Universidad Autónoma de Madrid

Facultad de Ciencias

Departamento de Biología Molecular

Structural analysis of intracellular transport, nuclear entry and egress of Herpes simplex virus 1 by cryo electron tomography

Dissertation presented by **Iosune Ibiricu Urriza** in candidacy for the degree of

'Doctora con Mención de Doctor Europeo'

The work presented in this dissertation has been performed at the Max Planck Institute of Biochemistry under the co-directorship of Dr. Jose Lopez Carrascosa and Dr. Wolfgang Baumeister and under the supervision of Dr. Kay Grünewald.

Madrid, 2009

Table of Contents

List of Abbreviations

2D	two dimensional
3D	three dimensional
BSA	bovine serum albumin
CCD	charge-coupled device
CHO	chinese hamster ovary cell
DHC	dynein heavy chain
D-MEM	dubleccos modified eagle medium
DMSO	dimethyl sulfoxide
DRG	dorsal root ganglia
DTT	dithiothreitol
EDTA	ethylenediaminetetraacetic acid
EGTA	ethylene glycol tetraacetic acid
EM	electron microscopy
ER	endoplasmatic reticulum
ESCRT	endosomal sorting complexes required for transport
ET	electron tomography
EtBr	ethidium bromide
FBS	foetal bovine serum
FEG	field emission gun
FM	fluorescence microscopy
FSC	Fourier shell correlation
GFP	green fluorescence protein
GTP	guanosine-5'-triphosphate
HFF	human foreskin fibroblasts
HSM	horse serum medium
HSV-1	Herpes simplex virus 1
HVEM	herpes virus entry mediator
IC	intermediate chain
IgG	Immunoglobulin G
IV	inclusion vesicle
KeV	kiloelectron volts
KHC	kinesin heavy chain
KLC	kinesin light chain
LC	light chain
LIC	light intermediate chain
L-particle	light particle
MEF	mouse embryo fibroblast
MEM	minimum essential medium
MES	2-(*N*-morpholino) ethanesulfonic acid
min	minutes
MOI	multiplicity of infection
MT	microtubule
MTOC	microtubule organizing centre

NBM	neurobasal medium
NPC	nuclear pore complex
PBS	phosphate buffered saline
PFU	plaque forming units
p.i.	post infection
PIs	protease inhibitors
PIPES	piperazine-N,N′-bis(2-ethanesulfonic acid)
PMSF	phenylmethanesulphonylfluoride
PrV	Pseudorabies Virus
RPMI	Roswell Park Memorial Institute medium
RT	room temperature
TEM	transmission electron microscope
wt	wildtype

Abstract

Herpes simplex virus 1 (HSV-1) is a complex enveloped double stranded DNA virus. The capsid containing the DNA is surrounded by a thick layer of tegument proteins and a lipid envelope with surface glycoproteins. In this work, cryo-electron tomography (cryo-ET), in combination with fluorescence microscopy, was applied to structurally analyze different stages of the HSV-1 'life' cycle *in situ* under close-to native conditions and without any chemical fixation. The focus of this study was on intracellular viral transport, attachment of capsids to nuclear pores and viral egress from cells.

After entry into host cells by membrane fusion, HSV-1 capsids are devoid of most of their tegument and preserve the so-called inner tegument. Capsids are then retrogradely transported towards the nucleus along microtubules, most probable by the cellular molecular motor complex dynein-dynactin. After replication, progeny capsids exit the nucleus and are anterogradely transported towards the cell membrane, most likely by the cellular molecular motor kinesin-1. At the final assembly site of the mature virus (virion) the capsids encounter membranous compartments that are associated with some of the tegument and viral glycoproteins. As a result, virions are further transported towards the cell membrane inside these compartments to exit the cell.

Transport of capsids was structurally analyzed *in vivo* and *in vitro* by cryo-ET and subtomogram averaging. Some of the inner tegument proteins are assumed to be essential for motor complex binding to the capsid during transport. However, the specific location of the inner tegument proteins and the attachment site of the motor complex have remained in dispute. Here it was revealed that the inner tegument was localized at the capsid vertices, binding to pentons and peripentonal hexons. This suggested that the motor complex binds only at the capsid vertices. Surprisingly, not only capsids containing DNA were transported *in vivo*, but also capsids devoid of DNA. Significant differences in tegumentation could be observed between these two groups.

An *in vitro* system was established to study the attachment of incoming capsids to nuclear pores. Extracted *Xenopus laevis* oocyte nuclei that were incubated with isolated capsids were spread and vitrified for cryo-ET observations. Several co-factors that potentially influence the attachment (cytosol, importin-ß and ATP) were tested.

Secondary envelopment, assembly and egress are the least understood processes in the HSV-1 'life' cycle. Cryo-ET of infected neurons provided new insights on the molecular structure of these events. An implication of clathrin during secondary envelopment and exit was revealed, as well as a specific orientation of the viral particles against the exit site. The formation of L-particles (non-infective viral particles produced during infection) was also characterized and showed many similarities to the egress pathway in virions.

The structural analysis of virus-host cell interactions *in vivo* and *in vitro* provided new relevant biological insights into the HSV-1 'life' cycle, complementing existing biochemical data.

1 Introduction

1.1 Herpes Simplex Virus 1

1.1.1 Classification, properties and clinical aspects

Herpesviruses are highly spread in nature and infect many different organisms like mammals, birds and reptiles (*Herpesviridiae*), fish and amphibians (*Alloherpesviridiae*) and oysters (*Malacoherpesviridiae*) (McGeoch *et al.* 2006). The *Herpesviridiae* encompass a large family of double stranded DNA viruses that can cause several illnesses in humans, like mucocutaneous lesions, keratitis, encephalitis, meningitis, chicken pox, roseola and Karposi´s sarcoma (Sedy *et al.* 2008). The members of this family share four significant biological properties (Fields 2007):

- They specify many enzymes related to the metabolism of nucleic acids, DNA synthesis and processing of proteins.
- The synthesis of viral DNA and the assembly of the capsid occur in the nucleus of the host cell. The final assembly of the mature infective virus, the so called virion, occurs in the cytoplasm.
- The production of infective viruses ultimately provokes the destruction of the infected cell.
- They are able to stay latent in their natural hosts, and they can produce recurrent infections.

This family is divided into three subfamilies: *Alphaherpesvirinae*, *Betaherpesvirinae* and *Gammaherpesvirinae* (**Table I**). Herpes Simplex Virus 1 (HSV-1) is the prototype of the subfamily *Alphaherpesvirinae*. This subfamily is characterized by their relatively short reproductive cycle and their ability to invade and persist in the neuronal tissue, where they remain latent and can be reactivated. HSV-1 is highly studied due to these biological properties, which provide a model and tool for the study of protein translocation, synaptic connections in the nervous system, membrane structure, gene regulation, gene therapy, cancer therapy and other biological and medical problems (Fields 2007).

In humans, HSV-1 infects first the epithelial cells of the oral or perioral cavity and then enters the nervous terminals that are in contact with the primarily infected epithelial cells. From here, it travels along the axons (retrograde transport) until it reaches the cell body and the nucleus of the neuronal cell in the dorsal root ganglia, where it remains latent. Reactivation can occur in response to different external stimuli like sun light, stress or fever. The virus is then transported to the area originally infected or to the proximities. It sheds viruses and infects further epithelial cells (**Figure 1**). These recurrent infections usually cause lesions near the oral cavity, but they can also provoke ocular lesions and in rare cases, typically in immunocompromised patients, they can cause encephalitis, which can have catastrophic results, even death (Fields 2007).

Table I: Classification of human herpesviruses (Fields 2007).

Official Nomenclature	Common name	Genus	Subfamily
Human Herpesvirus 1 (HHV-1)	Herpes simplex virus type 1 (HSV-1)	Simplexvirus	*α-herpesvirinae*
Human Herpesvirus 2 (HHV-2)	Herpes simplex virus type 2 (HSV-2)	Simplexvirus	*α-herpesvirinae*
Human Herpesvirus 3 (HHV-3)	Varicella zoster virus (VZV)	Varicellovirus	*α-herpesvirinae*
Human Herpesvirus 4 (HHV-4)	Epstein-Barr virus (EBV)	Lymphocryptovirus	*γ-herpesvirinae*
Human Herpesvirus 5 (HHV-5)	Human Cytomegalovirus (HCMV)	Cytomegalovirus	*β-herpesvirinae*
Human Herpesvirus 6A (HHV-6A)	HHV-6A	Roseolovirus	*β-herpesvirinae*
Human Herpesvirus 6B (HHV-6B)	HHV-6B	Roseolovirus	*β-herpesvirinae*
Human Herpesvirus 7 (HHV-7)	HHV-7	-	*β-herpesvirinae*
Human Herpesvirus 8 (HHV-8)	Kaposi´s sarcoma-associated herpesvirus (KSHV)	Rhadinovirus	*γ-herpesvirinae*

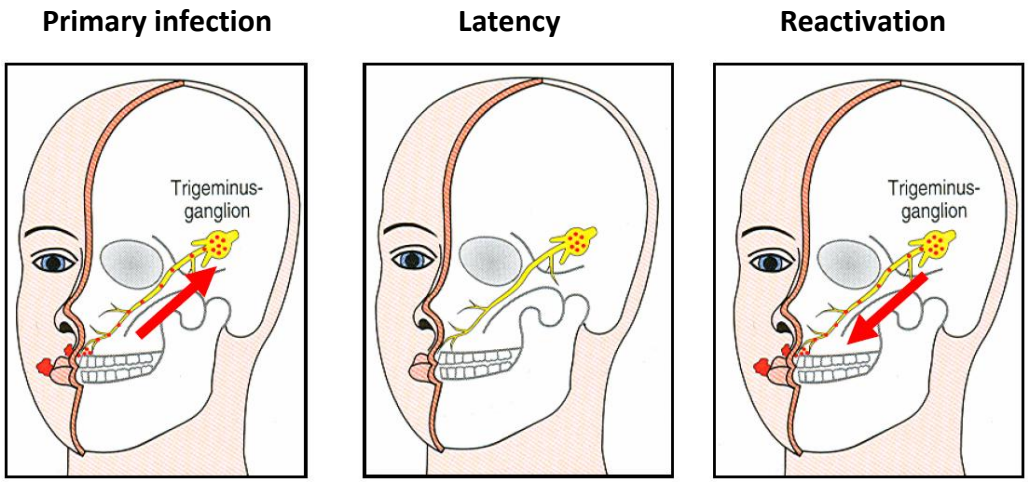

Figure 1. Schematic representation of the primary infection, latency and reactivation in HSV-1. After primary infection of the epithelial cells of the oral cavity the viruses infect the nerve terminals that are in contact with the epithelial cells and are transported along axons to the nucleus of the neuron, where they remain latent. In case of reactivation, they are transported again along the axon to the epithelial cells that were originally infected, resulting in recurrent infection (Döhner 2006).

1.1.2 Structure

1.1.2.1 Virions

The infectious HSV-1 particles (so called virions) are large (180-220 nm diameter) and of high complexity (**Figure 2**). They contain a highly packed 152 kbp double stranded DNA that is surrounded by an icosahedral capsid of about 125 nm diameter. The capsid has been studied in detail by cryo electron microscopy (cryo-EM) (Schrag *et al.* 1989; Zhou *et al.* 1994; Zhou *et al.* 2000; Bowman *et al.* 2003). It is composed of five major different proteins (**Table II**): VP5 (149 kD), VP26 (12 kD), VP23 (34 kD), VP19C (50 kD) and UL6 (74 kD). The crystal structure of the major capsid protein VP5 has been already resolved (Bowman *et al.* 2003). The largest morphological units inside the capsid are the capsomers: twelve are 5-coordinated (pentons, located at the vertices) and 150 are 6-coordinated (hexons). They are formed by five and six copies of VP5 respectively. The hexons also contain six copies of the protein VP26 that form a ring on top of the VP5 subunits. The triplexes form the connections between capsomers and are composed of one molecule VP19C and two molecules VP23 (Newcomb *et al.* 1993). One of the twelve vertices is different. It consists of a dodecameric ring formed by twelve copies of the UL6

protein, instead of the five copies of VP5 present in the rest of the vertices. This unique vertex is called portal, since it serves as an entry and possibly as an exit channel for the DNA (Newcomb *et al.* 2001; Trus *et al.* 2004; Cardone *et al.* 2007; Chang *et al.* 2007). It was suggested that the protein UL25 retains the DNA inside the capsid and might also provide a nuclear exit signal (Ogasawara *et al.* 2001; Rode 2007).

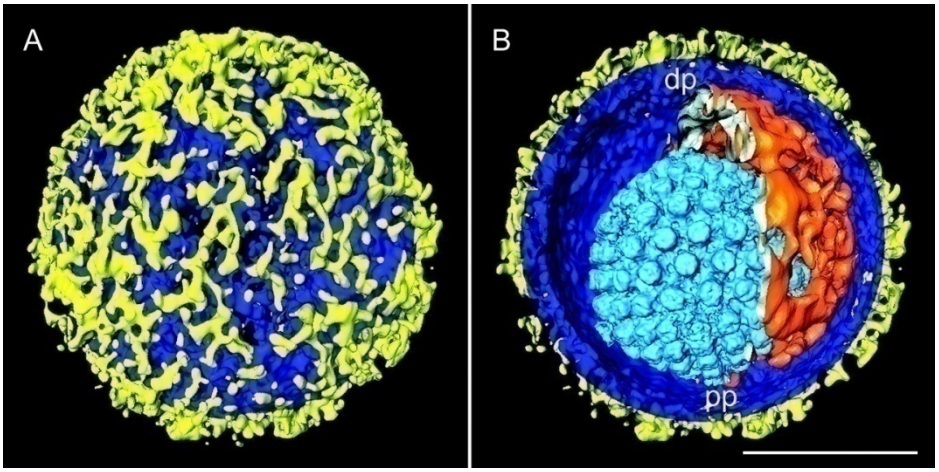

Figure 2. Surface representation of HSV-1, derived from cryo-electron tomography data. (A) Exterior of the virion, showing the glycoproteins (yellow) emerging from the envelope (blue). (B) Cut open view of the virion. The capsid (light blue) and tegument (orange) are shown inside the envelope (dark blue). pp: proximal pole; dp: distal pole; bar = 100 nm (Grünewald *et al.* 2003).

The virions are bound by a lipid bilayer called envelope that contains more than eleven different integral membrane glycoprotein species (**Table III**). Some of these glycoproteins are essential for cellular entry (Spear 2004) (**1.1.3.1**). Others are likely involved in virus assembly (Mettenleiter 2006).

An amorphous layer of at least 20 different proteins is located between envelope and capsid. This so called tegument has an irregular structure (Grünewald *et al.* 2003), although it is more regularly arranged near the capsid vertices (Zhou *et al.* 1999). Some of the proteins that form the tegument are of special interest due to their assumed role during the transport of the capsid towards the nucleus and the cell periphery (**Table IV**, **1.1.3.2, 1.1.3.4**). The capsid is positioned asymmetrically within the virion (Grünewald *et al.* 2003). The pole where the capsid is closest to the envelope has almost no tegument (proximal pole) and the opposite pole of the virion contains most of the tegument (distal pole) (Grünewald *et al.* 2003) (**Figure 2**).

Table II: Genes that code for HSV-1 capsid proteins. The mayor capsid proteins are highlighted (based on Fields 2007; Loret *et al.* 2008).

Gene	Protein	Function	Size
UL6		Forms the homodecameric portal at one vertex of the capsid	676 aa
UL17		Targets the procapsid to the site of DNA packaging	703 aa
UL18	**VP23**	Part of the triplex that connects capsomers	318 aa
UL19	**VP5**	Major capsid protein, six copies in hexons and five in pentons	1311 aa
UL25		Involved in viral DNA packaging into capsids	580 aa
UL26	VP24, VP21	Self cleavable protease with two scaffold proteins as product	635 aa
UL26.5	VP22a	Scaffold protein	326 aa
UL35	**VP26**	It forms an hexameric structure on the outer surface of each hexon	112 aa
UL38	**VP19c**	Part of the triplex that connects capsomers	465 aa

aa: amino acids

Table III: Genes that code for HSV-1 glycoproteins. The glycoproteins most relevant in HSV-1 entry are highlighted (based on Fields 2007; Loret *et al.* 2008).

Gene	Protein	Function	Size
UL1	**gL**	Forms a heterodimer with gH. Essential for entry	224 aa
UL10	gM	Forms a complex with gN and inhibits cell fusion	473 aa
UL20		Involved in nuclear egress	
UL22	**gH**	Forms a heterodimer with gL. Essential in cell-cell and virus-cell fusion	838 aa
UL27	**gB**	Binds cellular receptors. Essential for entry	904 aa
UL34		Required for primary envelopment. Essential for infection	
UL44	**gC**	Involved in attachment of virions to the cells via cellular receptors	511 aa
UL49A	gN	Forms a complex with gM. Required for its functional processing	
UL53	gK	Required for virus-induced cell fusion	338 aa
US4	gG	Function unknown	283 aa
US5	gJ	Blocks apoptosis	
US6	**gD**	Interacts with cellular receptors during entry. Essential for entry	394 aa
US7	gI	Forms a heterodimer with gE, viral receptor for monomeric IgG	390 aa
US8	gE	Forms a heterodimer with gI, viral receptor for monomeric IgG	550 aa

aa: amino acids

Table IV: Genes that code for HSV-1 tegument proteins. The best characterized ones are highlighted (based on Fields 2007; Loret *et al.* 2008).

Gene	Protein	Function	Size
RL1	ICP34.5	Viral neurovirulence factor	248 aa
α0	**ICP0**	Functions as an ubiquitin-kinase	775 aa
α4	**ICP4**	Functions as repressor and transactivator	1298 aa
UL4		Colocalizes with ICP22 before onset of DNA synthesis	199 aa
UL7		Involved in viral replication	296 aa
UL11		Involved in secondary envelopment	96 aa
UL13		Protein quinase, regulates viral replication	518 aa
UL14		Might facilitate the packaging of certain proteins	219 aa
UL16		Associates with cytoplasmic capsids, essential for infection	373 aa
UL17		Responsible for DNA packaging, essential for infection	703 aa
UL21		Binds to microtubules	535 aa
UL31		Primary tegument protein, essential for primary envelopment at the inner nuclear membrane	306 aa
UL36	**VP1-2**	Required for the transport of the capsid in the cytoplasm. Could be related to the DNA injection into the nucleus. Essential for infection	3165 aa
UL37		Attaches to the DNA and VP1-2. Essential for infection	1123 aa
UL41	**vhs**	Degrades mRNA in the early stages of infection	489 aa
UL46	**VP11/12**	Increments the activity of VP16	718 aa
UL47	**VP13/14**	Increments the activity of VP16	491 aa
UL48	**VP16**	Induces the expression of the α-genes. It is also required for the assembly of virions. Essential for infection	491 aa
UL49	**VP22**	Involved in egress transport of capsids	?
UL51		Unknown function	244 aa
US2		Unknown function	291 aa
US3		Promotes egress of capsids from the nucleus to the cell periphery	481 aa
US9		Required for the transport of virions to the cell periphery	234 aa
US10		Unknown function	312 aa
US11		Attaches to the RNA and is partially responsible for the virion packaging	161 aa

aa: amino acids

1.1.2.2 Light particles

In the early 90´s it was observed that infection with HSV-1 of different cell lines did not only produce virions but also non-infectious light particles (L-particles), characterized by the absence of capsid and DNA (Szilagyi *et al.* 1991). The morphology of these non-infectious particles has been analyzed in viral preparations and seems to be quite heterogeneous, covering a wide range of sizes and in many cases containing inclusion vesicles (IVs) that vary in size and number. These IVs could be associated with certain phosphoproteins (Szilagyi *et al.* 1994). Some of the polypeptides detected in L-particles are not observed in virions (Szilagyi *et al.* 1991). One of them was identified as the IE trans-activating polypeptide (McLauchlan *et al.* 1992). L-particles are not only present in HSV-1 but in all alphaherpesviruses tested so far (McLauchlan *et al.* 1992; Dargan *et al.* 1997). These particles have a function during infection, since they seem to be able to fuse with the cell and thus they deliver additional tegument proteins needed during HSV-1 replication (McLauchlan *et al.* 1992; Dargan *et al.* 1997).

The formation of L-particles was shown to be independent of the production of virions by infection with the temperature-sensitive mutant ts1203, which at non-permissive temperatures can not form capsids. Here, at non-permissive temperatures L-particles were produced but virion assembly did not take place (Rixon *et al.* 1992). Previous studies by classical electron microscopy showed that L-particles seem to be formed by budding of condensed tegument into Golgi-derived vesicles. Furthermore, they were observed budding simultaneously into a vesicle together with capsids, which suggests that virions and L-particles share the same secondary envelopment site and mechanism (Aleman *et al.* 2003).

1.1.3 Replication cycle

1.1.3.1 Cell entry

HSV-1 entry into cells is mediated by interactions of viral glycoproteins integral to the virion envelope and their cellular receptors. There are at least 11 different glycoprotein

species present on the envelope (**Table IV**), but only five of them play an important role during viral entry: gB, gC, gD, gH and gL (Spear 2004).

The virion attaches to the cell membrane by interaction of the glycoproteins gC and gB with heparan sulphate chains located at the cell surface (Campadelli-Fiume *et al.* 2000; Carfi *et al.* 2001) (**Figure 3A**). After attachment, entry of HSV-1 into the cell takes place in two different ways depending on the cell type (Milne *et al.* 2005):

1) Primary pathway: fusion of the viral envelope with the plasma membrane (Pelkmans *et al.* 2003). The glycoprotein gD provokes conformational changes after the interaction with the cell receptors herpesvirus-entry-mediator (HVEM), nectin-1 or specific sites in heparan sulphate (Shukla *et al.* 1999). The binding of gD to any of these receptors induces fusion. Once this binding takes place, certain domains of the receptors are exposed and interact with gB, gH and gL, finally leading to membrane fusion (Spear 2004). Recently, it has been reported that the interaction between glycoprotein gB and the cellular receptor PILRα is essential for the infection in certain cell types (Satoh *et al.* 2008). After fusion of viral envelope and plasma membrane, the capsid is released into the cytoplasm leaving behind most of the tegument (Maurer *et al.* 2008), but keeps the so called inner tegument attached to certain areas of the capsid. This entry pathway has been described for HFF, Ptk2 and Vero cells and is also typical for neurons, the natural host cells of the virus.

2) Secondary pathway: viral entry via endocytosis (Smith *et al.* 2004). It is followed by fusion of the viral envelope with the endosome membrane. This fusion is most probably also mediated by interaction of viral glycoproteins with receptors of the endosome membrane. In most of the cases, the fusion takes place only after acidification of the medium. This entry pathway has been shown for CHO and HeLa cells (Nicola *et al.* 2003; Milne *et al.* 2005). The release of the capsid into the cytoplasm is also characterized by the loss of most of the tegument while maintaining the inner tegument attached to the capsid. This remaining tegument seems to be crucial for the transport of the capsid towards the nucleus (Bearer *et al.* 2000; Antinone *et al.* 2006; Luxton *et al.* 2006). Some of the tegument proteins, like vhs, are separated from the capsid after fusion and act in the cytoplasm. Others, like VP16, are independently transported to the nucleus.

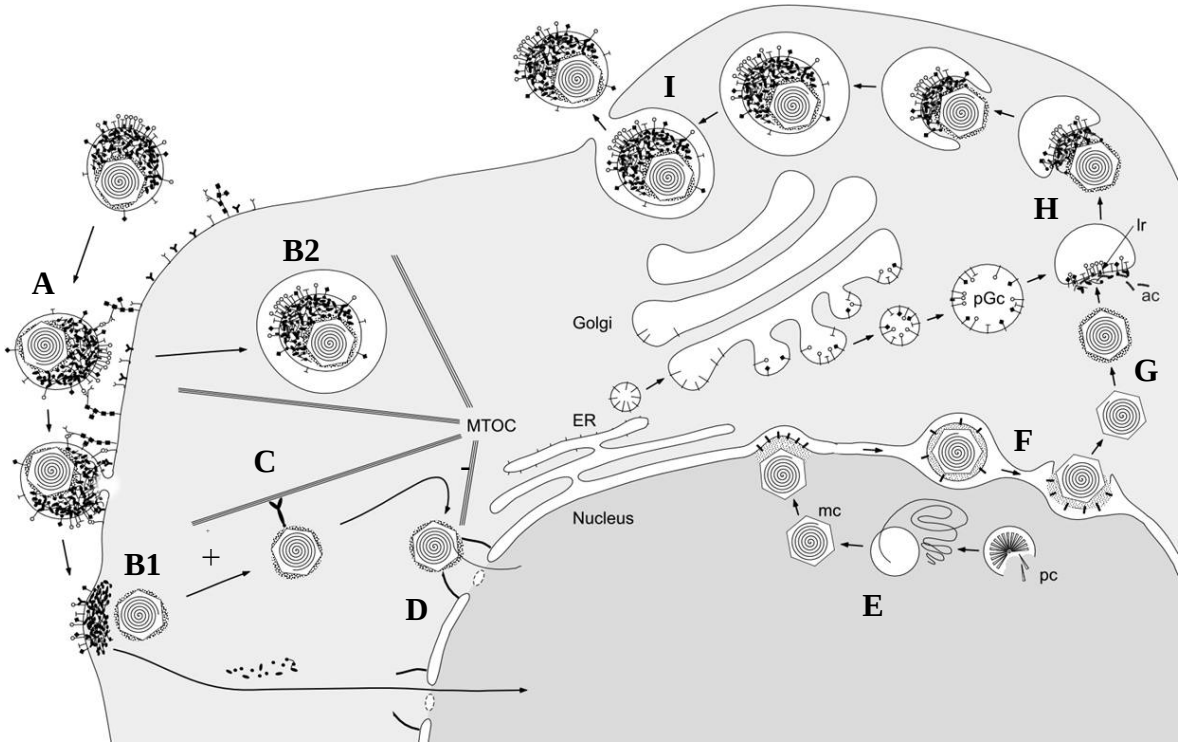

Figure 3. Scheme of the HSV-1 'life' cycle. (A) Attachment to the cell membrane and entry, by fusion of envelope and cell membrane (B1) or by endocytosis (B2). (C) Transport of the capsid towards the nucleus of the cell along microtubules, mediated by molecular motors. (D) Attachment of the capsid to the nuclear pore and DNA release into the nucleus. (E) Replication and capsid assembly. (F-I) Egress pathway, including (F) exit of the capsid from nucleus by envelopment-deenvelopment-reenvelopment, (G) anterograde transport of the capsid, (H) assembly by secondary envelopment of the virion and (I) exit from the cell. Figure by courtesy of Kay Grünewald.

1.1.3.2 Transport towards the nucleus

Once the capsid is released into the cytosol, it takes advantage of the cellular machinery to be transported towards the nucleus of the cell (**Figure 3C**; for details see **1.1.4**). The molecular motor used by HSV-1 capsids to be transported along microtubules from the cell periphery to the nucleus (retrograde transport or minus-end directed transport) is dynein and its cofactor dynactin (Sodeik *et al.* 1997; Döhner *et al.* 2002; Greber *et al.* 2006; Radtke *et al.* 2006). It has been observed how capsids accumulate at the microtubule organizing centre (MTOC) and then spread over the nuclear envelope (Sodeik *et al.* 1997; Döhner *et al.* 2002; Mabit *et al.* 2002). It is not known how capsids manage to get to the nuclear envelope from the MTOC. This spread might also involve active transport along microtubules using a plus-end directed motor like kinesin-1 (Janus 2008).

1.1.3.3 Attachment to the nucleus, DNA release and replication

When the capsid reaches the nucleus it binds to the nuclear pores at the nuclear envelope and releases its DNA inside (**Figure 3D**). It has been reported that importin-ß enhances the attachment of capsids to nuclear pores (Ojala *et al.* 2000). Nuclear pore complexes (NPCs) are huge supramolecular complexes that span the inner and outer nuclear membrane and mediate the bidirectional transport of several macromolecules. They have a doughnut-like central body from which fibres extend into both the cytoplasm and the nucleus. The nuclear fibres form a basket-like structure below the body of the pore (Stewart 2007). The structure and dynamics of NPCs have been extensively studied by cryo electron tomography (cryo-ET) (Beck *et al.* 2004; Beck *et al.* 2007).

The capsid orientation towards the nuclear pore and the mechanisms that induce the DNA release are not known. Some studies suggest that one of the vertices of the capsid is facing the nuclear pore during attachment (Sodeik *et al.* 1997; Ojala *et al.* 2000), probably the portal since it is as well the site for DNA entry into the capsid (Newcomb *et al.* 2001). Therefore, DNA injection into the nucleus might occur through one of the vertices of the capsid. It seems that DNA release is ATP dependent and some other factors involved in nuclear import might also be required (Ojala *et al.* 2000; Whittaker 2003). The DNA release by isolated capsids was tested in an *in vitro* system where capsids were able to release the DNA into mammalian nuclei. When those capsids were treated with trypsin, they lost the proteins VP1-2, VP13/14, VP16 and VP22, and DNA release was markedly affected. This indicates that at least some of these proteins are involved in the process (Ojala *et al.* 2000). VP1-2 is most probably involved since HSV-1 tsB7, a mutant defective in VP1-2, can attach to nuclear pores but is not able to release its DNA into the nucleus at non-permissive temperatures (Batterson *et al.* 1983).

After DNA release, the empty capsid remains attached at a distance of 50 nm from the centre of the pore until it is eventually released into the cytoplasm and degraded (Sodeik *et al.* 1997).

Once the DNA has entered the nucleus replication starts (**Figure 3E**). The new capsids are assembled by means of a scaffolding protein that helps to form spherical procapsids. This procapsid undergoes a maturation process to form the characteristic icosahedral capsid

(Heymann *et al.* 2003). After capsid maturation the double stranded DNA enters through the portal vertex and undergoes packaging. Three types of capsids (A-, B- and C-capsids) have been found in infected nuclei. C-capsids contain DNA and can mature to form infectious virions. A and B-capsids lack DNA but B-capsids still partially contain the scaffolding protein. A-capsids are assumed to be products of aborted DNA packaging (Newcomb *et al.* 1991). Recent studies showed that C-capsids have higher amounts of the proteins UL25 and UL17 than A and B-capsids. These minor capsid proteins form a heterodimer at the vertices of the capsid (Trus *et al.* 2007) and are involved in DNA packaging and capsid maturation (Salmon *et al.* 1998). All nuclear capsids are thought to be free of tegument and the recruitment of tegument proteins would start during primary envelopment and would mainly continue in the cytoplasm (Miranda-Saksena *et al.* 2002; Naldinho-Souto *et al.* 2006), although recent studies suggest that nuclear capsids could be already associated with the tegument proteins VP1-2 and UL37 (Bucks *et al.* 2007).

1.1.3.4 Viral egress

After replication and assembly and once the DNA is packaged, the mature capsid leaves the nucleus. The nuclear egress has created a lot of controversy. There are three different hypotheses for viral egress:

1) Envelopment-deenvelopment-reenvelopment model (**Figure 3F**): the capsid acquires a primary envelope at the inner nuclear membrane while getting into the perinuclear space (Epstein 1962). The proteins pUL31 and pUL34 interact at the inner nuclear membrane and form a complex that is required for the formation of the primary envelope. The kinase US3 is essential for the distribution of pUL31 and pUL34 in the nuclear membrane (Reynolds *et al.* 2002; Klupp *et al.* 2007). This way the primary enveloped virion would contain at least the proteins pUL31, pUL34 and US3. The tegument protein VP16 was also detected in primary enveloped particles (Naldinho-Souto *et al.* 2006). These particles exit the perinuclear space by fusion of the primary envelope with the outer nuclear membrane. (Skepper *et al.* 2001; Mettenleiter 2002; Mettenleiter *et al.* 2006). Once released into the cytoplasm, the capsid loses the primary tegument and is transported towards the cell periphery (anterograde transport), most likely using the molecular motor

Kinesin-1 (for more detail see **1.1.4**). The process of tegumentation that the capsid undergoes in the cytoplasm is not very well defined. It is known that certain tegument proteins are essential for the intracellular transport of capsids (see **1.1.4.3**). At the final assembly site of the virion, the newly formed capsids encounter cytoplasmic membranous compartments that are associated with some of the tegument and viral glycoproteins. These compartments originate from the trans-Golgi network and most likely also use a type of kinesin for plus-end directed transport (Loomis *et al.* 2001; Turcotte *et al.* 2005; Mettenleiter *et al.* 2006). The ESCRT multiprotein complexes (Endosomal Sorting Complexes Required for Transport) might also be involved in the seconday envelopment of HSV-1 (Crump *et al.* 2007). The result of the secondary envelopment is an enveloped virus particle that has budded topologically away from the cytoplasm into a membranous compartment derived from the trans-Golgi network. Inside this compartment the virion is further transported to the plasma membrane and exits the cell by exocytosis-like fusion of the transport compartment membrane with the plasma membrane (Mettenleiter 2002).

The site of secondary envelopment is also a controversial subject. In neurons it is suggested on one hand that it mainly takes place at the cell periphery, in particular at the axon terminals and sporadically also in varicosities. In this case, anterograde transport along the axon occurs with naked capsids (Miranda-Saksena *et al.* 2000; Luxton *et al.* 2005; De Regge *et al.* 2006; Snyder *et al.* 2006; Diefenbach *et al.* 2008). Varicosities are dilations of axons that represent residual growth cones left behind during growth of the axon terminal. They typically contain actin, microtubules and vesicles (Lucic *et al.* 2007; Diefenbach *et al.* 2008). On the other hand studies done with Pseudorabies virus (PrV), another member of the *Alphaherpesvirinae* family, suggest that the capsid is enveloped close to the cell body and anterograde transport occurs once the capsid acquires an envelope (Antinone *et al.* 2006; Lyman *et al.* 2007; Lyman *et al.* 2008).

HSV-1 exits the neuron from varicosities as well as from axon terminals (Miranda-Saksena *et al.* 2000; Smith *et al.* 2001; Smith *et al.* 2004; Luxton *et al.* 2005; Saksena *et al.* 2006; Snyder *et al.* 2006).

2) Single envelopment model: after getting into the perinuclear space, the enveloped capsid is transported to the Golgi cisternae via the endoplasmatic reticulum cisternae, which are in direct connection with the perinuclear space. It then uses the secretory pathway of the Golgi for its transport inside the cell by the formation of vacuoles that can contain one or more virions (Darlington *et al.* 1968; Lycke *et al.* 1988; Leuzinger *et al.* 2005). These vacuoles are transported towards the cell periphery along microtubules, most probably by the molecular motor kinesin-1. Once the vacuole gets to the cell membrane, both membranes fuse and the viruses are released to the extracellular space. In this model, the viruses abandon the perinuclear space already with all the tegument and glycoproteins characteristic for virions and travel in the cytoplasm along microtubules already in a mature form. Since nearly all the tegument proteins are exclusively cytoplasmic, this model is not likely.

3) Expansion of the nuclear pores model: it is the most controversial model. It was proposed that the NPCs expand in such a way that the capsid is able to exit the nucleus through them (Leuzinger *et al.* 2005). Once free in the cytoplasm, it would acquire the tegument and would invaginate inside Golgi cisternae to be enveloped and form a mature virion. From here it would use the secretory pathway of the Golgi like in the first and second model to exit the cell. This model is also not likely since such sized NPCs would not be functional any longer and the cell would die within a short time. However, live cell microscopy reveals that cells survive viral egress for several hours.

1.1.4 Intracellular trafficking of viral particles

The intracellular transport of viral particles is mediated by molecular motors of the cell. These are protein complexes able to move along microtubules and are used by the cell to transport different types of cargo, like vesicles and organelles. The mechanism they use to obtain energy for the movement is ATP hydrolysis. This reaction causes a small conformational change in one of the globular motor domains that is amplified and translated into a step-wise movement (Schliwa *et al.* 2003). The molecular motors are essential for the transport of HSV-1 since the cytoplasm is crowded with different

organelles, cytoskeleton and a high concentration of proteins, which restricts the free diffusion of particles bigger than 500kDa (Dauty *et al.* 2005).

1.1.4.1 Microtubules

Microtubules are part of the cytoskeleton of eukaryotic cells and are formed by the polymerization of α and β tubulin dimers. They are cylinders of 25 nm diameter and variable length (Nogales 2000). Originally, they have been described as empty cylinders. However, recently it has been observed in mammalian cells including neurons that the lumen of microtubules can be filled with globular particles (Garvalov *et al.* 2006). The minus (-) end of a microtubule is localized at the microtubule organizing centre (MTOC) and the plus (+) end is oriented towards the cell periphery. This plus end is continuously polymerising and depolymerising. Microtubules have different functions inside the cell. They are part of the cytoskeleton and help to maintain the shape of the cell. Moreover, they act as 'highways' for the transport of different organelles and vesicles and they form the mitotic spindle, which segregates the sister chromatids during cellular division.

1.1.4.2 Molecular motors

The minus-end directed transport of viral particles is mediated by dynein, which has a molecular weight of 1.4 MDa and contains two heavy chains (DHC, 520 kDa) that bind to the microtubule and hydrolyze ATP to generate movement (**Figure 4**). It also has six light chains (LCs) that belong to three protein families (LC8/PIN, tctex and LC7/roadblock), two light intermediate chains (LIC, 53-57 kDa) and two intermediate chains (IC, 74 kDa) (Vale 2003). LCs, LICs and ICs are involved in the attachment of the viral particle (Vallee *et al.* 2003; Greber *et al.* 2006; Radtke *et al.* 2006). It has been shown by single molecule measurements that dynein makes steps of 8-32 nm length depending on the load (Mallik *et al.* 2004; Reck-Peterson *et al.* 2006). Dynein requires the protein complex dynactin to be fully functional (**Figure 5**) (Sodeik *et al.* 1997; Döhner *et al.* 2002; Culver-Hanlon *et al.* 2006).

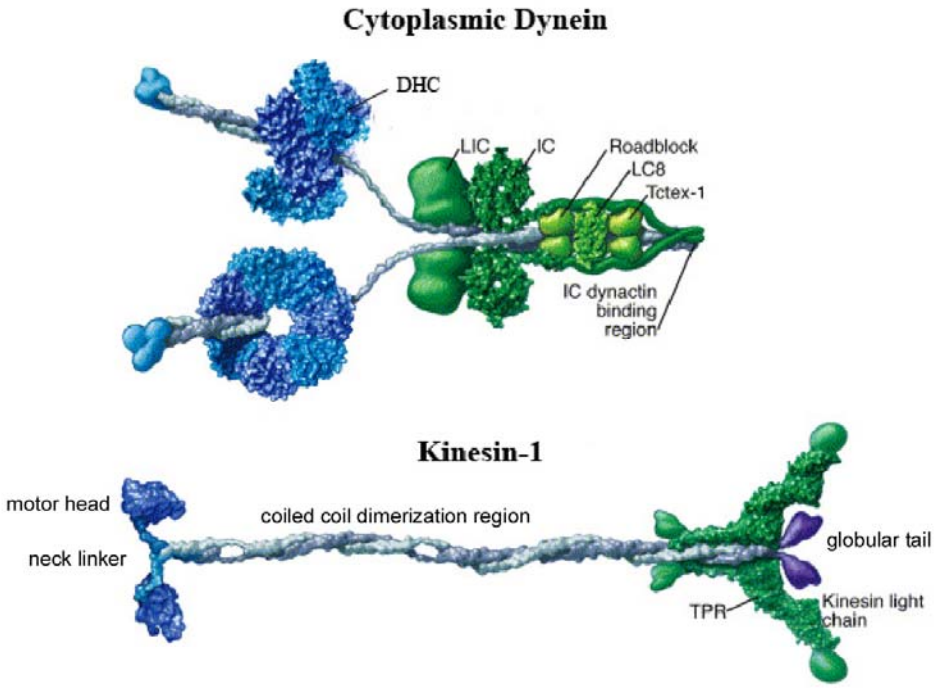

Figure 4. Schematic representation of the molecular motors dynein and kinesin-1. DHC: dynein heavy chain; LIC: light intermediate chain; IC: intermediate chain (Vale 2003)

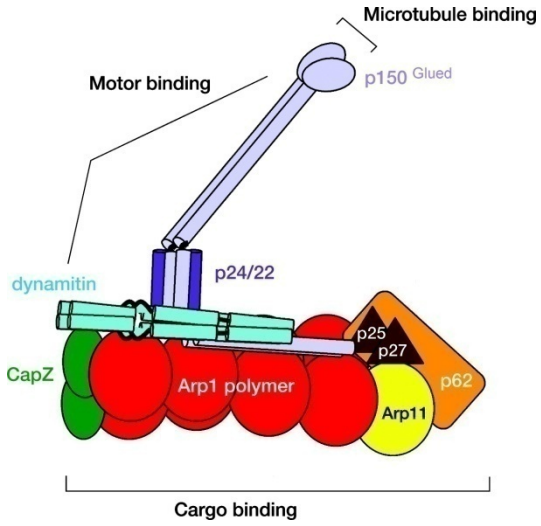

Figure 5. Schematic representation of dynactin. It shows the areas that bind to cargo, microtubules and molecular motors (Schroer 2004).

The plus-end directed transport of viral particles is most likely mediated by the molecular motor kinesin-1 (**Figure 4**), which contains two heavy chains (KHC, 120 kDa) and two light chains (KLC, 64 kDa). Each heavy chain consists of a motor head that attaches to the microtubule, a neck linker, a long coiled coil dimerization region and a globular tail. The light chains attach to the viral particle. Kinesin-1 is responsible for usually taking care of the transport of cellular organelles and cargo from the nucleus to the cell periphery. Kinesin-1 was shown to interact with dynein via KLC and DIC (Ligon *et al.* 2004). It moves along microtubules moving the two motor heads with a step size of 8 nm (Yildiz *et al.* 2005).

The intracellular transport of viral particles is not always continuous; it often changes direction and becomes bidirectional (Gross 2003). Therefore, it is assumed that not only one of the motors is present, but both of them are attached to the viral particle at the same time (**Figure 6**). In peroxisomes *in vivo* it was observed that up to eleven kinesins or dyneins can work together to transport the same cargo at higher speed (Kural *et al.* 2005). A regulation of the motor activity is needed to ensure that dynein and kinesin do not concomitantly pull in opposite directions. This coordination of movements is probably mediated by dynactin, which has a binding site called p150/Glued that attaches to the DIC domains in dynein and to the XCAP domain in kinesin-1 inducing their activation (Schroer 2004). It is believed that only one of the motors can be attached to dynactin at the same time. Therefore, when one of the motors is attached to dynactin, it is activated and in contact with the microtubule, moving the cargo in one direction, while the other motor remains inactivated and detached from the microtubule but still connected to the cargo. It is hypothesized that detachment of the motor from both microtubule and dynactin could be mediated by a protein functioning as a spring, which would disconnect one of the motors while the other one remains active. This protein could be associated either to the cargo or to dynactin (Gross 2003).

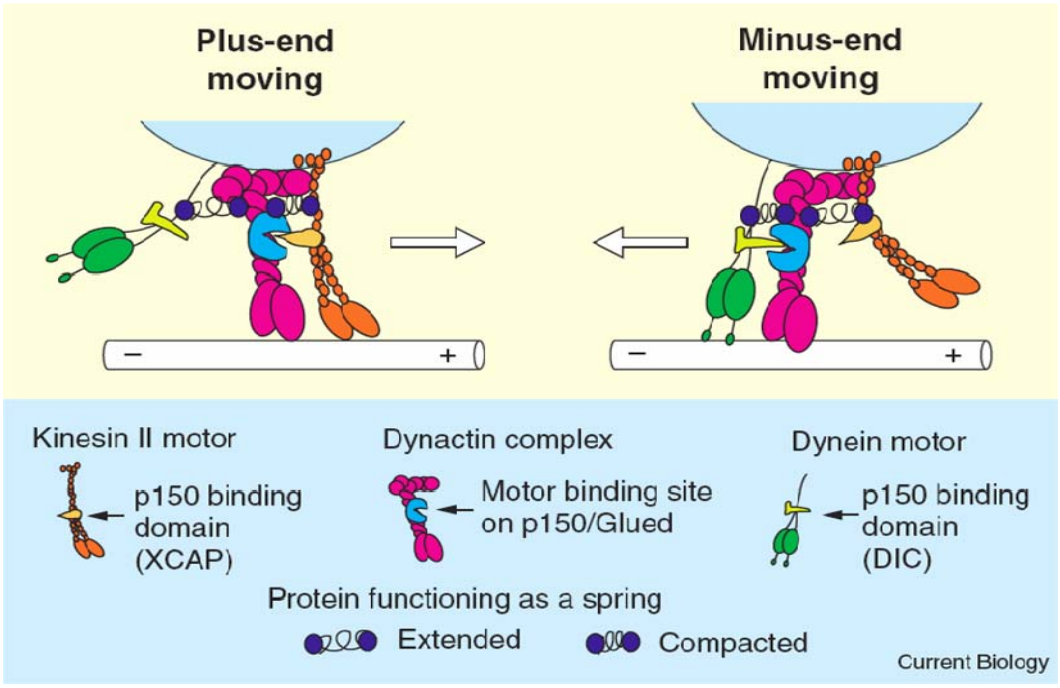

Figure 6. Schematic representation of the coordination of the molecular motors dynein and kinesin mediated by the complex dynactin (Gross 2003).

1.1.4.3 Capsid-tegument-motor interactions

Where the attachment sites of the capsids to molecular motors are and how the viral proteins are involved in the attachment are questions that have been only partially answered. Several tegument proteins are essential during intracellular transport of viral particles and are most likely binding sites for the molecular motors. Studies of PrV indicate that the tegument proteins VP1-2 and UL37 are required for intracellular transport of capsids (Luxton *et al.* 2005; Luxton *et al.* 2006). The deletion of the gene UL36 (its product is VP1-2) leads to the accumulation of HSV-1 capsids in the cytoplasm that could not release the DNA into the nucleus (Desai 2000). The fact that VP1-2 seems to be strongly associated to HSV-1 capsids in comparison to other tegument proteins also corroborates the hypothesis that VP1-2 plays an important role in intracellular transport (Spear *et al.* 1972). Previous studies of intact isolated virions have shown that a small portion of tegument is connected to the vertices of the capsid, in particular to the capsid protein VP5 (Zhou *et al.* 1999). Based on the size of the density, the author suggested this to be VP1-2. Furthermore, earlier electron microscopy studies showed capsids inside cells

with substantial density found at the vertices (Sodeik *et al.* 1997). This suggests that the molecular motors might attach to the vertices of the capsid, most probably interacting with tegument proteins like VP1-2 and UL37. There are other tegument proteins like VP16, VP13-14 and VP22 that might also be involved in transport of newly produced capsids to the periphery of the cell, since they have been sometimes localized together with capsids during egress although not after entry (Luxton *et al.* 2005).

1.1.4.4 Membrane protein-motor interactions

Assuming that anterograde transport of HSV-1 takes place when the virion is fully assembled and inside a transport vesicle (see **1.1.3.4**), there must be binding sites on the virus containing compartment for attachment of molecular motors for transport to take place. One candidate is the cytosolic tail of the membrane protein UL34, which seems to interact with the DIC subunit of dynein (Ye *et al.* 2000). UL34 is located at the inner nuclear membrane and after primary envelopment would be present in the envelope of the virus. Another candidate could be the membrane protein UL56, which in HSV-2 was shown to interact with KIF1A, a member of the kinesin-3 family (Koshizuka *et al.* 2005).

1.2 Approaches for structural analysis

1.2.1 Transmission electron microscopy

The electron microscope was invented by Ernst Ruska and Max Knoll at the beginning of the thirties, displacing the light microscope as the visualization technique for higher resolution at that time. Since then it has gone through a number of technological improvements to obtain higher resolution. Nowadays, transmission electron microscopes (TEM) can reach 3-4 Å resolution for biological specimens, although the basic concepts are still the same (**Figure 7**). Electrons emitted from a source (electron gun) are accelerated by high voltage (for biological specimens typically 100-300 KeV) to form an electron beam. This beam is focused with electrostatic and electromagnetic lenses over a thin sample situated in the microscope column. This column is kept at high vacuum to prevent scattering of electrons by air molecules (Yonekura *et al.* 2002).

The beam is focused with the condenser lenses onto the specimen. Some of the electrons transit the specimen without interfering with it, whereas others are retained or scattered by the atoms of the specimen. There are two different types of scattering: elastic and inelastic. In elastic scattering there is no loss of kinetic energy. It is essential for the contrast increase in the final image (see **1.2.2**). In inelastic scattering there is an excitation of the specimen and loss of electron energy (Reimer 1997). Furthermore, the inelastically scattered electrons produce noise that degrades the quality of the final image. The proportion of electrons that undergo scattering depends directly on the sample thickness and density.

This way, an image is formed by the electrons that pass through the specimen. The objective lens and the projector lenses magnify the image, which is projected on a fluorescent screen situated at the end of the column. Alternatively, the image can be also captured by a TV camera, by photographic film or by a CCD (charge-coupled device) detector. The last one is able to form digital images directly, first converting the electron image into photons by a phosphorescent layer and transferring the light image to the CCD sensor.

Some electron microscopes are equipped with an energy filter, being able to select electrons within a narrow energy window. When operated in zero-loss energy mode it removes the electrons that have been inelastically scattered and therefore increases the signal to noise ratio in the final image. There are two different implementations of energy filters: in-column (e.g. Omega design; implemented by Zeiss and JEOL) and post-column energy filters (e.g. Gatan Imaging Filter; GIF).

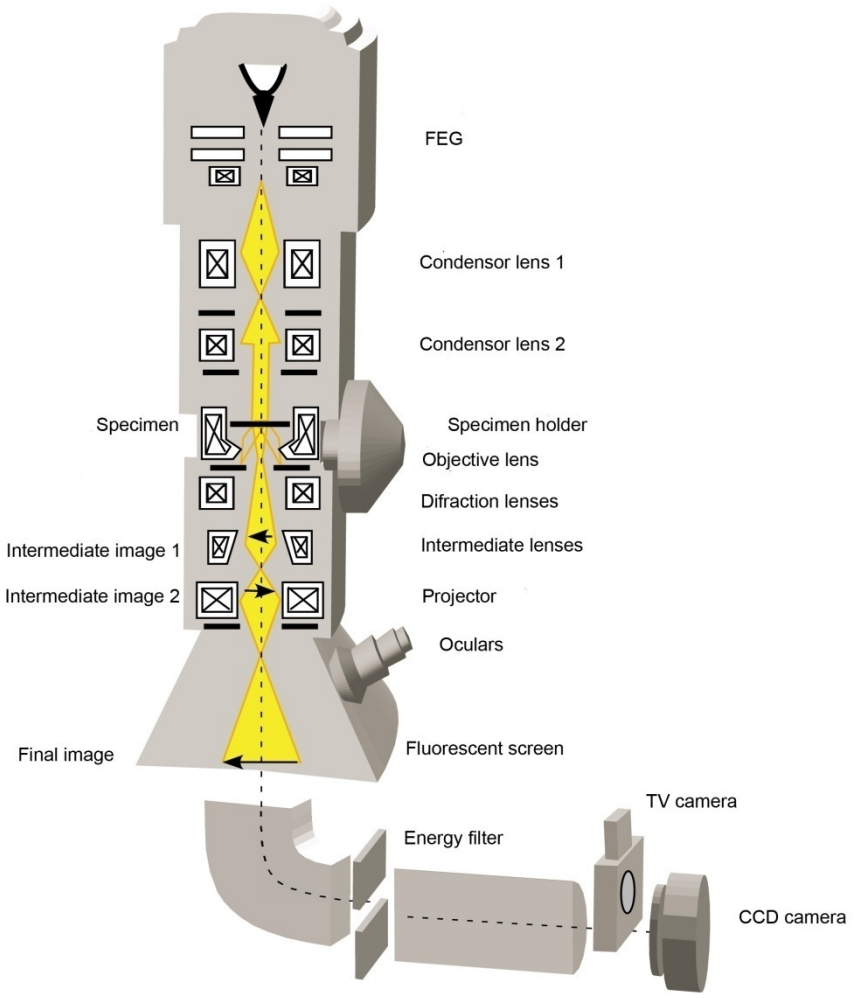

Figure 7. Scheme of the inner structure of the Phillips CM300 TEM equipped with a column energy filter, a TV camera and a CCD camera (Schweikert 2004).

1.2.2 Image formation

An electron micrograph is a two-dimensional (2D) projection of an object observed in TEM. The image resolution is limited essentially by the contrast, defined as the relative difference of intensity between a spot in the image and what is surrounding it. The contrast is essential to differentiate the image elements from the background.

In preparations with heavy metals staining the contrast is increased due to the high density of the sample. This is the amplitude contrast, also called scattering contrast, and it is produced by the electrons that are scattered at large angles when they interact with high density areas of the sample and thus do not contribute to the formed image.

In vitrified biological specimens the phase contrast, also called interference contrast, is more important. It is the result of the interference between the elastically scattered electrons and the non-scattered electrons (Erickson 1971). Without staining, the atoms of the sample have very similar density to the surrounding ice layer (see **1.2.4**) and scatter very weakly. Therefore, in this case phase contrast is more important than amplitude contrast. Phase contrast is enhanced by the combination of defocus and lens aberration. By applying defocus the phase of the scattered electrons varies more from those of the non-scattered electrons, which enhances the phase contrast. However, too high defocus will limit the resolution and lead to formation of artefacts in the image. For biological specimens, the optimal focus to balance contrast and resolution is slightly under the perfect focus (underfocus).

The contrast transfer function (CTF) specifies the relative contrast of details in the image as a function of spatial frequency and depends on the spherical aberration of the objective lens defocus and electron energy. The CTF is defined in Fourier space, where images are represented by the spatial frequencies they contain. The Fourier principle says that any periodical function can be divided into the infinite addition of sines and cosines, and thus has a unique representation in Fourier space. Therefore, the transformation to Fourier space is very useful for image processing.

1.2.3 Preparation of biological specimens for electron microscopy

Biological specimens typically contain high water contents (up to 90% of the specimen). Since the column of the microscope is under high vacuum and the specimens are exposed to a high voltage electron beam, a biological specimen would be completely destroyed if it would not be treated so its water content is eliminated or immobilized. Therefore, biological samples for TEM have to be fixed.

The traditional method of preparation consists of chemical fixation followed by staining with heavy metals, dehydration with organic solvents and embedding with plastic or resin. After that the sample is sectioned into slices that are again stained with heavy metals to further increase their contrast. These treatments are very harsh for the sample and can cause artefacts and leakage of molecular components.

The cryo-fixation was introduced at the end of the eighties to overcome these problems, and has revolutionized the biological electron microscopy world (Adrian *et al.* 1984; Dubochet *et al.* 1988). With this method the sample is vitrified and stays hydrated. Thus, structures are kept in a close-to native state conditions and do not suffer any further chemical treatment. To achieve specimen vitrification the sample is rapidly frozen in cooled liquid ethane to a temperature of ca. -180°C. Fast freezing avoids the formation of ice crystals that would expand and destroy the sample and the formation of hexagonal ice that would lead to unwanted electron diffraction. Instead, in vitrification the water is transformed into glass-like ice of amorphous consistency, similar to the consistency of liquids but with a very high viscosity (**Figure 8**). In addition, the low temperature has a cryo-protecting effect that reduces the radiation damage caused by the electron beam during imaging in TEM. On the other hand, samples thicker than ~10 µm cannot be properly vitrified with the above described method. For thicker specimens, alternative methods like high pressure freezing and subsequent sectioning of the frozen-hydrated specimens at ca. -140 to -160°C have been recently developed (CEMOVIS; Al-Amoudi *et al.* 2004).

1.2.4 Cryo electron microscopy

Once vitrified, the samples are stored in liquid nitrogen (-196°C). The samples are inserted into the column inside a cryo-holder. This type of holder can be cooled with liquid nitrogen and is able to keep the specimen at ca. -180°C. Once the sample is introduced, it is important to keep the electron dose applied as low as possible to avoid sample damage. Since there is no staining with heavy metals, the contrast of the vitrified sample is low and it comes just from the specimen material. Biological specimens are composed mainly of hydrogen, carbon, oxygen, phosphorus, nitrogen and sulphur. These are soft materials that produce low contrast compared to heavier elements (e.g. gold).

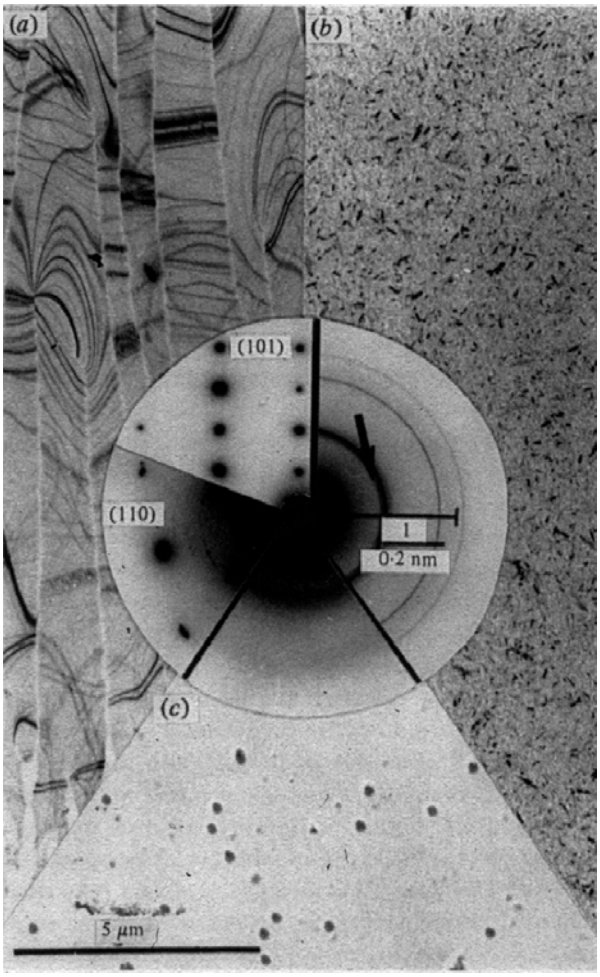

Figure 8. Typical images and diffraction patterns of different types of ice. (a) Hexagonal ice. It is a 60 nm thick layer. The dots in the diffractograms indicate a crystalline organization (101,110). (b) Cubic ice, obtained after heating up a layer of vitrified ice. The arrow indicates the presence of some hexagonal ice. It is a layer of 70 nm thickness. (c) Vitrified ice. The layer has 70 nm thickness. The polystyrene beads added for the focusing are visible. All images were taken at a magnification of 7500x (Dubochet *et al.* 1988).

1.2.5 Cryo electron tomography

Tomography is a technique that allows the generation of three-dimensional (3D) volumes of objects (tomograms). When combined with cryo-EM, it is referred to as cryo electron tomography (cryo-ET). ET is based on the principle discovered by Radon in 1917, which describes how a tomogram can be formed from the different projection images of an object. This principle was later on developed and was finally put into practice in 1968 (De Rosier 1968). By cryo-ET it is possible to obtain tomograms of a wide range of biological specimens, from cells to molecules, allowing the study of the function–structure relation of such specimens (Lucic *et al.* 2005). Specifically, cryo-ET allows the observation of

details from the surface and the interior of an object that cannot be detected in single projections using the same total electron dose (**Figure 9**). The details are better isolated and recognized in tomography while in 2D, structures can overlap and be obscured by another object. The resolution of a cryo-electron tomogram is typically in the order of ~5 nm.

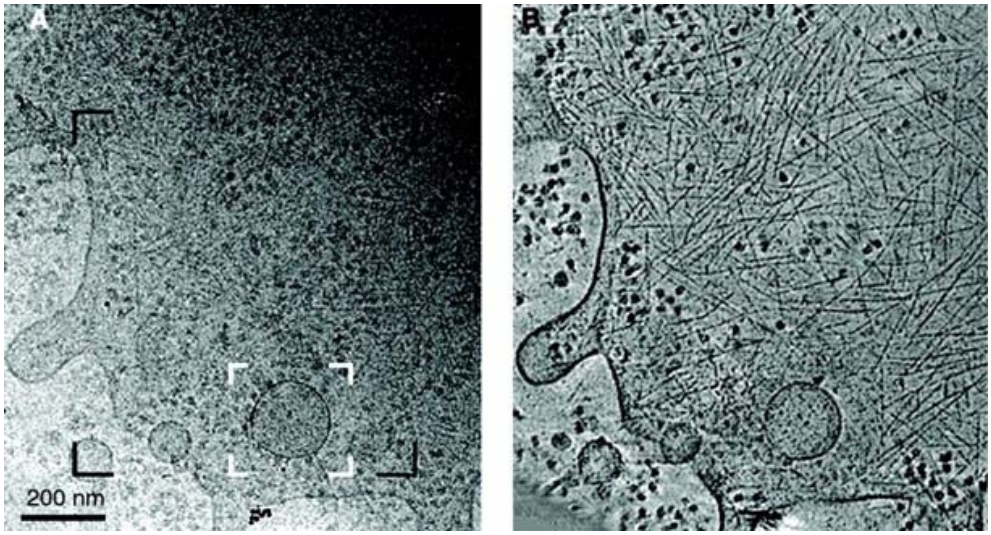

Figure 9. Periphery region of a Dictyostelium cell analyzed by cryo-ET. (A) Electron micrograph presenting the projection image of the object. (B) Slice extracted from the volume of the tomogram in 3D taken in the same area as in (A). In (B) the actin filaments and other cellular complexes are visible in much more detail (Medalia *et al.* 2002).

1.2.5.1 Tilt series acquisition

The procedure consists of recording a series of electron micrographs from a specimen at different angles (**Figure 10, left**). There are two fundamental requirements for tomogram acquisition: the object of interest has to stay inside the field of view during all the image acquisition and all the micrographs have to be taken at the same magnification and under similar defocus values and electron dose. To obtain the projection images of the sample at different angles, the sample holder is rotated around its axis perpendicular to the electron beam. The specimen holder and the goniometer performing the rotation are not mechanically perfect and after tilting there are usually shifts of the object of interest in

the field of view. It is therefore necessary to readjust these shifts by centering the object in the field of view.

Manual adjustments take a lot of time and electron dose, thus automatic procedures for data acquisition have been developed (Koster *et al.* 1992; Dierksen 1993). The automatic acquisition follows three different steps: focusing, tracking and exposure. Focusing compensates for the defocus changes occurring when the specimen is tilted. (Koster 1989). The defocus is determined by comparison of two images acquired at different beam tilt angles. Tracking corrects the shifts of the specimen compared to the previous tilt angle. For this an image with very low electron dose is recorded and compared to an image of the same area taken at a previous tilt angle. Exposure is the acquisition of the final image. Typically, the areas of focusing and tracking are distant from the exposure area to minimize the radiation damage in the area of interest.

1.2.5.2 Three-dimensional reconstruction

To reconstruct the 3D volume from the projection images, it is first necessary to align all the projections with respect to each other and then combine them to create the volume (**Figure 10**). The alignment compensates for the remaining small shifts of the specimen inside the field of view. It can be done with markers or by cross-correlation. The markers are small, electron dense particles added evenly to the sample. Usually, colloidal gold particles are used but also quantum dots have been recently applied as markers for vitreous sections (Masich *et al.* 2006; Gruska *et al.* 2008). The coordinates of the markers are located for every projection image manually or automatically. The reconstruction of the tomogram is done once the alignment is defined. The way how the 3D information is recovered from the images in 2D can be explained in Fourier space: the Fourier transform of a projection corresponds to a central slice in the Fourier space of the visualized object. Thus, projections from different directions will sample different parts of the Fourier representation of the object. The way of reconstruction most commonly used in ET is weighted back-projection. In this method the projections are projected back to obtain the 3D volume. A simple back-projection will lead to an artificial intensification of the low

frequencies, which makes it necessary to apply a weighting that eliminates this effect in Fourier space (Harauz G. 1986).

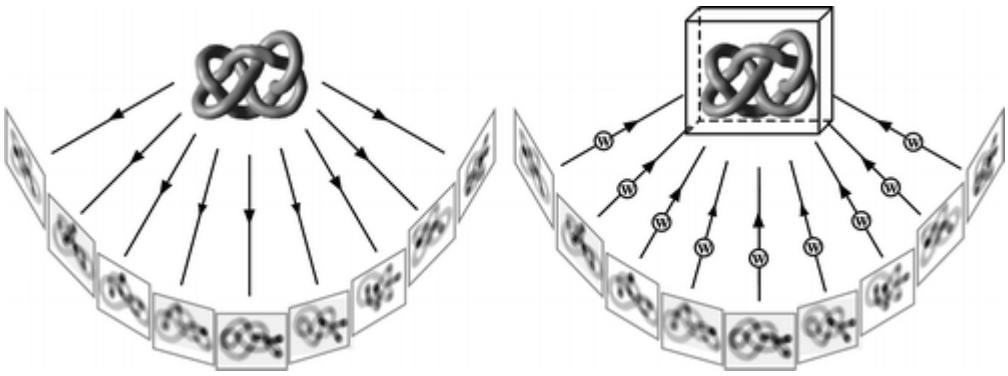

Figure 10. Tomography principle. Left: projection images from an object at different angles are collected. Right: The three-dimensional reconstruction is obtained by backprojection (Lucic *et al.* 2005).

1.2.5.3 Limitations due to electron exposure

The biggest limitation in cryo-ET is the damage induced in the sample when exposed to the electron beam. In chemically fixed and heavy metal treated samples the dose that can be applied is much higher than in cryo-samples. When a cryo specimen is exposed it suffers a modification due to ionization and formation of free radicals. Although these processes are not temperature dependent the resulting damage, loss of mass and the diffusion of free radicals are temperature dependent (Lucic *et al.* 2005). Therefore, the electron dose must be kept under the critical limit where the sample starts to degrade. As a consequence the contrast is lower than in the chemically fixed samples, where one can apply a higher total dose. Typically, the total dose tolerable by a cryo specimen is around 60-80 $e^-/Å^2$, but depends on the specimen and must be determined experimentally. The better specimen preservation achieved with a lower total dose must be balanced against the lower signal to noise ratio (and thus resolution) of the acquired images.

Thicker specimens (e.g. cells) will scatter and absorb more of the electron beam. For these specimens, a high acceleration voltage (300 KeV) is needed because of its larger penetration depth.

1.2.5.4 Limitations due to the missing wedge

There is a limitation for the data acquisition in tomography due to the specimen holder design. The tilt range cannot be larger than ± 70 degrees. This obstructs the visualization of certain regions in the object. The information inside the non sampled part of Fourier space is lost (missing wedge) so the reconstruction of the object cannot be complete (for a whole reconstruction of an object it would be necessary to tilt ± 90 degrees) (**Figure 11**). Due to the missing wedge, the resolution of the tomogram is direction dependent (anisotropic). Objects can appear elongated in the direction of the electron beam and some structures remain unresolved (**Figure 11**). The acquisition of tomograms by double tilt acquisition schemes can minimize this effect. In this case two tomograms of the same object are taken, rotating the sample 90 degrees in the horizontal plane after acquiring the first one. This has to be done with the same total dose available, i.e. either the tilt increments have to be bigger in both series, or the electron dose spent per image has to be reduced.

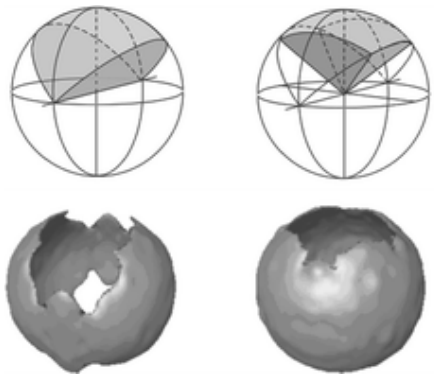

Tilt range	Single	Double
±70°	78%	93%
±60°	67%	84%
±45°	50%	67%

Figure 11. Sampling coverage by single and double axis tilting. The scheme above shows the volume parts that are not sampled in Fourier space. In the case of single tilting there is a missing wedge (left) and in the double tilting a missing pyramid (right). The objects below are simulated reconstructions of an object (a hollow sphere) as they would appear with the tilting scheme above. The table shows the percentages of Fourier space covered by each tilting type for different angles (Lucic *et al.* 2005).

2 Aim of the study

The aim of this study was the structural analysis of crucial aspects in the interactions of Herpes simplex virus 1 (HSV-1) with its host by cryo electron tomography (cryo-ET). This poses a technical and histological challenge, since hitherto virus-cell interactions had not been studied directly in a native state by cryo-ET. This would allow gaining three-dimensional structural and functional insights at the level of macromolecular complexes. The particular focus of the project was on the following aspects:

1) Interaction of viral structures with molecular motors and cytoskeletal elements of the host allowing for directional capsid transport: The aim was to visualize the sites of capsid-tegument and motor protein interactions during intracellular transport of capsids both *in vivo* and *in vitro* and thus gain structural information of the molecular complexes involved in transport. To achieve this, several eukaryotic cellular host systems needed to be tested, established and optimized for flat growth on electron microscopy grids to allow for cryo-ET imaging. Time lapse-fluorescence microscopy needed to be used to determine the time point of maximal intracellular virus transport.

2) Association of capsids with the nuclear pore complexes and release of the viral DNA into the nucleus: Direct *in situ* capsid binding to the nuclear pores by cellular cryo-ET is not possible due to the inherent thickness limit in cryo-ET. Therefore, there was a need to establish a suited subcellular investigation system that would allow studying capsid attachment to nuclear pores by cryo-ET. Once such a subsystem compatible with the technical requirements of cryo-ET would be found, co-factor requirements for capsid attachment had to be tested.

3) Secondary envelopment of capsids in neurons and release of virions from the host cell: The aim was to structurally analyze the secondary envelopment of HSV-1 inside cells in native preserved conditions and to contribute to the ongoing discussion whether secondary envelopment occurs before or after axonal transport of particles. Secondary envelopment of HSV-1 typically occurs in cell areas too thick for cryo-ET. Therefore, cellular systems allowing imaging these sites needed to be explored. This would include neuronal cells, the most native system, which would provide a particular challenge as it involves primary cell cultures. Furthermore analysis of exit sites was performed. This largely neglected process involves membrane fusion and its analysis provided first mechanistic insights. This was of particular interest since the virus can be used as marker for the exocytotic event. It was needed to explore and analyze suitable cellular models for the structural analysis of secondary envelopment.

4) Morphology and formation of L-particles: L-particles have been previously analyzed isolated or in chemically fixed cells and only in 2D. Therefore, there was a need to study them in 3D and analyze their assembly in comparison to virion formation *in situ* by cryo-ET. This would contribute to a more accurate description of the L-particle morphology and would help to better understand the mechanisms of virion formation.

Beyond the immediate interest in the pathogen–host interaction these topics aimed to reveal general principles of cellular functions using the virus as probe.

3 Material and methods

3.1 Cell culture

3.1.1 Cell lines, media and supplements

Several cell lines were cultured and tested for cryo-ET (**Table V**).

Table V: List of cell lines, media and supplements.

Cell line	Origin of the cell line	Medium	Medium supplements
Hippocampal neurons	Rat hippocampus (provided by Frank Radtke, MPI Neurobiology, Germany)	HSM, NBM	1:50 B27 (Gibco) + 1:400 L-glutamin (Invitrogen; only for NBM)
DRG neurons	Rat dorsal root ganglia (provided by Frank Radtke, MPI Neurobiology, Germany)	NBM	1:50 B27 (Gibco) + 1:400 L-glutamin (Invitrogen)
Ptk2	Epithelial kidney cells from *Potorous tridactylis* (CCL-56, ATTC)	MEM	100 U/ml Penicillin + 100 µg/ ml streptomycin + 10% FBS
HeLa	Human cancerous cells from cervix (CCL-2, ATTC)	MEM	100 U/ml Penicillin + 100 µg/ ml streptomycin + 10% FBS
Vero	Epithelial kidney cells from african green monkey (CCL-81, ATTC)	D-MEM	100 U/ml Penicillin + 100 µg/ ml streptomycin + 10% FBS
BHK-21	Baby hamster kidney fibroblasts provided by Beate Sodeik, Hannover Medical School, Germany)	MEM	100 U/ml Penicillin + 100 µg/ ml streptomycin + 10% FBS
MEF-Cdc42	Mouse embryo fibroblasts (provided by Reinhard Fässler, MPI Biochemistry, Germany)	D-MEM	100 U/ml Penicillin + 100 µg/ ml streptomycin + 10% FBS
HFF	Human foreskin fibroblasts (provided by Prashant Desay, Baltimore university, USA)	MEM	100 U/ml Penicillin + 100 µg/ ml streptomycin + 10% FBS

- HSM: horse serum medium (16050130; Gibco)
- NBM: neurobasal medium (21103049; Gibco)
- D-MEM: Dubleccos modified eagle medium (31966; Gibco)
- MEM: alpha-minimum essential medium (11900; Gibco). Added 5% $NaHCO_3$
- FBS: foetal bovine serum (Sigma-Aldrich)

3.1.2 Procedures for the cell culture

All non-neuronal cell lines were cultivated as follows: after thawing, cells were incubated at 37°C with an atmosphere of 5% CO_2 in culture flasks for 2-3 days in their respective medium (see **3.1.1**) until they formed a confluent monolayer covering the entire surface of the flask bottom. The medium was then removed and cells were washed with PBS and detached from the surface with Trypsin-EDTA (Gibco). Cells were either subcultivated into new flasks to continue dividing or frozen and stored in liquid nitrogen. The medium used for the freezing contained 20% FCS + 10% DMSO (Gibco).

3.2 Virus preparation

3.2.1 Viruses

The following viruses were used during the experiments:

- wt HSV-1 strain 17+ (Prashant Desai, Baltimore University, USA)

- wt HSV-1 strain KOS (Beate Sodeik, Hannover Medical School, Germany)

- VP26-GFP-HSV-1 (Prashant Desai, Baltimore University, USA)(Desai *et al.* 1998)

- ts-B27-HSV-1 (Prashant Desai, Baltimore University, USA)(Desai *et al.* 1998)

3.2.2 Procedures for viral preparation

- Infection: BHK, Vero or HFF cells were cultured until they reached 90-95% confluency. Viruses were diluted in CO_2 independent medium (Gibco) + 20 mM Hepes (pH 7) (Sigma) + 0.1% BSA (Sigma). The medium was removed from the flasks, they were washed with PBS and HSV-1 was added with a multiplicity of infection (MOI) of 0.003-0.01. The bottles were left on a rocking platform at room temperature for 1 hour. Medium was added and the flasks were incubated at 37°C, 5% CO_2 until 95% of the cells were rounded and 80% detached from the surface when knocking the flask. This usually occurred after 2-3 days for both wt and mutant.

-Virus harvest: after knocking the flasks the medium was collected into 50 ml Falcon tubes and centrifuged to pellet down the cellular material (3500 xg, 20 min, 4°C). The pellet containing the cellular material was frozen for later purification of nuclear capsids. The supernatant was centrifuged (21500 xg, 90 min, 4°C) and the pellet containing the virions was resuspended in MNT buffer (20 mM MES, 100 mM NaCl, 30 mM Tris, pH 7.4) for 1-2 days at 4°C. To further soften and detach, the pellet was carefully pipetted up and down.
- Gradient purification: The gradient was prepared in tubes for the SW28 rotor (Ultraclear, Beckmann) as follows: tubes were half filled with 10% Nycodenz in MNT buffer and then 40% nycodenz in MNT buffer was carefully underlayed using a syringe with a long needle until the interphase was at half height of the tube. The gradient was prepared in a gradient master (BioComp Instruments, Fredericton, New Brunswick, Canada) according to manufacturer´s instructions.
The diluted viral pellet was applied to the top of the gradient and centrifuged (72000 xg, 105 min). The band containing the virions was collected, frozen in liquid nitrogen and stored at -80°C.

3.2.3 Plaque tritation

The MOI of a viral preparation was determined by a plaque assay. Vero cells were cultured in 6 well plates until they covered the plate surface completely. A dilution series of the virus inocula was done as in **Table VI**.

Table VI: Dilution series for HSV-1 plaque assay.

Control	1200 µl RPMI / 0.1% BSA	500 µl/well
10^{-2}	1485 µl RPMI/BSA + 15 µl virus	500 µl/well
10^{-3}	1080 µl RPMI/BSA + 120 µl 10^{-2}	500 µl/well
10^{-4}	1080 µl RPMI/BSA + 120 µl 10^{-3}	500 µl/well
10^{-5}	1080 µl RPMI/BSA + 120 µl 10^{-4}	500 µl/well
10^{-6}	1080 µl RPMI/BSA + 120 µl 10^{-5}	500 µl/well
10^{-7}	1080 µl RPMI/BSA + 120 µl 10^{-6}	500 µl/well
10^{-8}	1080 µl RPMI/BSA + 120 µl 10^{-7}	500 µl/well
10^{-9}	1080 µl RPMI/BSA + 120 µl 10^{-8}	500 µl/well

Cells were washed with 2 ml RPMI/BSA per well and 500 µl of each dilution was added for each well. The plates were shacked at room temperature for 1 hour. Afterwards the medium containing the viruses was removed and substituted by 2 ml medium with 20 µg/ml IgG per well. The plates were incubated for 2-3 days at 37°C and 5% CO_2 until there was plaque formation. The medium was then removed and cells were fixed with 37% formaldehyde diluted 1:4 in PBS. After 10 minutes, the formaldehyde was removed and the plates were dried at room temperature for 10-20 minutes. Cells were stained with 0.1 % crystal violet in 2% ethanol for 10 minutes. The stain solution was removed and wells were rinsed with distilled water and let dry. The plaques were counted and the PFU/ml was determined.

3.3 Sample preparation for electron microscopy

3.3.1 Vitrification

3.3.1.1 Cells grown on grids

Once the cells had reached the desired state for observation they were vitrified. 1-2 µl of 10 nm colloidal gold in PBS/BSA was added to serve as fiducial markers for tomogram alignment. The grids were placed in special tweezers that can be mounted into the vitrification device (designed and produced by Rudolf Gatz; MPI of Biochemsitry, Germany). The excess of liquid was removed with a filter paper (Watmann) by slightly pressing it towards the back side of the grid for 2-3 seconds. The tweezers were then fast released into cooled liquid ethane (-180 °C). After that the grid was rapidly transferred into liquid nitrogen (-196 °C) and stored.

3.3.1.2 Specimens in suspension

A droplet of 4-5 µl sample in suspension is added to 200 mesh copper grids with holey carbon support film (Cu R2/1 200 mesh, Quantifoil) or copper grids 200 mesh with lacy carbon support film. Colloidal gold is added and sample is vitrified as described in **3.3.1.1.**

3.3.1.3 Spread *Xenopus laevis* oocyte nuclei

After spreading and washing the nucleus on a Cu Quantifoil grid, Colloidal gold is added and sample is vitrified as described in **3.3.1.1.**

3.3.2 Negative stain

To rapidly check samples in the electron microscope (excluding cells), negative stain was used. A droplet of 3-5 µl sample was applied to a grid with continuous carbon film. A droplet of 1 % uranyl acetate was put on the sample and was incubated for one minute at room temperature (RT). The drop was blotted from the side and grid was dried at RT.

3.4 Study of HSV-1 'life' cycle *in situ* by cryo-ET

3.4.1 Non-neuronal cell lines

For the observation of cells in cryo-ET, 200 mesh gold grids with holey carbon support film were used (Au R2/1, Quantifoil). They were treated on a plasma cleaner for 30 seconds to make them more hydrophilic and then floated on a drop of fibronectin overnight (dilution 1:100 of 1 mg/ml fibronectin in PBS) to make the surface of the grid adherent for the cells. On the next day grids were placed in medium for some hours on a Petri dish and then transferred to a new dish with fresh medium. After trypsin treatment, the cells were pipetted over the grids to allow them to attach and spread. This incubation lasted for 1-2 days (37°, 5% CO_2) until the cells were flat enough to be observed by cryo-EM. Once ready the cells were infected with HSV-1 with an MOI of 100 by adding the virus inocula directly to the medium. They were incubated at 37 °C and 5% CO_2 the time necessary to observe the different stages of the infection (see **3.7**). After that they were vitrified (see **3.3.1.1**).

To study transport right after entry, the Petri dish containing the non-neuronal cells was cooled on ice. After adding the viral inocula to the medium, cells were incubated for 2 hours on ice to allow the virions to attach to the cell surface. At 4°C virions can attach to

the cell but were not able to enter (Sodeik *et al.* 1997; Maurer *et al.* 2008). Grids were then transferred to 37°C and 5% CO_2 and incubated for 5-10 minutes before vitrification.

3.4.2 Neurons

Primary rat neurons were isolated and dissociated before each experiment (kindly provided by Boyan Garvalov and Liane Meyn, MPI of Neurobiology, Germany). There was no cell culture since neurons do not divide. For the observation of cells in cryo-ET, 200 mesh gold grids with holey carbon support film were used (Au R2/1, Quantifoil; C-flat).

3.4.2.1 Hippocampal neurons cultivation

Grids and Petri dishes were sterilized under UV light for 15 minutes. A poly-L-lysine solution of 1 mg/ml in Borate buffer (1.24 g boric acid + 1.9 g borax in 400 ml distilled water, pH=8.5) was prepared and filtered through a 0.22 μm filter (Millex). The filtered solution was carefully spread over the grids to be incubated over night. On the next day grids were repeatedly washed with distilled water and covered by horse serum medium (**Table V**). They were incubated for one day and then the medium was exchanged for neurobasal medium. After that the neurons were added to the grids (120.000 neurons per 60 mm diameter Petri dish, 6 grids per Petri dish) and incubated (37° C, 5% CO_2) for 7 days. In this time the neurons could adhere and developed axons and dendrites. They were then infected with HSV-1 with an MOI of 100 and, after incubation at 37°C and 5% CO_2 for the time necessary to reach a specific stage of infection (see **3.7**), they were cryo-fixed (see **3.3.1.1**). Due to the sensitivity of neurons to any external manipulation including temperature shifts, the 2 hours incubation at 4°C for attachment of virions to the cells was avoided.

3.4.2.2 DRG neurons cultivation

After treatment of the grids with poly-L-lysine (see **3.4.2.1**), and washing with distilled water, the grids were treated with laminin (Roche, 0.5 mg/ml) diluted 1:10 in neurobasal medium and incubated for 1 hour at 37°C. After that the DRG neurons were pipetted over the grids (120000 cells per 60 mm diameter Petri dish, 6 grids per Petri dish). After incubation (37° C, 5% CO_2) during 5-6 days they were infected with HSV-1 at an MOI of

100. They were then incubated at 37°C and 5% CO_2 the time necessary to observe the desired stage of infection (see **3.7**) and vitrified (see **3.3.1.1**).

3.5 *In vitro* study of capsid-tegument-motor interactions

3.5.1 Materials

- HSV-1 virions (wt strain KOS, VP26-GFP)
- 50 µl *Xenopus laevis* egg extract (provided by Thomas Mayer, MPI of Biochemistry).
- MKT-buffer: 20 mM MES, 100 mM KCl, 30 mM Tris, pH 7.4
- 2x lysis-buffer (2% TX-100 in 2x MKT, pH 7.4) with either 200, 1000 or 2000 mM KCl
- 20% sucrose (w/v) in MKT with either 100, 500, 1000 mM KCl
- 30% sucrose (w/v) in acetate-buffer, pH 7.4, adjusted with KOH
- 1 M DTT stock
- 10 mg/ml DNase II (Sigma) in PBS
- 10 mg/ml Rnase (Roche) in PBS
- 10 mg/ml BSA in MKT
- BRB80: 80 mM PIPES, 1 mM EGTA, 2 mM $MgCl_2$. pH 6.8 with KOH
- TNE-buffer: 0.-5 M NaCl, 1 mM EDTA, 20 mM Tris-HCl, pH 7.5
- Acetate-buffer: 100 mM potassiumacetate, 3 mM magnesiumacetate, 5mM EGTA, 10 mM HEPES +/- 5% (w/v) Sucrose; pH 7.4 with KOH
- 20x E-Mix: 150 mM Creatinphosphat, 20 mM ATP, 2 mM EGTA, 20 mM $MgCl_2$, pH 7.7
- 2000 U/ml Hexokinase (Roche) in 2x Acetate-buffer and 50% Glycerin
- 1 M $MgCl_2$ stock
- Protease inhibitors (PIs): 500x AEL (Sigma), 500x ABP (Sigma), 250x PMSF (Sigma)
- 1 M D-Glucose-stock (Sigma)
- 20 mg/ml BSA in Acetate-buffer (for supplementing cytosol)
- 25 mM Nocodazol (Sigma) (diluted in DMSO)
- Tubulin (provided by Beate Sodeik, Hannover medical school, Germany)
- 4 mM Taxol (Sigma)
- 100 mM GTP

3.5.2 Capsid detegumentation

This method is based on a previous study (Wolfstein *et al.* 2006).

100 µl virions of 10^9 PFU/ml were mixed with the same amount of 2x lysis buffer with 200, 1000 or 2000 mM KCl so that the viral envelopes are lysed by the detergents and the tegument is partially removed by the high salt concentration. PIs and 10 mM DTT were also added. The mix was incubated at 4°C for 30 min and the ultracentrifuge tubes for the SW 50.1 rotor were blocked meanwhile for 10 min with 10 mg/ml BSA. The capsids were pelleted through a 5 ml 20 % sucrose cushion with the respective salt concentration and 10 mM DTT (30 min, 84000 xg, 4°C). The pellet was incubated overnight at 4°C together with 200 µl BRB80 with 10 mM DTT, 10 mM $MgCl_2$ and PIs and sonicated.

A 5 µl aliquot was applied directly to a copper grids 200 mesh with lacy carbon support film grid, previously treated in a plasma-cleaner for 10 seconds and vitrified (see **3.3.1.2**). For experiments involving incubation of capsids together with molecular motors, RNAse and DNAse II were added to the pellet to a final concentration of 100 µg/ml and incubated at 37 °C for 30 minutes. Capsids were then sedimented (Airfuge ultracentrifuge, Beckman A-100-30 rotor, 77500 rpm, 8 min, RT) and resuspended in 70 µl cytosol that contained a high concentration of molecular motors (see **3.5.3**). For direct observation of such capsids, the pellet was resuspended in 70 µl BRB80 and vitrified (see **3.3.1.2**).

3.5.3 Cytosol preparation from *Xenopus laevis* egg extract

Xenopus laevis egg extract with a protein concentration of 22 mg/ml was used for the isolation of cytosol. It was diluted 1:5 in acetate buffer with 5% sucrose and 5 µl E-mix. This stock could be frozen at -80°C and used later for capsid binding to the NPCs (**3.6**). For the attachment of motors to capsids the cytosol was clarified by centrifugation (Airfuge, A-100-30 rotor, 30 min, 85200 rpm, RT) and the supernatant was diluted 1:10 in acetate buffer with 5% sucrose and had a final concentration of the following materials: 20 U Hexoquinase, 10 mM glucose, 10 mM $MgCl_2$, 10 mM DTT +100 µg/ml DNAse, 100 µg/ml RNAse, 50 µM Nocodazol, 1 mg/ml BSA and PIs.

3.5.4 Immunogold labeling of dynein

To check for attachment of molecular motors to detegumented capsids, capsids incubated with cytosol as described in **3.5.2** were mixed with 5% BSA in PBS and incubated for 5 minutes at 4°C. Then 3 µl of the mixture were placed over a continuous carbon film grid and after 1 minute at room temperature were blotted from the side. For blocking, a drop with 0.15% BSA in PBS was added and blotted from the side (repeated twice). A drop with 10 µg/ml primary antibody (anti-mouse dynein intermediate chain, MAB1618, Chemicon) with 0.15% BSA in PBS was added and incubated for 30 minutes in a wet chamber. After blotting from the side the grid was washed with drops of 0.15% BSA in PBS (repeated three times). Then the grid was incubated for one hour with a secondary antibody coupled to gold (GAM IgG 6 nm gold, Aurion) diluted 1:20 with 1% BSA in PBS. After incubation the grid was washed three times with 0.15% BSA in PBS, two times with distilled water and was prepared by negative stain as described in **3.3.2.** Control grids were prepared by following the same procedure but without prior incubation of capsids with cytosol.

3.5.5 Attachment of capsids to motors and microtubules

To form microtubules 2 µl of tubulin were polymerized by adding 4 µl BRB80, 1.5 mM GTP, 30 µM taxol and incubating the mix for 30 minutes at 37°C. The microtubules were afterwards diluted 1:30 in BRB80, 1.5 mM GTP, 30 µM taxol.

A 4 µl aliquot of the so polymerized microtubules was added to the EM grid and incubated for 3 minutes to allow attachment. Afterwards, 4 µl of detegumented capsids (500 mM KCl, see **3.5.2**) and cytosol were added. The mixture incubated on the grid at RT for 10 minutes. After that the specimen was vitrified (see **3.3.1.2**).

3.6 *In vitro* system for the attachment of capsids to nuclear pores

3.6.1 Isolation and cryo-ET of mammalian nuclei

Vero cells were harvested from one confluent cell culture flask by washing them 3 times with ice-cold 1x PBS and cell scraping. The cells were pelleted at 400 xg for 5 min and resuspended in 2 ml of LSB buffer. The cells were then lysed with 20 strokes in a Dounce homogenizer and the nuclei were pelleted at 750 xg for 5 min and resuspended in 1 ml of LSB buffer supplemented with 100 µg/ml RNAseII and DNAse. After 30 minutes incubation at 37°C the nuclei were pelleted at 750 xg and resuspended in 5 ml LSB buffer. A 5 µl drop was applied to a grid with a holey carbon support film (Quantifoil) and vitrified (see **3.3.1.2**).

3.6.2 Isolation of nuclei from *Xenopus laevis* oocytes

Stage V oocytes were extracted from *Xenopus Laevis* frog ovaries (kindly provided by Valentin Stein, MPI Neurobiology, Martinsried, Germany). For the nuclei extraction they had to be of good quality and not older than 5 days after operation (during this time they were kept at 18°C). A good oocyte was characterized by its clear separation between the black and the white pole of the egg. Eggs were incubated at room temperature in LSB buffer (10 mM HEPES pH 7.5, 1 mM KCl, 0.5 mM $MgCl_2$) and 1 µl PIs for 15 minutes. The hypotonic buffer caused the oocyte to swell. The oocyte was then punctuated with sharp tweezers at the rim between the black and the white halfs, the membrane was spread, and once the transparent appearing nucleus was isolated it was carefully moved to a Petri dish with fresh LSB buffer. The isolated nuclei could be kept intact for a couple of hours at 17-22°C.

3.6.3 Preparation of capsids and cytosol

Partially detegumented capsids were prepared as described in **3.5.2**. This time 2x lysis buffer with 1000 mM NaCl was used. The pellet containing the capsids was dissolved in 20 µl acetate buffer. To test the best concentration of cytosol for attachment, capsids

isolated from VP26-GFP-HSV-1 virions were incubated with 8-10 isolated *Xenopus* nuclei in the presence of 120 µl of 220, 22, 2.2, 0.22 or 0.022 µg/ml cytosol diluted in acetate buffer (preparation in **3.5.3**). After 30 minutes incubation at RT the nuclei were washed by gently pipetting up and down in acetate buffer and the nuclear rim was observed by fluorescence microscopy. Importin ß and ATP were also tested to see if this could improve attachment of capsids.

3.6.4 Preparation of capsids attached to *Xenopus laevis* nuclei for cryo-ET

For the cryo-ET experiments 120 µl of cytosol with a concentration of 0.22 µg/ml supplemented with 0.3 µM importin-ß were mixed. 8 µl of capsids and 8-10 isolated nuclei were added and incubated at room temperature during 30 minutes. Holey carbon support films (Quantifoil) on copper grids were treated in the plasma cleaner for 30 seconds and placed in a pair of tweezers. After the incubation with the capsids and the cytosol, the nucleus was transferred to the grid with a cut pipette tip and spread with very sharp glass tipped capillaries (Word Precision instruments). The nuclear membrane was washed three times by adding 6µl acetate buffer and the excess of liquid was blotted with a filter paper from the side. At the end 2 µl of 10 nm colloidal gold in PBS/BSA was added and the grid was vitrified (see **3.3.1.3**).

3.6.5 Labeling of capsid DNA with ethidium bromide

To label the viral DNA, VP26-GFP capsids isolated as in **3.6.3** were incubated with 20 µg/ml ethidium bromide (EtBr) for 45 minutes at 37°C and then centrifuged through a sucrose cushion with 500 mM NaCl. The pellet was resuspended in 20 µl acetate buffer.

3.7 Light and fluorescence microscopy

To determine the time points of infection in cells and to test capsid attachment to isolated nuclei, VP26-GFP-HSV-1 virions were used (kindly provided by Phrasant Desai)(Desai *et al.* 1998). The cells were cultivated on a Petri dish modified with a glass

bottom or on an IBIDI slide. Once the cells were ready, they were infected with an MOI of 100 and incubated at 37°C and 5% CO_2 for different times.

For life cell imaging an Axiovert 200M (Zeiss) fluorescence microscope equipped with a CCD camera (AxioCam HRm; Zeiss) was used. The microscope was controlled by the software Axiovision 4.1 (Zeiss). The temperature and amount of CO_2 in the atmosphere was controlled by means of a chamber around the microscope (EMBL workshop). Imaging was done at 37°C and 5% CO_2 with the 63x and 100x oil objectives. Two different types of experiments were performed:

- Long time-lapse experiments: They were used to determine the time points for the different stages of infection. The area to study was selected and the microscope was then programmed to take a phase contrast image of the area followed by a fluorescence image, every hour for 21-24 hours.

- Short time-lapse experiments: They were used to observe the transport of single viral particles during a certain period of time. The area to study was selected by searching for active transport and a phase image was acquired. The microscope was then programmed to take a fluorescence image every 1-3 seconds for 3-10 minutes.

After the experiment, the phase and fluorescent images were superimposed.

For verifying capsid attachment to nuclear pores, capsids were isolated from VP26-GFP-HSV-1 and incubated with isolated nuclei (**3.6**) before observation by fluorescence microscopy.

3.8 Transmission electron microscopy

All the tomograms were obtained on a Phillips CM300 or on a FEI Polara transmission electron microscope. Both microscopes were equipped with a field emission gun (FEG) operated at 300 KeV acceleration voltage, an energy filter with a CCD camera (Gatan GIF 2002) of 2048x2084 pixels. In the case of the Phillips CM300 a conventional cryo-holder (model 626, Gatan) was used. In the case of the Polara a multi-specimen holder was used. It can contain six grids at the same time inside cartridges that are inserted in the column

of the microscope with an insertion holder, all at cryo temperatures (-180°C). The cryo temperature was obtained by cooling the holder with liquid nitrogen.

The tilt series were usually acquired from -60° to 60°, and tilt increments of 2-3°. The defocus was set to values between -8 µm and -12 µm with an accuracy of ± 500 nm. The pixel size of the acquired images was 0.68 nm (CM300) and 0.805 nm (Polara).

3.9 Image processing

3.9.1 Tomogram reconstruction

Tilted images were aligned respective to each other and tomograms were either reconstructed with the TOM-Package software (Nickell *et al.* 2005), a part of the program MATLAB (The MathWorks Inc.), or the software IMOD (Kremer *et al.* 1996). The volume of the reconstructions for visualization was typically 512x512x256 pixels, after the images obtained in the microscope (2048x2048 pixels) were binned twice. Visualization and further processing of the tomograms was done with the EM software (Hegerl 1996) and Bsoft (Heymann *et al.* 2007). Surface visualization in 3D was done with the program Amira (TGS Inc., Bourdeaux, France). To remove noise from the tomograms anisotropic diffusion algorithms were used (Frangakis *et al.* 2001).

3.9.2 Subtomogram acquisition of capsids and averaging

The procedures used for the subtomogram extraction and averaging of subtomograms were from Bsoft. In detail, the capsids were picked with the procedure *bshow* from unbinned tomograms. The subvolumes were extracted with the procedure *bpick* and had a size of 180x180x180 pixels. The orientation of the particles against a reference was found with the procedure *bfind* and the oriented particles were averaged with *badd*. Icosahedral symmetry was applied to the averages with *bsym*. After applying symmetry the new average was used as a reference and several iterations of refinement were performed.

The resolution of the averages was determined by Fourier Shell Correlation (FSC), 0.5 criterion (Stewart *et al.* 1999). Here particles are divided randomly into two data sets and the averages of both sets are compared.

3.9.3 Vertex classification

Capsid vertex classification was done with the program JSubtomo (developed by Juha Huiskonen, Martinsried). Vertexes were divided into five parts going from the centre of the penton towards the centre of the neighbouring hexon, giving 60 different volume parts and orientations per capsid. These volumes were classified into two classes: with or without extra density. For the class 1 a template with extra density was used (result of the average of all capsids from the same group of detegumented particles before classification) and for the class 2 a template without extra density (result of the manual removal of the extra density). The templates were masked so that only one fifth of a penton was visible. To correlate the fifths of a vertex with each template the command *jsubtomo* was used (mode refine). Then the difference between the cross-correlation values for class 1 and 2 was calculated and, in the case of detegumented capsids, only the 50% of the particles with higher cross-correlation values against one of the templates was selected to obtain a finer average of both classes. After averaging, the particles from each class were masked to one fifth of a penton (FOP) and several iterations of refinement and classification were performed. To form the whole vertex average C5 symmetry was applied to the masked average.

3.9.4 Difference mapping

To be able to calculate the difference map of two averages it was necessary to set them to the same resolution level (*bfilter*) and to scale them to the same gray values with Bsoft (*bar*). The difference of densities was then calculated (*bop*).

4 Results

4.1 Study of cell lines for cryo electron tomography

To enable the analysis of HSV-1 infection directly inside cells by cryo-ET, it is first necessary to determine which cell lines are suitable for this approach. For our cryo-ET studies, whole cells vitrified by plunging are used (see **3.3.1.1**). Since cryo-ET is limited to areas with a maximal thickness of ~1µm (Lucic *et al.* 2005), only adherent cells that are thin enough in some areas after freezing can be used.

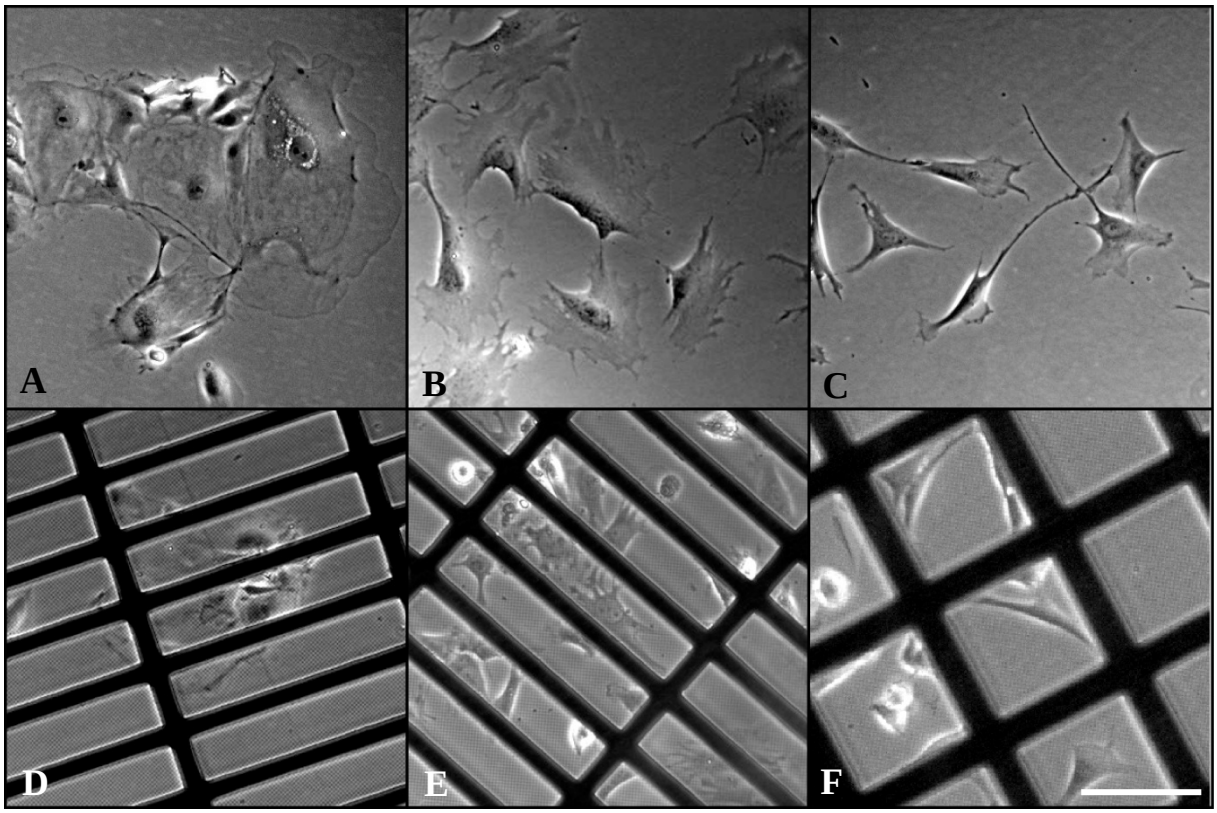

Figure 12. Non-neuronal adherent cell lines suitable for cryo-ET. Cells cultured on a Petri dish (A, B, C) or on a holey carbon support film (Au Quantifoil) (D, E, F). (A, D) Ptk2 cells. (B, E) Mouse embryo fibroblasts (MEF) cells. (C, F) Human foreskin fibroblast (HFF) cells. Bar: 200 µm.

The cell lines used for the tests are listed in **3.1.1, Table V.** All cell lines were found to grow better on gold grids (Au Quantifoil, Au C-flat) than on copper grids. The coating of the carbon support film on Au grids with fibronectin was tested to see whether the

attachment and spreading of the non-neuronal cells would be improved. This was not the case. Neither the amount of cells able to attach to the grid nor the spreading and flatness of the cells was improved. Since the addition of a coating might also interfere with the quality of the vitrified ice, the best approach for culture of non-neuronal cell lines on grids was using holey carbon support film gold grids without any coating. Cells appeared flattest after one day incubation at 37°C and 5% CO_2. The cell line found to be more suitable for cryo-ET due to its flatness was Ptk2. The HFF and MEF cells were also flat enough in many areas and also suitable for cryo-ET, but not as much as Ptk2 (**Figure 12**). Cellular parts closer to the nucleus were always too thick to be visualized. Only the rims of cells were flat enough and thin filopodia were most suitable.

Since the natural hosts of HSV-1 in humans are neurons, they were the first choice. This required the use of primary cells rather than stable cell lines. Rat dorsal root ganglia (DRG) neurons were tested but the amount of cells found on the grids was low and the suitable areas for microscopy were rare due to the notable thickness of the samples. Therefore, events of the HSV-1 replication cycle in DRGs by cryo-ET could not be observed. On the other hand, in rat hippocampal neurons it was likewise not possible to image the cell body with cryo-ET due to its thickness, but axons and axon terminals were often thin enough. Furthermore, these cells developed axons more easily on the grid than DRGs. Consequently, the final experiments for the observation of the HSV-1 'life' cycle were performed with hippocampal neurons.

4.2 Early studies with HSV-1 infection of non-neuronal cell lines

In the first experiments, Ptk2 and MEF cell lines were used to study retrograde transport during HSV-1 entry. After adding the virions and incubation at 4°C for 2 hours, samples were warmed to 37°C for 5-10 minutes and then vitrified. Despite numerous attempts, only a total number of five viral particles (inside an endosome or as a cytosolic capsid) were found inside epithelial cells vitrified 5-10 minutes p.i.. The reason why these events were so rarely observed was probably that once the virus enters the cell, the transport towards the nucleus occurs very rapidly. Therefore, it was difficult to observe capsids in the peripheral areas suitable for tomography.

4.3 Viral particle interactions with molecular motors and cytoskeleton during transport

Viral-host interactions were studied in rat hippocampal neurons. Therefore, it was necessary to determine the optimal growth of isolated hippocampal neurons concerning two criteria: flatness of the axon and infectivity. For this purpose, neurons were grown on IBIDI slides for different amount of days and both flatness and infectivity were tested. When neurons were grown for 4 days, they presented undeveloped axons and when infected with VP26-GFP-HSV-1 with an MOI of 50, the amount of intracellular capsids observed was small. In contrary, hippocampal neurons grown for 7 days on IBIDI slides showed higher axonal development (long and thin axons) and a substantial increase of intracellular capsid transport. Neurons grown for 14 days had a very high development of axons and dendrites, which formed a very dense network. 14 days old neurons showed a very good infectivity, but when grown on holey carbon support Au grids, vitrified and observed by cryo-EM, the tight network of axons and dendrites appeared too electron-dense. Therefore, the final experiments were done with neurons grown for 7 days.

4.3.1 Determining time-points of infection by fluorescence microscopy

To determine the time course of infection, fluorescence microscopy experiments in hippocampal neurons infected with VP26-GFP-HSV-1 were performed. Rat hippocampal neurons grown on IBIDI slides for 7 days were infected at an MOI of 50. With the long time-lapse experiments (one image per hour), it was observed that capsids reached the nuclei of the cells at 3 hours p.i. and newly produced viral particles were transported along the axons from 15 to 24 hours p.i.. After 24 hours p.i. there was still production of viruses but many cells were dying. The production of viruses had its peak at around 16 hours p.i.. (**Figure 13**).

At this time point, short time-lapse experiments were performed by collecting images of an area every 3 seconds. The particles did not move constantly towards one direction inside the axons but rather shifted directions quite frequently. Anyhow, a predominant tendency for transport towards the cell periphery was observed 16 hours p.i..

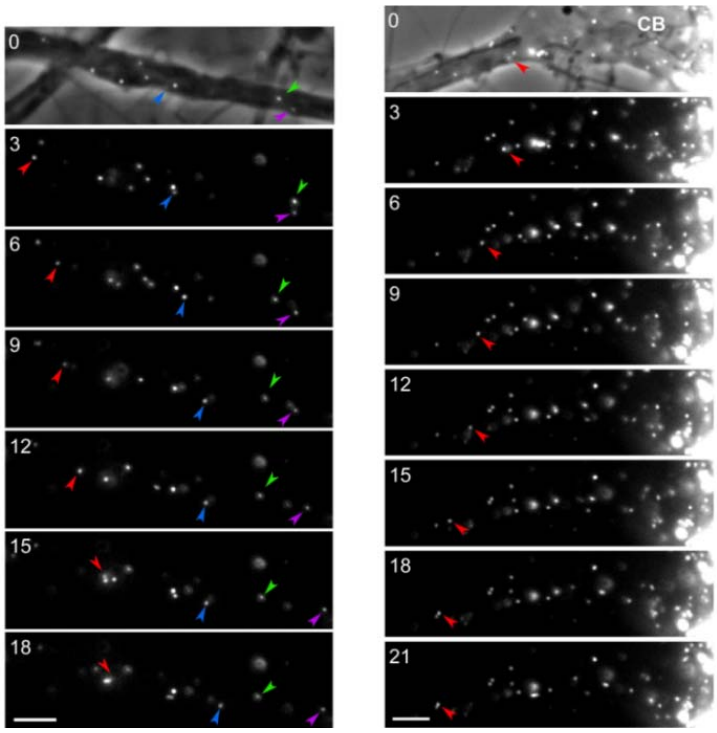

Figure 13: Short time-lapse experiments in hippocampal neurons infected with GFP-VP26-HSV-1. The fluorescence images were taken 16 hours p.i. in 3 seconds intervals. Bright field images (top) were taken to show the shape of the cell and axons. An axon with viral particles in a mid-axon region (left column) and an axon near the cell body (right column). Arrows show the position of the viral particles. CB: cell body. Bar: 2 µm.

4.3.2 Cryo-ET of transport of HSV-1 in hippocampal neurons

Hippocampal neurons grown for 7 days on holey carbon support films on Au grids were infected with wt HSV-1 strain KOS at an MOI of 50 and were vitrified at different times after infection depending on the type of experiment.

4.3.2.1 Transport of intracellular capsids

To study retrograde transport of capsids, cells were vitrified 5-10 minutes p.i.. The search of capsids was performed by following intact axons and visualizing them at low magnification and very high defocus (-100 µm). Once a spot suitable for tomography was found, a tilt series was collected from -60° to 60°, with an angular increment of 3°. The images had a final pixel size of 0.805 nm. The total electron dose received at the specimen level was kept between 60 and 90 electrons/A^2 and the exposure time was

adjusted to the tilt angles by a 1/cos scheme. The defocus applied was -12 µm to gain contrast and to be able to distinguish structures inside the cell. As in the case of non-neuronal cell lines, the amount of viral particles observed right after entry was very small. In this case, after many trials, one event of capsid transport was observed at 5-10 min p.i. in neurons (**Figure 14B, C).** Here a capsid was found inside an axon close to the axon terminal. After 3D-reconstruction, a high number of microtubules inside the axons and the actin network, as well as other cellular structures, became visible. Electron-dense material seemed to connect the capsid with the adjacent microtubule (**Figure 14C**). Actin was always present in varicosities, while it did not appear in other areas of the axon, apart from the axon terminal.

Anterograde transport of cytosolic capsids was observed in neurons vitrified 16 hours p.i.. These events were much more frequently observed than retrograde transport events (**Figure 14D-G)**. Fully assembled capsids (cytosolic C-capsids), usually in groups of at least two capsids per field of view, were observed inside axons at 16 hours p.i.. Capsids without DNA (cytosolic A- and B-capsids, the latter contained the scaffold protein) were also found, although less frequently. Like after entry, capsids were usually found in proximity to microtubules and in some cases electron-dense material was detected in between.

4.3.2.2 Transport of intracellular virions

Besides non-enveloped capsids (**Figure 14**), Enveloped virions inside membranous compartments and close to microtubules were visualized in middle regions of axons (varicosities) (**Figure 15**). Typically there was only one virion inside a compartment. Occasionally, they were found in areas close to other vesicles associated to glycoproteins or clathtrin. No densities resembling molecular motor complexes could be detected binding to the viral membranous compartments, but smaller densities were very often observed associated to the outer side of the compartment.

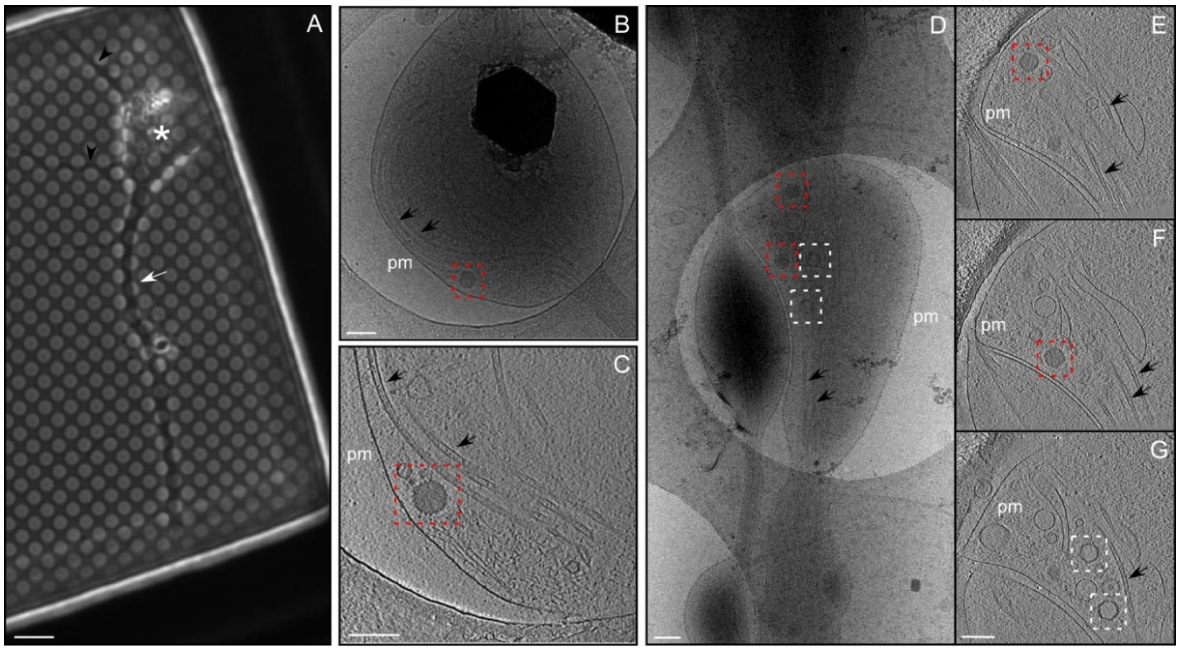

Figure 14. Transport of HSV-1 capsids in neurons during entry and egress. (A) Hippocampal neuron grown on a holey carbon support film. Axon: white arrow; dendrites: black arrow heads; cell body is marked by an asterisk; bar: 6 µm. (B) Projection image of an axon vitrified 5 minutes p.i.. Bar: 200 nm. (C) Slice through the 3D-volume obtained in the same area as (B). Electron-dense material is located attached to the capsid (framed in red) and in contact with the neighbouring microtubule. An actin network is situated at the periphery of the axon region (likely a varicosity). Bar: 200nm. (D) Projection image of an axon at 16 h p.i.. Cytosolic C-capsids are framed in red and cytosolic A-capsids in white. (E–G) Slices through the tomogram taken at the area shown in (D). pm: plasma membrane; black arrows: microtubules; bars: 200 nm.

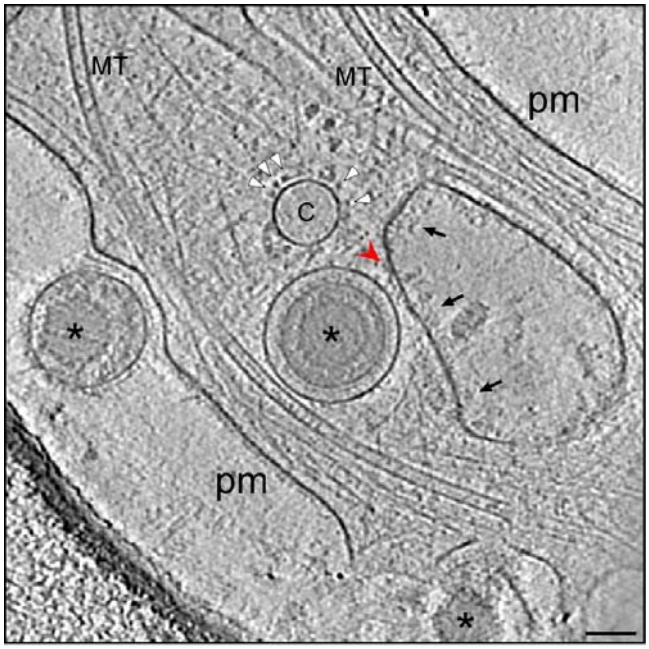

Figure 15. Transport and exit of enveloped cytoplasmic virions in an axonal varicosity. Slice of a tomogram where a virion is visible inside a membranous compartment in the cytoplasm close to a microtubule. Another virion that just had exited the cell is observed in the same field of view. A coated vesicle and a vesicle associated with glycoprotein-like structures (arrows, red arrow head) appear close to the transported virion. White arrow heads: coat; C: coated vesicle; pm: plasma membrane; MT: microtubule; bar: 100 nm.

4.3.3 Capsid-tegument-motor interactions during transport in neurons

To visualize the interactions between capsid and tegument and (if possible) molecular motors during egress in neurons, cryo-ET and subtomogram averaging of 48 cytosolic C-capsids (containing DNA) during anterograde transport was performed. The averaged 3D structure (**Figure 16D**) had a resolution of 6.9 nm resolution (FSC=0.5 criteria).

To study which densities correspond to tegument, the average was compared to nuclear capsids, in particular to C-capsids isolated from infected nuclei. These capsids are thought to be free of tegument. Therefore, cryo-ET and subtomogram averaging was applied on 143 isolated nuclear C-capsids. An average with a resolution of 5.6 nm was obtained (**Figure 16B**). Cryo-ET and subtomogram averaging was also applied to 158 nuclear A-capsids isolated from neurons (**Figure 16A**). The nuclear C-capsids were used for comparison to the capsids found inside neurons, since these presented a small extra density located at the hexons surrounding the vertices that probably corresponds to the minor capsid protein UL25 (Ogasawara *et al.* 2001). This protein is present in substantially lower amounts in A-capsids (Trus *et al.* 2007). This way, the difference of densities between the control (nuclear C-capsid average) and the capsids from neurons would only be tegument. There were clear differences between the transported cytosolic capsids and isolated nuclear C-capsids. Extra density was found at the vertices of the average of transported cytosolic C-capsids. It was mainly present over the pentons and connecting further to the two adjacent triplexes (Tc and Ta in nomenclature of Zhou *et al.* (1994) marked in **Figure 16 A3**) and to one side of the neighbouring hexons (**Figure 16D, Figure 17**). The rest of the hexons did not have significant extra density attached. The transported cytosolic C-capsid average appears larger than the averages of nuclear capsids.

The procedure described above was repeated for 26 ‘defective’ capsids (without DNA and partially with scaffolding protein) found inside axons during anterograde transport, to see if there were any differences with the cytosolic C-capsids found during egress. The average was resolved to 9.7 nm resolution (**Figure 16C**). Extra density was observed by comparison with nuclear C-capsids at the side of the hexons surrounding the vertices that connected to the triplexes adjacent to the penton (Ta). Surprisingly, the amount of extra

density in 'defective' capsids from neurons was much smaller than in cytosolic C-capsids from neurons and the pentons did not present any extra density on top (**Figure 17**). The channel of the penton seemed to be empty in comparison to the capsids that were filled with DNA (nuclear C-capsids and cytosolic C-capsids from neurons). The small extra densities were only detected at the hexons surrounding the vertices while the rest of the capsid contained no extra density.

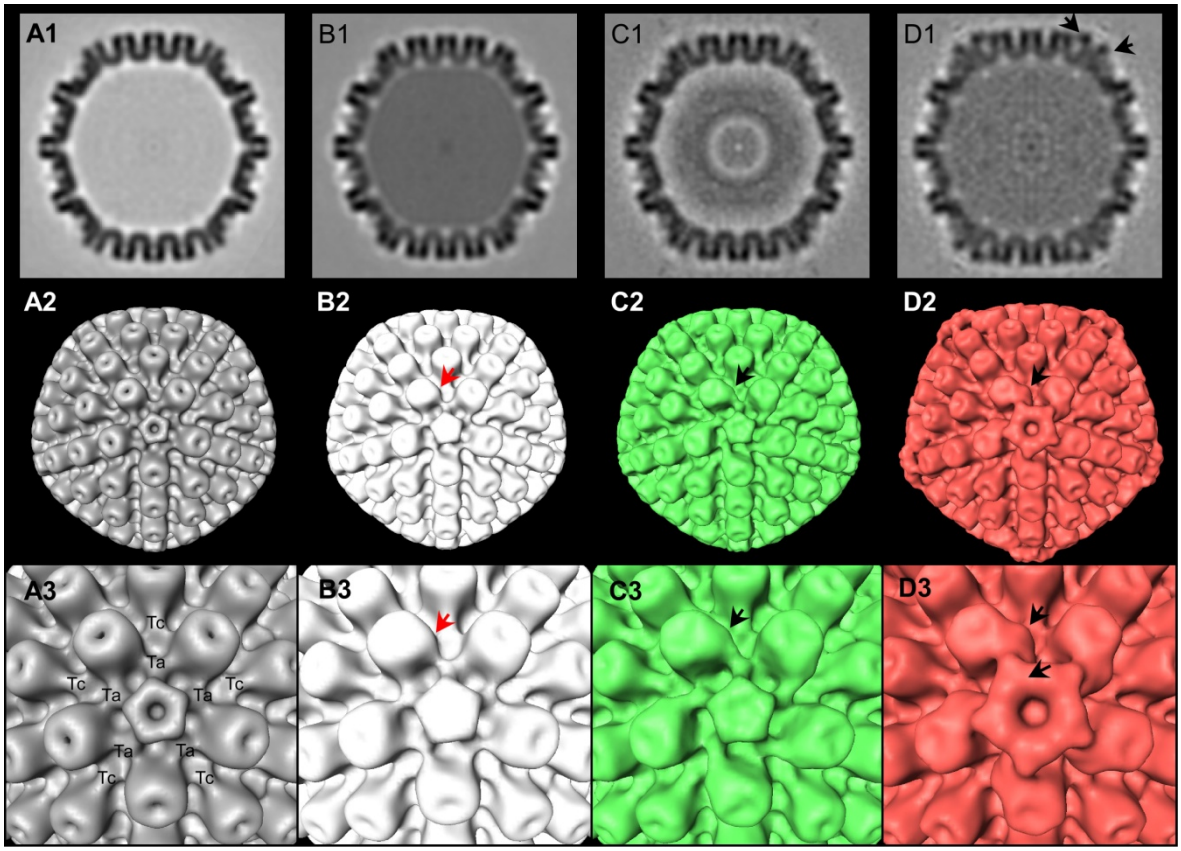

Figure 16. Averages of (A) isolated nuclear A-capsids, (B) isolated nuclear C-capsids, (C) cytosolic 'defective' capsids and (D) cytosolic C-capsids. (A1-D1) Middle slice of the volumes in their original orientation. The electron-dense material visible inside the capsid shell in (B1) and (D1) corresponds to DNA. In (C1) it corresponds likely to the scaffolding protein. (A2-D2) Isosurface representation of the averages. (A3-D3) Close-up view of a single vertex. Isolated nuclear A-capsids do not present tegumentation in the vertices. Isolated nuclear C-capsids have a small extra density (red arrow) at the right side of the hexons that surround the penton. Cytosolic 'defective' capsids have more extra density than nuclear C-capsids (black arrow), also at the right side of the hexons that surround the penton, but also connecting to the adjacent triplexes (Ta). Cytosolic C-capsids present big amounts of extra density (black arrows) on top of the pentons, connecting to the right side of the neighboring hexons and to the adjacent triplexes (Ta, Tc). Icosahedral symmetry has been applied on the averages.

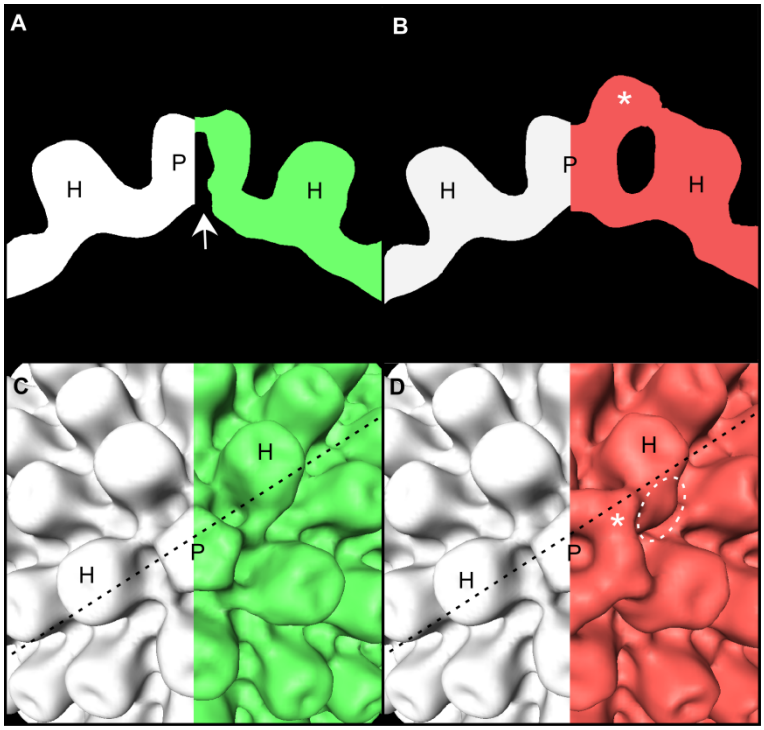

Figure 17. Side by side comparison between nuclear C-capsid average (white) and the averages from transported cytosolic C-capsids (red) and 'defective' capsids (green). (A, B) Surface cuts along one vertex. (C, D) Close-up view of a vertex. Dashed lines show where the surface cut was made. Extra density is clearly observed in cytosolic C-capsids, going from the top of the pentons (asterisk) towards the neighboring hexons (surrounded by dashed circle). 'Defective' capsids have a small extra density located at the right side of the hexons and the pentons do not have any extra density attached. The channel of the penton is open (white arrow). H: hexon. P: penton.

4.3.4 Vertex classification of intracellular capsids in neurons

The average of transported 'defective' and cytosolic C-capsids showed that the extra density was located at the vertices. Next, to know if these densities are homogeneously distributed throughout all vertices or if they rather appear only in some of them, classification was applied. By classifying the vertices into 'tegumented' and 'not tegumented' it is possible to know more about the distribution of the tegument. In case the number of vertices without tegument was high enough to influence the average, a more defined structure of the tegument would be obtained after classification.

Therefore, subtomogram classification of the 'defective' and cytosolic C-capsids was performed. The template for the class-1 (with tegument) came from the unmodified average of all capsids. The template for the class-2 (without tegument) came from the

modification of the average of all capsids by manual deletion of the extra densities located at the vertices. A mask was created which, after applied to the averages of the capsids before classification, masked away the whole capsid except one fifth of a penton. Therefore, the templates used for classification of the capsid subtomograms were only one fifth of a penton (**Figure 18**).

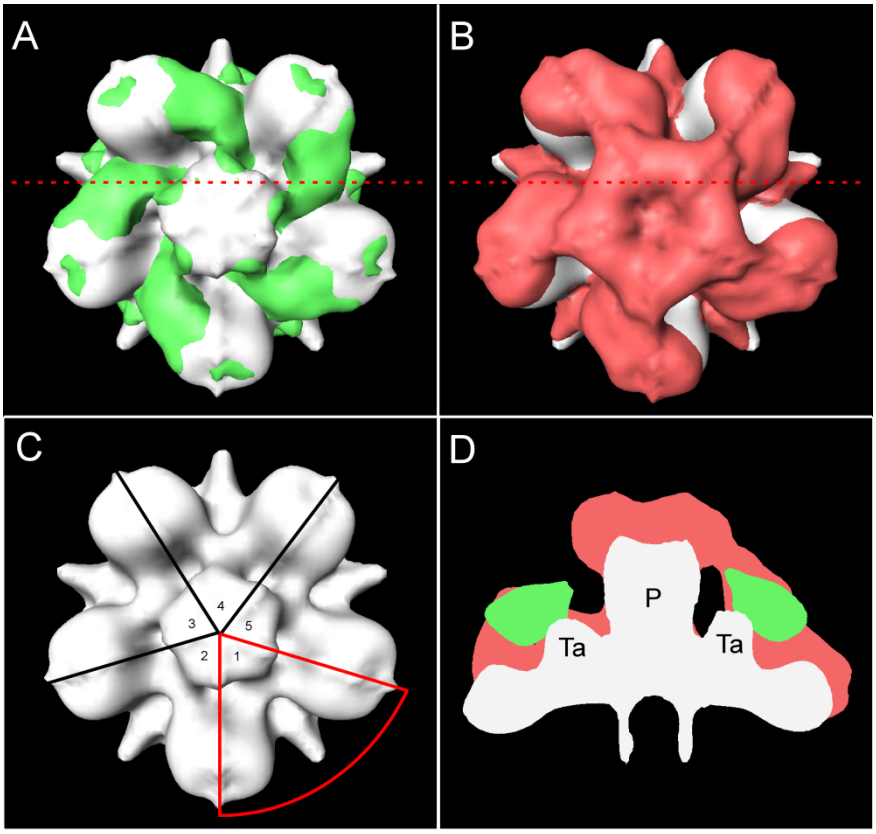

Figure 18. Classification of vertices in cytosolic capsids found inside neurons. In (C) the division of a vertex into five equal parts is represented. Divisions go from the middle of the penton towards the middle of the neighboring hexon. Templates for classification are one fifth of a vertex (C, framed in red). In (A) and (B) the nuclear C-capsid average (white) is superimposed with the class-1 averages of 'defective' (A, green) and cytosolic C-capsids (B, red). (D) Surface cut of the volumes along the direction indicated by dashed lines in (A) and (B). In (A), (B) and (D) 5-fold symmetry is applied to the 'one fifth'. P: penton; Ta: adjacent triplex.

Since every capsid has 12 vertices and every vertex can be divided into five parts (by creating divisions that go from the middle of the penton towards the middle region of the neighbouring hexons), there was a total of 60 fifths of a penton ('one fifths') subtomograms that could be extracted per capsid. The reason why only a fifth of a

penton was used as template was to be more selective in the classification, since it could be that for the same vertex the tegument is not equally distributed throughout all the neighbouring hexons (5/5), but it attaches with a ratio of 1/5, 2/5, 3/5 or 4/5.

This way, each 'one fifth' was classified as being with (class-1) or without tegument (class-2). After every iteration the subtomograms for every class were extracted and averaged. This process was repeated for three iterations.

4.3.4.1 Vertex classification of transported cytosolic C-capsids

The classification of the vertices of cytosolic C-capsids showed that almost all extracted subvolumes (91%) had a higher cross-correlation value with the class-1 template (with tegument). Subsequently, the comparison to nuclear C-capsids of the average of all subvolumes selected in class-1 showed a similar additional density than before classification (**Figure 18B, D**).

4.3.4.2 Vertex classification of transported 'defective' capsids

For the 26 'defective' capsids, about half of the extracted subvolumes showed a higher cross-correlation with the class-1 template and the other half with the class-2 template. That means that around 50% of the 'one fifths' had tegument attached. The average of the subvolumes had a resolution of 5.8 nm for both classes. The additional density in the class-1 was significantly bigger and more defined than in the average of all capsids without classification (**Figure 18A, D)**. The comparison between class-1 and nuclear C-capsids showed that class-1 had extra densities located at the right side of the hexons that surround the penton. This density connected to the triplexes adjacent to the penton. The penton presented a very small amount of extra density attached.

The distribution of class-1 and class-2 'one fifth' subvolumes was analyzed for 'defective' capsids to observe whether the tegument is randomly distributed over all vertices or it rather covers some of the vertices while others are empty. This assessment (**Figure 19**) showed that when all 'one fifth' subvolumes were analyzed, the majority of vertices presented 40 to 60% tegument coverage, i.e. 2/5 or 3/5 and when only the 50% 'one

fifths' with the higher cross-correlation values against one of the templates were analyzed, the distribution showed that most vertices had either small amount of tegument (20%) or relatively high amount (80%). The data shows that when all particles were taken into account, the distribution of tegument seemed to be random throughout all vertices, while when only the best particles were analyzed, vertices appeared either almost empty or with high amount of tegument. It is important to notice that including only the best 50% subvolumes can result in cases where this score is calculated on the basis of less than five 'one fifths' per vertex. In these cases, 3 out of 3 or 4 out of 4 coverage with tegument was considered as 100% coverage.

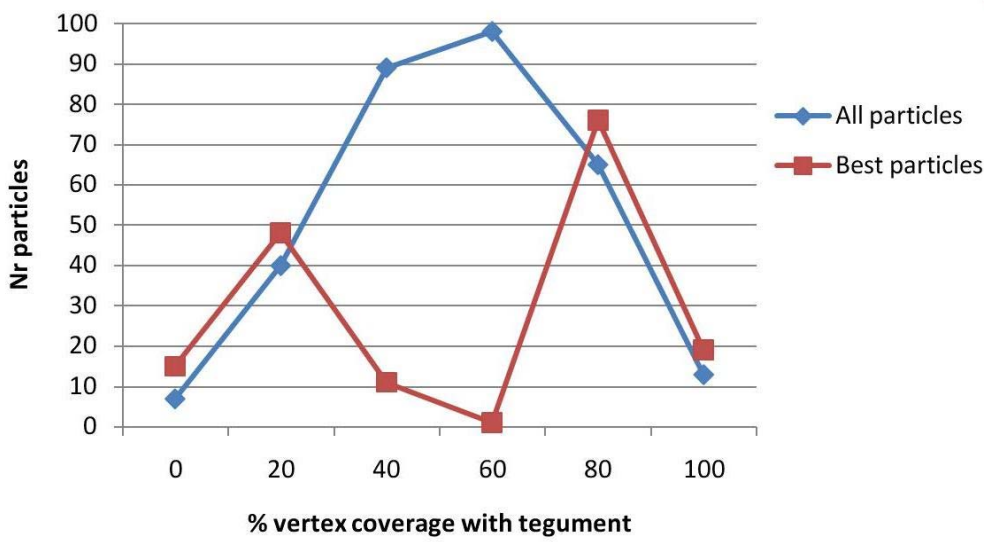

Figure 19. Tegument distribution within 'defective' capsids, when taking into account all particles or only the 50% best particles (higher cross-correlation values against one of the templates).

4.3.5 Capsid-tegument interactions *in vitro*

Since the number of capsids found inside neurons was limited, an *in vitro* system was used to obtain a higher resolution structure of the tegument. For this, capsids isolated from virions and detegumented by high salt concentration buffers were used. This treatment partially removed the tegument from virions but left some tegument proteins still attached to the capsid. Three different concentrations of high salt concentration buffers (100 mM, 500 mM and 1000 mM KCl) were used to detect density differences

between each group. ‘100 mM’ capsids are associated with most tegument proteins and ‘500 mM’ capsids are associated with more tegument proteins than ‘1000 mM’ capsids.

After capsid preparation, capsids were applied to an EM-grid and vitrified. Capsids had a high tendency to attach to the carbon film of the grid. Since the quality of the tomograms taken in the holes of the holey carbon film is better than the ones taken on carbon, grids with lacy carbon were used. These grids have a minimal carbon surface. Even if the sample was sonicated before applying it to the grid, in some cases the capsids aggregated and were sometimes surrounded by amorphous layers of electron-dense material most likely corresponding to clusters of tegument.

After collecting tilt series from -60° to 60° with an angular increment of 3°, subtomogram averaging was performed for every group of the salt-treated capsids. Only non-aggregated capsids present in holes of the carbon support film were selected. The ‘1000 mM’ capsid tilt series were obtained on a Phillips CM300 and on a FEI Polara electron microscope with different magnifications (final pixel size of 0.68 nm and 0.805 nm respectively). Therefore, all subtomograms coming from the CM300 were rescaled to the size of the Polara subvolumes. The microscopes were operated at 300 KeV, and the total electron dose applied for each tomogram was 60 e^-/A^2. The defocus applied was -8 µm. The data collection for the ‘100 mM’ and ‘500 mM’ capsids was performed on the FEI Polara microscope.

An average of 183 capsids, 246 capsids and 217 capsids was obtained from the ‘1000 mM’, ‘500 mM’ and ‘100 mM’ salt treated capsids, respectively. A difference map was then calculated between the averages of each group and the average of nuclear C-capsids (control) at a resolution of 5.6 nm (**Figure 20**). There were no significant differences observed between the ‘1000 mM’ average (**Figure 20A, D**) and the control. However, a clear difference in density was observed in one hand between the ‘500 mM’ average and the control (**Figure 20B, E**), and on the other hand between the ‘100 mM’ average and the control (**Figure 20C, F**). In both cases, the difference was located at the vertices and neighbouring hexons while the rest of hexons were free of extra density. The amount of extra density at the vertices and neighbouring hexons was bigger for the ‘100 mM’ average than for the ‘500 mM’ average. As in the case of cytosolic C-capsids found in

neurons, the extra density for the ‘500 mM’ average and for the ‘100 mM’ average was protruding from the side of the pentons to the right side of the neighbouring hexons.

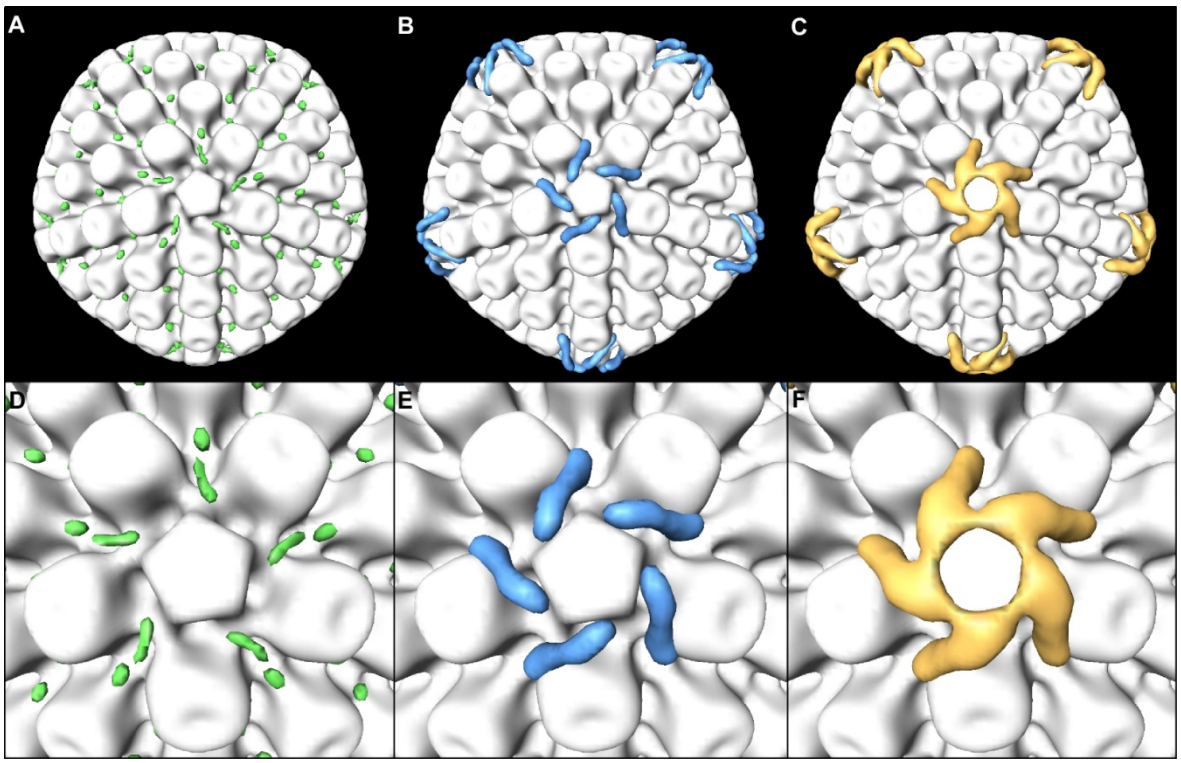

Figure 20. Isosurface visualization of the difference maps between the averages of salt treated capsids and nuclear C-capsids, superimposed with the average of nuclear C-capsids (white). (D-F) Close-up view of a vertex. Green: extra density present in the ‘1000 mM’ group. Blue: extra density present in the ‘500 mM’ group. Yellow: extra density present in the ‘100 mM’ group.

4.3.6 Vertex classification of *in vitro* detegumented capsids

As in the case of capsids found in neurons, the average of salt treated capsids showed that the remaining tegument locates at the vertices. To know the tegument distribution throughout the vertices and to get a more defined structure of the tegument density, vertex classification (as in **4.3.4**) was performed. Each group of subvolumes was classified into class-1 (with tegument) and class-2 (without tegument). The reference templates were again one fifth of a penton that came from the unmodified original average for class-1 (**4.3.5**) and from the average after manually deleting the extra densities for class-2. After each iteration, not all the subvolumes were averaged but only ~50% (the ones with higher cross-correlation values against one of the templates) (**Table VII**). The process

of classification was repeated for four iterations. In ‘1000 mM’ capsids, class-1 contained 45% of the subvolumes, while class-2 had only 13%. In ‘500 mM’ and ‘100 mM’, the subvolumes were equally distributed between class-1 and class-2.

The gold beads added before vitrification for subsequent alignment of the tomograms tended to stick to the capsids that were treated with 100 mM KCl, most probably due to the high amount of tegument still present in these capsids. Since the gold is highly electron-dense, it influenced the classification. To minimize this influence, a mask was applied to the ‘100 mM’ capsids to remove everything located further than away than 81 voxels distance (66 nm) from the centre of the capsids.

After classification (**Figure 21**), the tegument structure in the class-1 average (with tegument) was better defined than in the average of whole capsids without classification (**Figure 20**). The resolution was set to 4.2 nm for all averages to allow their comparison. The findings after classification for ‘1000 mM’, ‘500 mM’ and ‘100 mM’ capsids are summarized below:

- ‘1000 mM’ capsids: class-1 presented extra density located on top of the pentons. There was not significant extra density located at the neighbouring hexons of the penton but there was some at the adjacent triplexes Tc and Ta (**Figure 21 A2, A3**). Class-2 (without tegument) had a small extra density located at the right side of the neighbouring hexons (**Figure 21 A1**).

- ‘500 mM’ capsids: class-1 presented a large density on top of the pentons that connected to the right side of the neighbouring hexons and to the triplexes Tc and Ta (**Figure 21 B2, B3**). Class-2 did not present any clear extra density attached (**Figure 21 B1**).

- ‘100 mM’ capsids: class-1 presented extra density on top of the pentons that, as for the ‘500 mM’ capsids, connected to the right side of the neighbouring hexons and to triplexes Tc and Ta (**Figure 21 C2, C3**). Due to the mask for gold applied to the particles before averaging, the density appeared cut from the top. Class-2 average presented small extra densities that connected to the right side of the hexons surrounding the vertex and to the adjacent triplexes. The penton in class-2 was smaller than in nuclear C-capsids (**Figure 21 C1**).

Table VII: Distribution of the (~) 50% best subvolumes into classes after four iterations.

Salt concentration	Nr particles class-1 (with tegument)	Nr particles class-2 (without tegument)
1000 mM	4968 (45%)	1463 (13%)
500 mM	3711 (23%)	4465 (28%)
100 mM	2838 (23%)	3947 (32%)

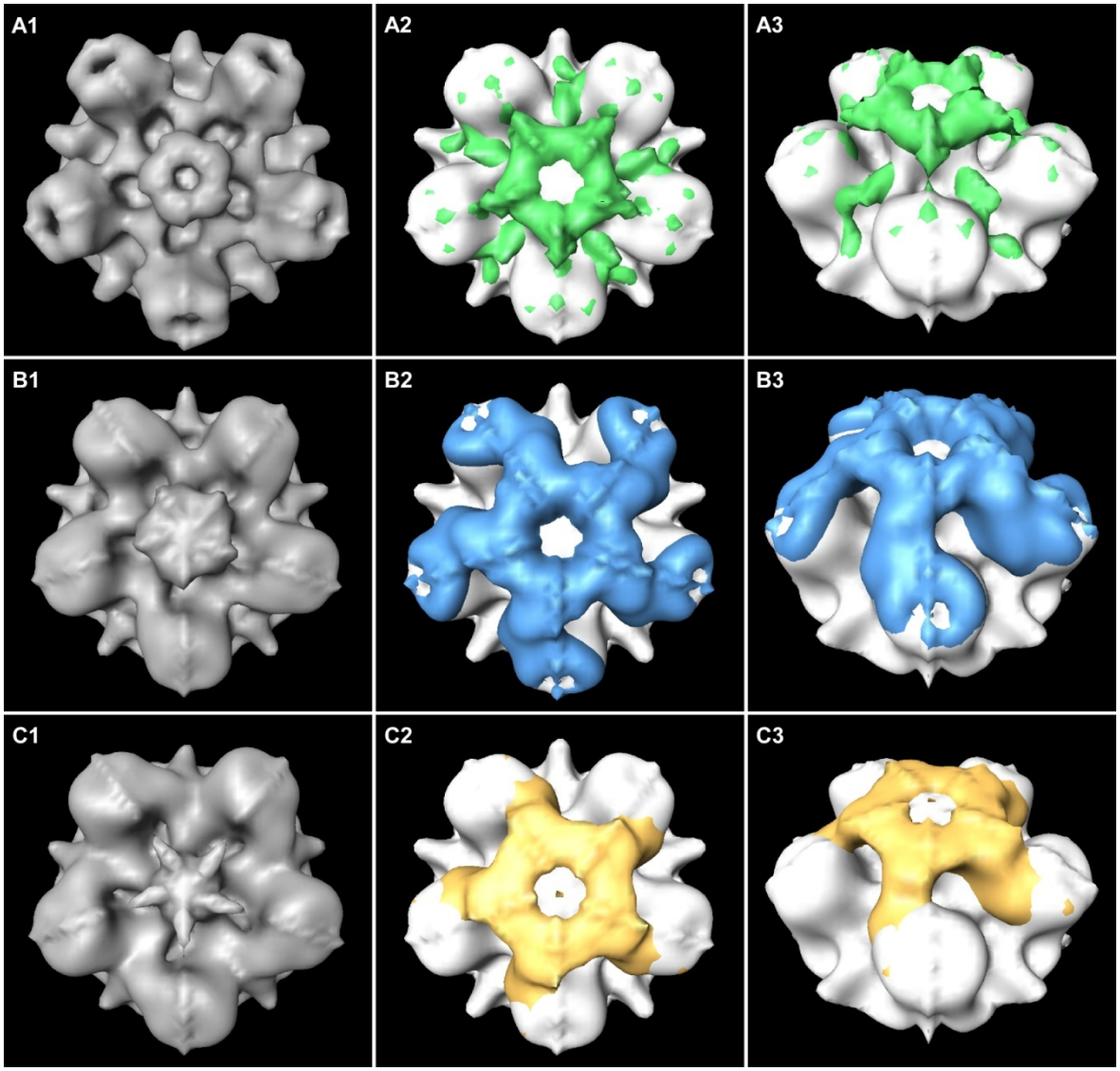

Figure 21. Classification of vertices for (A) 1000 mM, (B) 500 mM and (C) 100 mM KCl-treated capsids. (A1-C1) Class-2 average (without tegument). (A2-C2) Class-1 average (with tegument) superimposed to the average of C-capsids (white). (A3-C3) Rotation of the volume shown in (A2-C2) around a horizontal axis.

4.3.7 *In vitro* binding of capsids to molecular motors and microtubules

To study the interactions of molecular motors with HSV-1 detegumented capsids and microtubules *in vitro*, the first step was to see if there was attachment of isolated capsids to dynein by incubating 500 mM KCl treated capsids with *Xenopus laevis* oocyte cytosol and labeling with an anti-mouse dynein intermediate chain primary antibody and a secondary antibody coupled to gold. Control capsids (not incubated with cytosol) were also tested to see whether the labeling was specific. After applying negative stain, it was observed by EM that control capsids did not have gold labeling (**Figure 22B**), although sometimes gold beads were found on the carbon film. Capsids that were incubated with cytosol clearly showed labeling (8-15 gold beads per capsid) (**Figure 22C**), although densities attributed to molecular motors could not be detected by eye in the EM projection images.

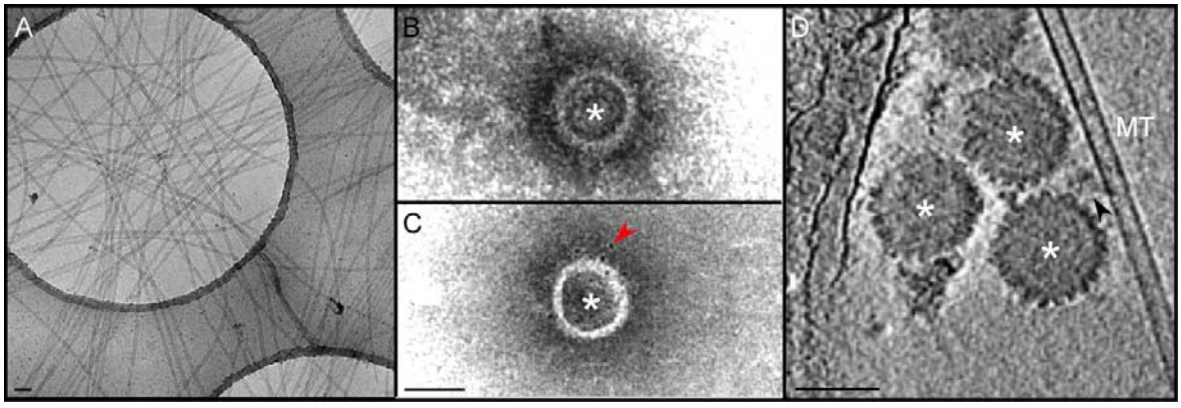

Figure 22. *In vitro* study of molecular motor binding to capsids and microtubules. (A) *In vitro* polymerized microtubules vitrified on a holey carbon support film. Immunogold-labeling of a control capsid (B) and of a capsid incubated with cytosol (C) in negative stain. A gold bead is pointed by the red arrow (D) Slice through a tomogram of vitrified detegumented capsids incubated with cytosol and *in vitro* polymerized microtubules. There is density located in between a capsid and the microtubule (black arrow). Capsids: marked with an asterisk; MT: microtubule; bars: 100 nm.

Inspired by a report of *in vitro* active transport of isolated capsids along polymerized microtubules (Wolfstein *et al.* 2006), the experiment was adjusted for cryo-EM conditions. Here, microtubules were polymerized and vitrified at different concentrations and observed by cryo-EM to find the suitable concentration for the latter incubation with

motors and capsids. They usually formed large networks homogeneously distributed over the whole grid.

After these initial experiments, 500 mM KCl treated capsids were incubated together with *X. laevis* cytosol and *in vitro* polymerized microtubules on Cu grids with holey carbon support film. Samples were then vitrified and observed by cryo-ET. Tilt series were collected from -60° to 60°, with an angular increment of 3° and the images had a final pixel size of 0.68 nm. The acceleration voltage was 300 KeV and the defocus applied was -8 µm. The percentage of capsids close to microtubules was ~20 %. Instead of showing a preferential binding to microtubules, capsids were rather homogeneously distributed over the ice and the carbon support film. Structures attributed to molecular motors were not obvious in the tomograms, although sometimes there were densities in between capsid and microtubule (**Figure 22D**).

4.4 Binding of capsids to nuclear pores

4.4.1 Cryo-ET of mammalian nuclei

Mammalian nuclei were isolated from Vero cells, vitrified and observed by cryo-EM. They were too electron-dense to be visualized properly and the nuclear membrane was always surrounded by other vesicular material that prevented the visualization of nuclear pores. Therefore, mammalian nuclei were no further explored for the study of capsid attachment to nuclear pores.

4.4.2 In vitro capsid binding to *Xenopus laevis* oocyte nuclei

Based on the existing literature showing the possibility to spread nuclear envelopes from isolated *X. laevis* oocyte nuclei for structural studies (Stoffler *et al.* 1999; Stoffler *et al.* 2003), this experimental system was explored here.

4.4.2.1 Detection of capsid attachment by fluorescence microscopy

The binding of capsids to nuclear pores was studied by using an *in vitro* system that included isolated *X. laevis* oocyte nuclei, isolated capsids from virions detegumented with 500 mM NaCl, and *X. laevis* oocyte cytosol.

The experiments conducted with VP26-GFP-HSV-1 capsids and different cytosol dilutions indicated that the best attachment of capsids to the nuclear envelope of *X. laevis* nuclei occurred at a concentration of 0.22 µg/ml cytosol (**Figure 23**). Successful capsid binding was detected as single fluorescent spots likely corresponding to single viral particles visibly located at the nuclear rim using the 63x oil objective. Fluorescence experiments done with nuclei incubated with 0.22 µg/ml cytosol supplemented with ATP did not show a significant increase of the nuclear rim staining. Addition of importin-ß also did not increase the fluorescence at the nuclear rim. Therefore, for the cryo-ET experiments the cytosol was used at a concentration of 0.22 µg/ml. Even though importin-ß did not seem to increase the fluorescence, it was applied to the cryo-EM experiments since it was reported to mediate nuclear binding (Ojala *et al.* 2000).

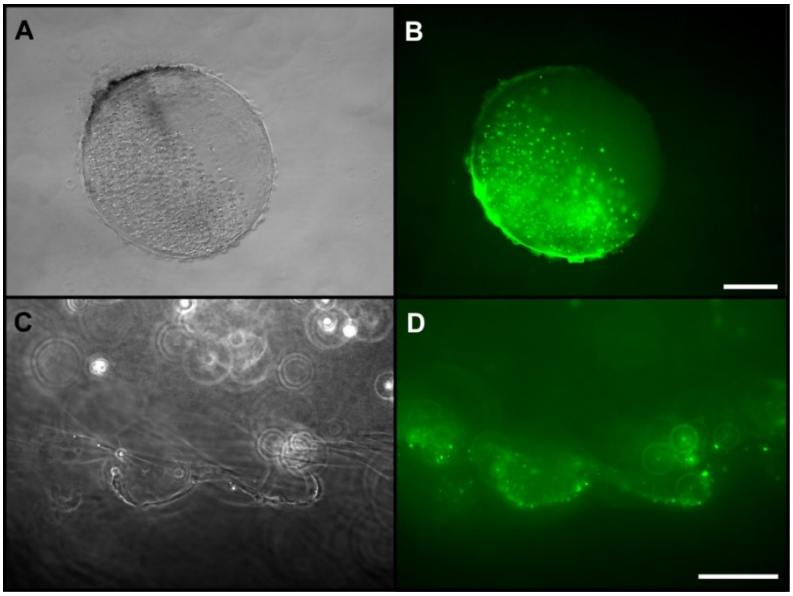

Figure 23. Attachment of isolated VP26-GFP-HSV-1 capsids to isolated nuclei by fluorescence microscopy. (A) Bright field image of a *Xenopus laevis* oocyte nucleus at 10x magnification. The respective GFP-fluorescence image is shown in (B). Bar: 100 µm. (C) Bright field image of the nuclear rim at 63x magnification and corresponding GFP-fluorescence signal (D). Bar: 20 µm.

4.4.2.2 Labeling of capsid DNA with ethidium bromide

To test if there was active release of DNA from capsids into the nuclear pore complexes (NPCs), the DNA of VP26-GFP capsids was labeled with EtBr (see **3.6.5**). After incubation, VP26-GFP capsids showed red fluorescence in more than 50% of the particles detected by GFP-fluorescence, which proved the successful labeling of DNA by EtBr. When these capsids were incubated with isolated nuclei, the fluorescence signal of the capsids was disappearing at the same speed for both red and green fluorescence. Therefore, it was not possible to distinguish between photo-bleaching of the fluorescence signal and DNA release.

4.4.2.3 Cryo-ET of capsids attached to *X. laevis* nuclear envelopes

After carefully spreading the *X. laevis* nuclei previously incubated with capsids and cytosol on an EM-grid, the sample was vitrified and observed by cryo-ET. The aim was to visualize the interaction between capsid and nuclear pore complex (NPC). It was possible to find suitable areas for tomography where the nuclei were well spread and the NPCs were nicely visible (**Figure 24**). Nuclear pores were covering almost the whole surface of the nuclear envelope and had an external diameter of ~125 nm. Often capsids were found bound to the outer nuclear envelope. Tilt series were collected from -60° to 60°, with an angular increment of 2° and with a defocus of -12 µm. The tomograms showed that the capsids present in these areas were not always located directly on top of a NPC but were also found at the sides of nuclear pores. Some of the capsids were full of DNA while others were empty or had the scaffold protein inside. It was not possible to clearly visualize whether the capsids were indeed bound to nuclear pores since in all the areas with capsids, the nuclear envelope was laying parallel to the grid and the missing wedge effect (see **1.2.5.4**) was therefore always strongest in the direction perpendicular to the membrane plane i.e. where the capsid and the NPC were supposed to interact.

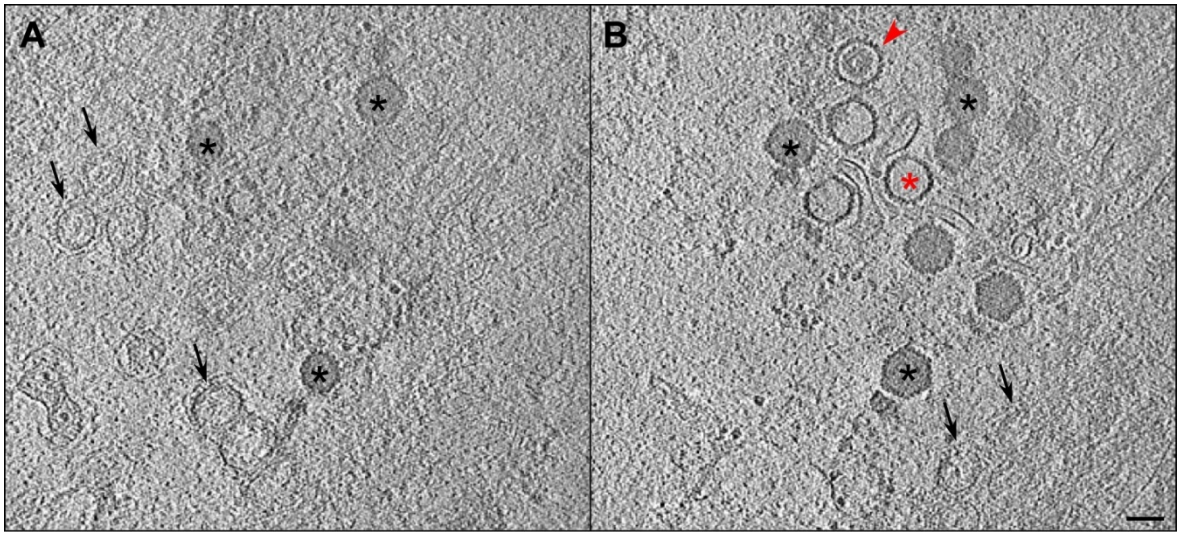

Figure 24. Slices from a tomogram 33 nm spaced and 8 nm thick, showing the nuclear envelope of a *X. laveis* oocyte that was incubated together with detegumented capsids and cytosol. Capsid are located at the outer nuclear membrane. Most of them still contain DNA (black asterisk), but others are empty (red asterisk) or contain the scaffold protein (red arrow head). They are in contact with NPCs (black arrows). Ribosomes and endoplasmatic reticulum membranes are visible on the surface of the envelope. Bar: 100 nm.

4.5 Secondary envelopment of HSV-1 in hippocampal neurons

4.5.1 Secondary envelopment of virions

Hippocampal neurons grown on grids for 7 days for development of axons were infected with wt-HSV-1 strain KOS with a titer of 10^9 PFU/ml at an MOI of 50 and were vitrified at 16 hours p.i.. To find events of secondary envelopment, axon terminals and middle regions of axons that were suitable (i.e. thin enough) for cryo-EM were screened. The cell bodies were always too thick to be imaged by cryo-ET.

Secondary envelopment of HSV-1 was observed in axon terminals. Here, capsids were found occasionally interacting with vesicles that had a characteristic curvature towards the capsid (**Figure 25**). These vesicles were studded with spikes, likely glycoproteins pointing from the membrane into the lumen of the vesicle. Sometimes, the density attached on the outside of these vesicles appeared as well spike or coat-like. Between the vesicle and the capsids electron-dense material, most likely tegument proteins, was detected. The tegument accretion was seen at the vesicle side showing the highest density of glycoprotein-like structures at the inner side of the enveloping vesicle. Notably,

this side of the vesicle had a changed curvature, appearing concave. Capsids were usually found in groups of at least two. The areas of active envelopment were characterized by the lack of microtubules and the presence of an actin network surrounding the area, but being absent inside the so formed quasi-compartment around the vesicles and capsids. 3D analysis revealed that some of the vesicles showing the typical curvature towards the capsids were not large enough to envelope the capsids. There were often several vesicles present in the areas of active envelopment. These vesicles could be differentiated into two groups: some of them were associated with glycoprotein-like and other densities while other vesicles showed a very smooth inner and outer membrane surface.

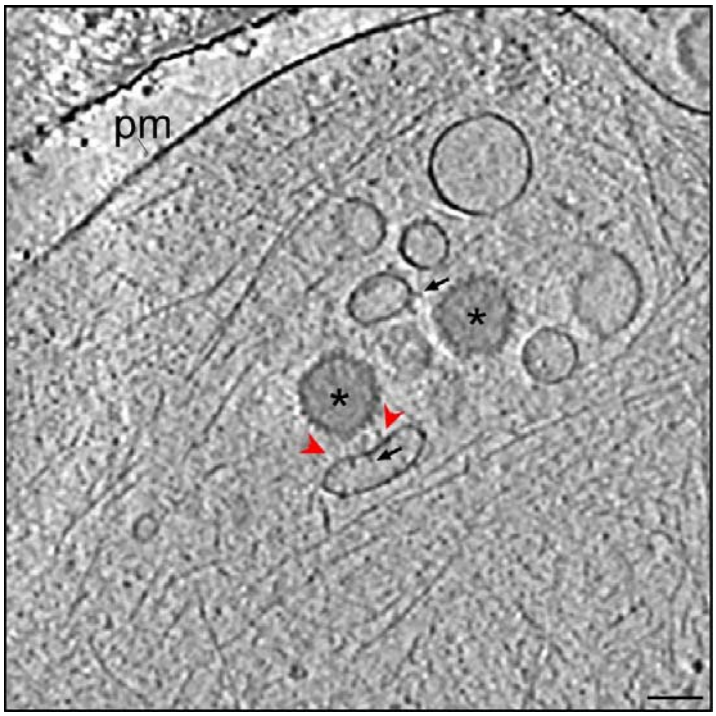

Figure 25. Site of secondary envelopment of virions in an axon terminal, shown on a slice through a tomogram. Here one of the vesicles that is studded with glycoprotein-like densities and tegument presents a concave curvature on the side facing the adjacent capsid. There is an accumulation of dense material (red arrow heads), most likely tegument proteins, in between capsid and vesicle. Glycoprotein spike-like densities are protruding from the inner side of the vesicle (black arrows), mainly from the side in contact with the tegument. The area presents other vesicles, sometimes associated to glycoprotein-like structures and sometimes clean. The whole group of vesicles and capsids is surrounded by actin. The tomogram was denoised using anisotropic diffusion logarithms. Asterisk designates capsids; pm: plasma membrane; bar: 100 nm.

In mid-axon regions, events of capsid envelopment were not observed, but there were areas resembling former envelopment sites. These areas were characterized by the presence of vesicles clearly being associated with glycoprotein-like densities and tegument, as well as the presence of enveloped virions. In some cases, virions were exiting the cell by fusion of the transport compartment with the plasma membrane close to the hypothetical envelopment site (**Figure 15**; exit in more detail in **5.4**). In these middle regions of axons, besides microtubules there was clearly actin present as well. Coated vesicles were also present.

4.5.2 L-particle formation

After 7 days incubation on grids, hippocampal neurons were infected and vitrified like described in **4.5.1**. Tilt series were also collected like in **4.5.1**.

L-particles were recognized as vesicles that showed glycoprotein spikes on their surface, contained tegument densities and in some cases inclusion vesicles (IVs). Sites of L-particle assembly were observed in axon terminals of neurons (**Figure 26**). Some of the vesicles in these areas were clearly associated with tegument and glycoproteins, and had a characteristic curvature around the inclusion vesicle (IV) being enveloped. As for capsids, tegument accretion was observed in between the IV and the enveloping compartment. Glycoprotein-like densities protruded from the inner side of the enveloping compartments into its lumen predominantly at the contact site with the tegument but were also present in lower abundance in other areas of the vesicles. Interestingly, some of the enveloping compartments showed a coating on the outside that provoked a curvature of the membrane (**Figure 26**; **Figure 27**). This coating protruded out of the membrane ~27 nm (**Figure 28**) and was regularly arranged forming pentagons and hexagons that were visible in the slices tangential to the compartments (**Figure 27**; **Figure 28**). Viral capsids were also found in areas of L-particle envelopment (**Figure 26**). Some of them were B-capsids, which are characterized by the lack of DNA and the presence of a scaffolding protein ring (Newcomb *et al.* 1990). The presence of many vesicles of 60 to 100 nm diameter that often showed glycoprotein-like densities on their inner surface was typical for these areas.

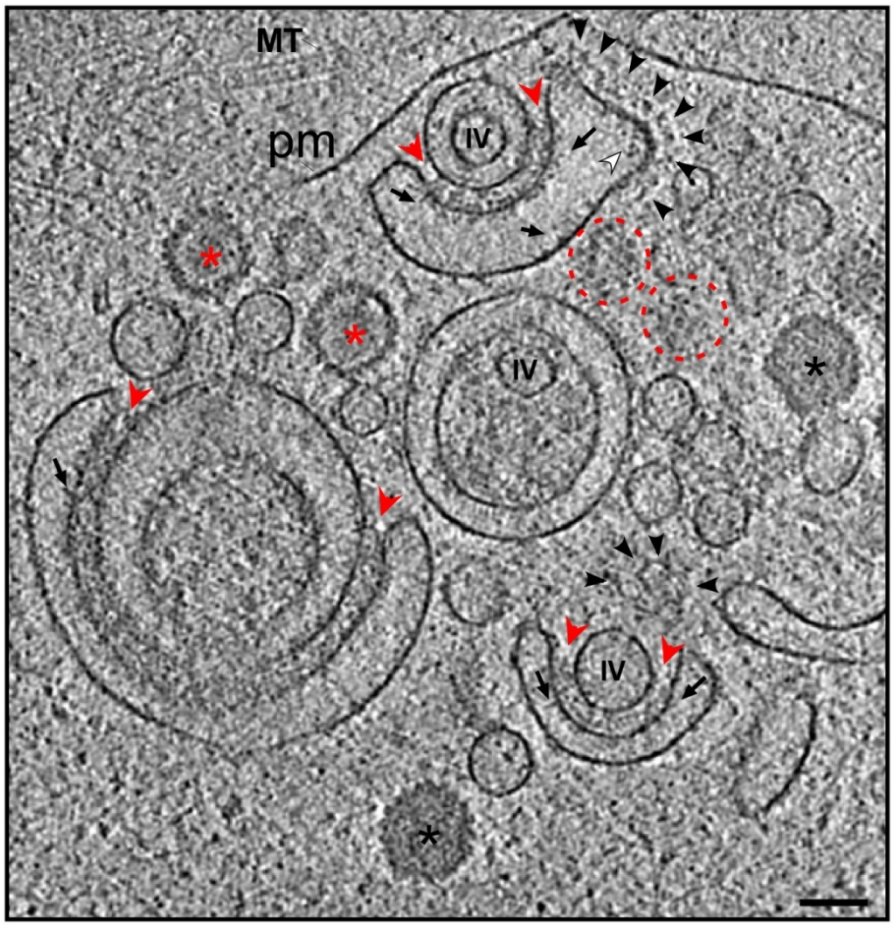

Figure 26. Slice through a tomogram of a secondary envelopment site in an axon terminal. Inclusion vesicles (IV) and capsids (asterisk) are enveloped by membranous compartments studded with glycoprotein-like densities at their inner surface (arrows) and associated with tegument (red arrow heads). Two of these compartments are partially coated, most likely with clathrin (groups of black arrow heads, upper group: side view of coating, bottom group: top view). The top view onto the coating allows the visualization of the hexagonal-pentagonal arrangement typical for clathrin. Here the coated membrane is continuous with the membranous compartment right underneath. There is accumulation of material (white arrow head) at the inner side of the coated membrane. Furthermore, in coated regions the membranous compartment has a different curvature. B-capsids are also visible (red asterisk, red dashed circles show top views of B-capsids where the capsomers are recognizable). pm: plasma membrane; bar: 100 nm.

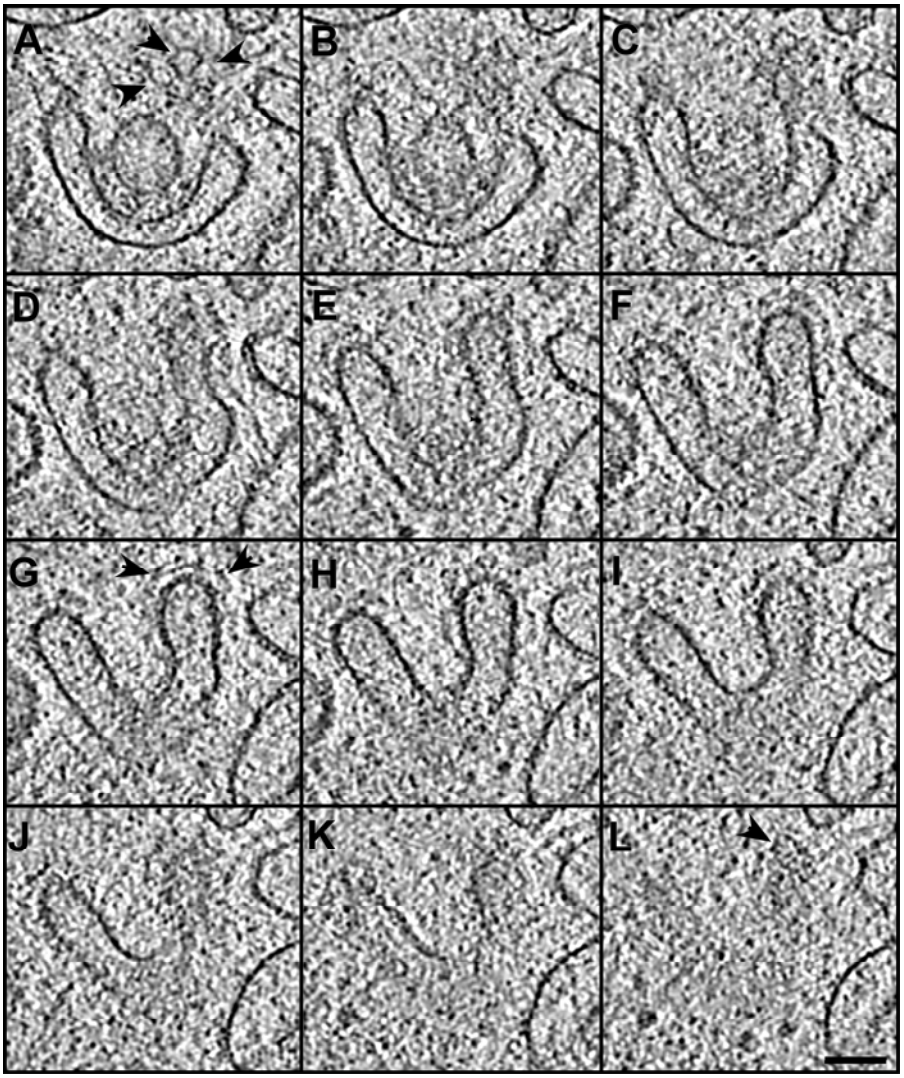

Figure 27. Parallel consecutive slices (thickness 10 nm) from a tomogram visualizing an envelopment site. Clathrin coats are visible at the edges of the compartment (arrow heads). In the views tangential to the membrane (e.g. A), the frontal hexagonal-pentagonal organization of the clathrin coat is clearly recognizable. Bar: 80 nm.

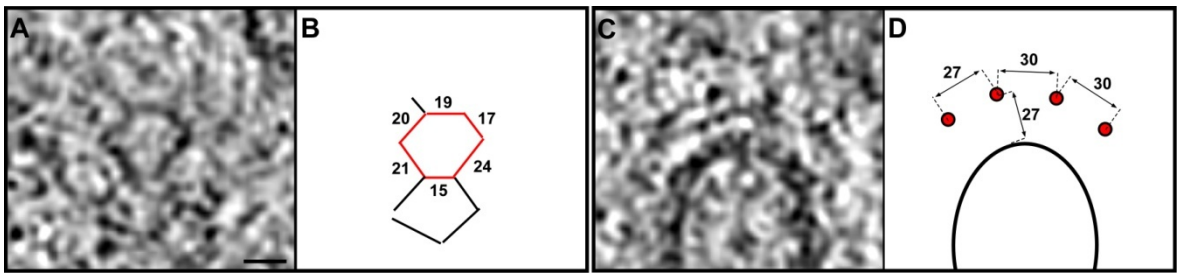

Figure 28. Top (A) and side view (C) of the clathrin coat. Close-up views from the figure 27A and G respectively. (B) and (D) are diagrams that represent the coat arrangement in (A) and (C) respectively. The numbers represent measured distances (in nm). The curve in (D) represents the enveloping compartment membrane. Bar: 20 nm.

4.5.3 Comparison between egress of virions and egress of L-particles

When comparing individual states in the virus and L-particle egress pathway, a number of structural similarities were observed. For a better evaluation they are presented side by side in **Figure 29**.

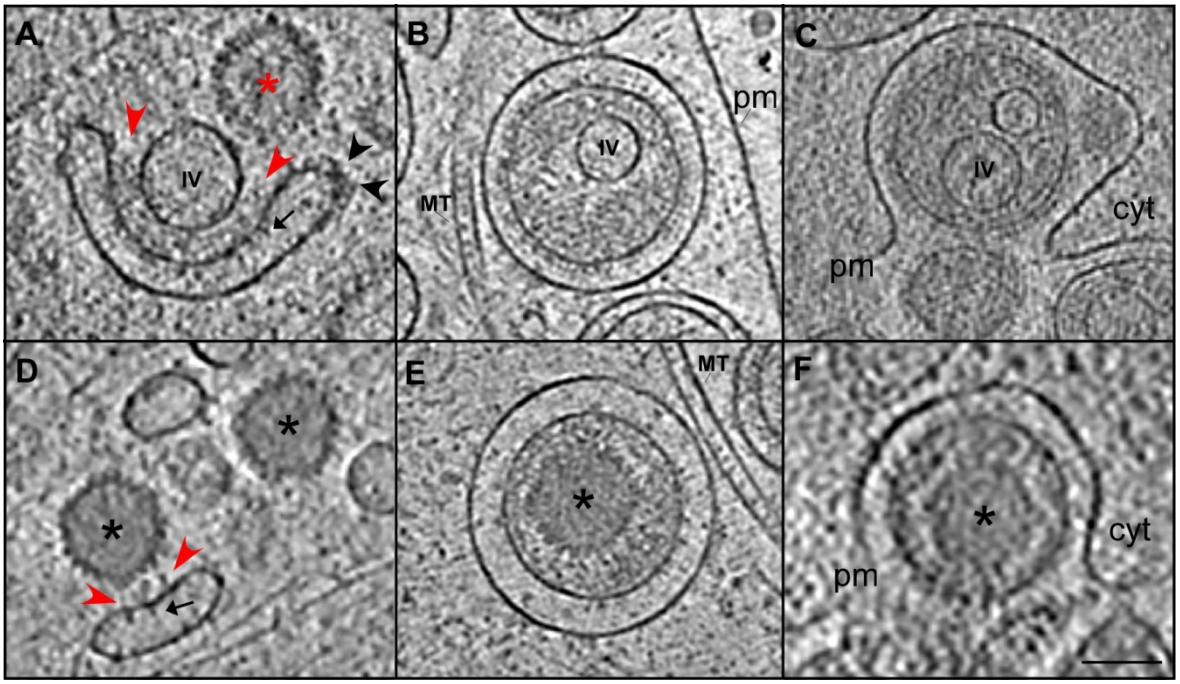

Figure 29. Slices through tomograms showing secondary envelopment, already enveloped particles and exit for HSV-1 L-particles (A-C) and virions (D-F). Both L-particles and virions undergo a similar process: at the site of secondary envelopment (A, D) membranous compartments with glycoprotein-like densities (arrows) and tegument densities (red arrow heads) surround IVs and capsids (asterisks). Newly formed L-particle (B) and virion (E) respectively inside a membranous compartment were found in close proximity to a microtubule (MT). (C, F) depicts exit by fusion of the membranous compartment with the plasma membrane (pm). Red asterisk: B-capsid; Black arrow heads: coat. pm: plasma membrane; cyt: cytoplasm; bar: 100 nm.

4.6 Structural characterization of L-particles

The appearance of L-particles found inside membranous compartments in neurons was compared to the morphology of isolated L-particles from a viral preparation (**Figure 30**). This viral preparation was from HSV-1 strain 17 produced in human foreskin fibroblast, and had a titer of 10^{10} PFU/cell. Aliquots were vitrified by plunge-freezing.

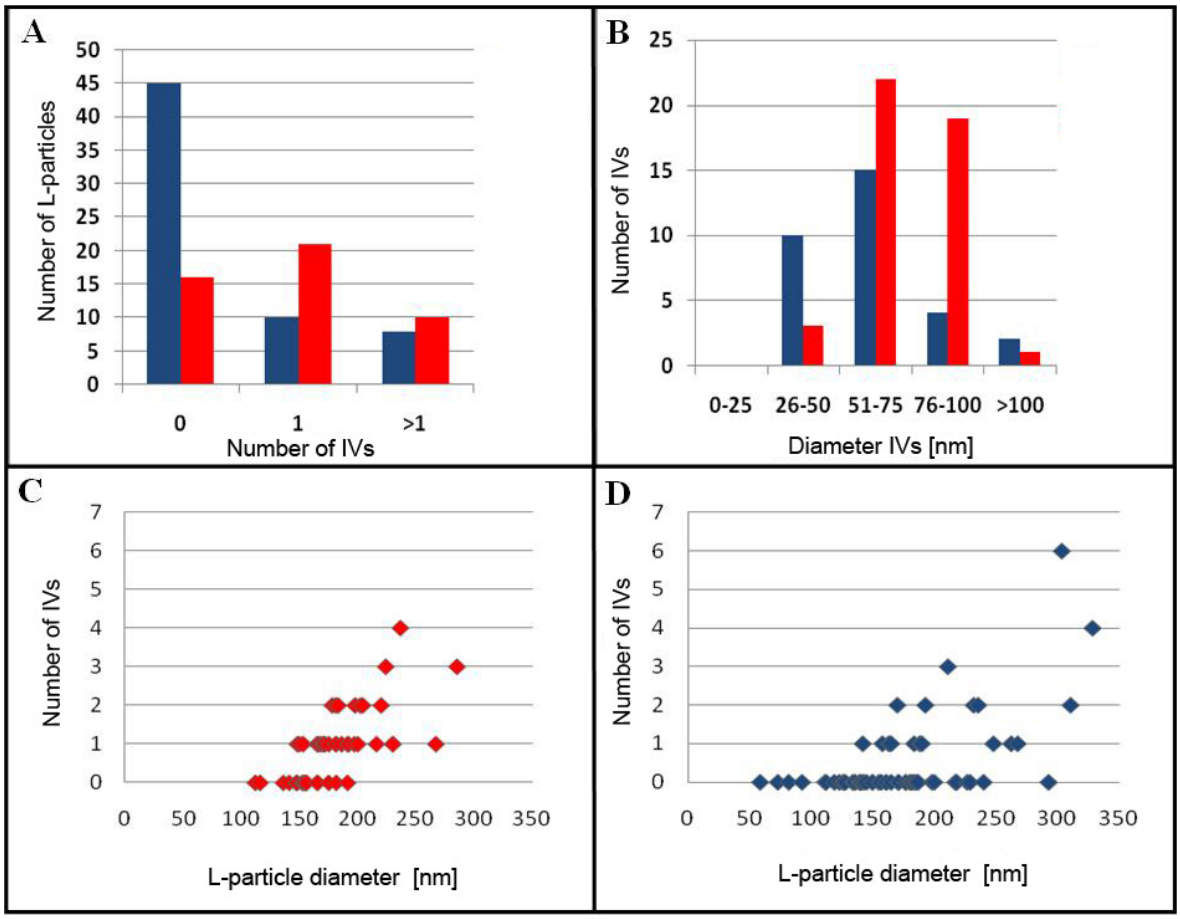

Figure 30. Size distribution of HSV-1 L-particles and contained inclusion vesicles (IVs) in virus preparations (blue) and inside neurons (red). (A) Number of IVs per L-particle. (B) Diameter distribution of IVs. (C) Distribution of number of IVs compared to L-particle diameter in neurons. (D) Distribution of number of IVs compared to L-particle diameter in viral preparations.

In viral preparations, L-particles had a wide range of sizes and shapes. Therefore, only L-particles that had a more or less spherical shape were taken into account. Sizes ranged from 59 to 328 nm diameter (average 177 nm) (**Figure 30D**). Around 16% of the L-particles contained one IV, while 71% did not contain any and 13% contained two or more vesicles (with a maximum of six in one case) (**Figure 30A**). The average size of IVs in viral preparations was 61 nm diameter (**Figure 30B**).

Inside neurons, L-particles were more homogeneous in size and shape than in viral preparations. Here they were always more or less spherical and their size ranged from 112 to 285 nm diameter (average 180 nm) (**Figure 30C**). In neurons, 45% of L-particles contained one IV, while 34% did not contain any and 21% contained two or more

(maximum was 4) (**Figure 30A**). The average size of the IVs in neurons was 71 nm diameter (**Figure 30B**).

There was a clear correlation between L-particle diameter and number of IVs present for both neurons (**Figure 30C**) and viral preparations (**Figure 30D**). The number of IVs was higher in L-particles of bigger diameter.

4.7 Exit of viral particles from host cells

4.7.1 Exit of HSV-1 from growth cones

After developing axons on grids for 7 days, hippocampal neurons were infected and vitrified like described in **4.5.1**. Tilt series were also collected like in **4.5.1**.

The axonal growth cones were identified as flat and relatively broad areas free of microtubules. It was not always possible to identify which terminals belonged to which axons, as gridbars obscure the view and hidden the exact tracking of an axon. This is particularly difficult since the axons tend to form a network over the grid and a minimum amount of cells present in the media during axonal growth is essential for their correct development. At 16 hours p.i., these terminals presented exit hot spots characterized by high concentrations of enveloped virions inside the neuron and released virions in the extracellular space next to those sites (**Figure 31**). There were different viral formations present in the cytoplasm; the majority were single virions surrounded by a membrane of the enveloping compartment. Some of these compartments contained two virions (**Figure 31B**), or a virion together with an L-particle (**Figure 31E**). There were as well single L-particles and vesicles associated with tegument contained in the compartments (**Figure 31D**). Viral particles containing empty capsids and capsids with scaffolding protein were also found (**Figure 31D, G**). Virions were found to undergo fusion of the membranous transport compartment with the plasma membrane at the axon terminals (**Figure 31H**). As a result of fusion the virion was released into the extracellular space.

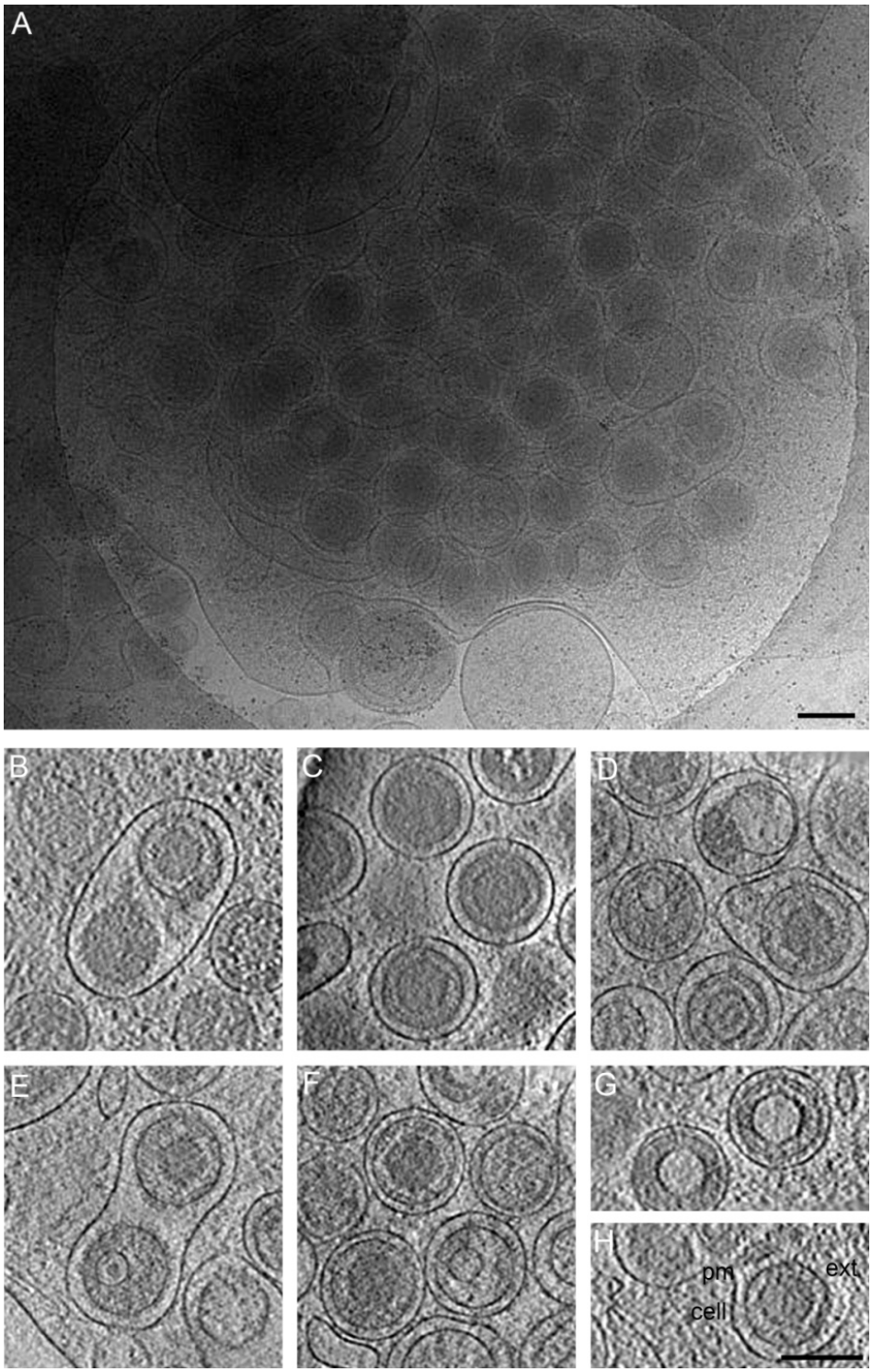

Figure 31. Exit of virions from growth cones. (A) Projection image of an axon growth cone, vitrified 17 h p.i.. Virions surrounded by an enveloping compartment are visible. (B-H) Tomographic slices through the corresponding tomograms taken in different growth cones. The viral particles can be found in several formations surrounded by a membrane: two virions together (B), single virions (C, F), a virion together with an L-particle (D), single L-particles (D, F), viral particles with B-capsids inside (D) and viral particles with empty capsids inside (G). (H) Virion exiting the growth cone after fusion of the transport vesicle with the plasma membrane (pm). cell: cytoplasm; ext: extracellular space; bars: 200 nm.

4.7.2 Exit of HSV-1 from varicosities

As in growth cones, HSV-1 was found to exit from middle regions of axons resembling varicosities (**Figure 32**) by exocytosis-like fusion of the membranous transport compartment with the plasma membrane. Microtubules were present throughout the whole axon. Varicosities contained vesicles of different sizes, and a network of actin filaments was located close to the exit sites. In some cases, virions released from the cell into the extracellular space were still found attached to the plasma membrane. The attachment sites showed connecting densities between the released virions and the plasma membrane (**Figure 34**, black arrow heads show the connection). In all cases, the plasma membrane was sharply kinked at the rim of the area of the exit site that was still connected by these densities (**Figure 32C**, red arrows). The distance between released virus and the plasma membrane was consistently ~30 nm. In some cases, a coat-like density of regular shape was recognizable at the cytoplasmic side of the membrane at the exit site (**Figure 33**). Its thickness ranged from 25 to 32 nm in the centre of the exit site, but being closer to the plasma membrane at the immediate rim of the exit site.

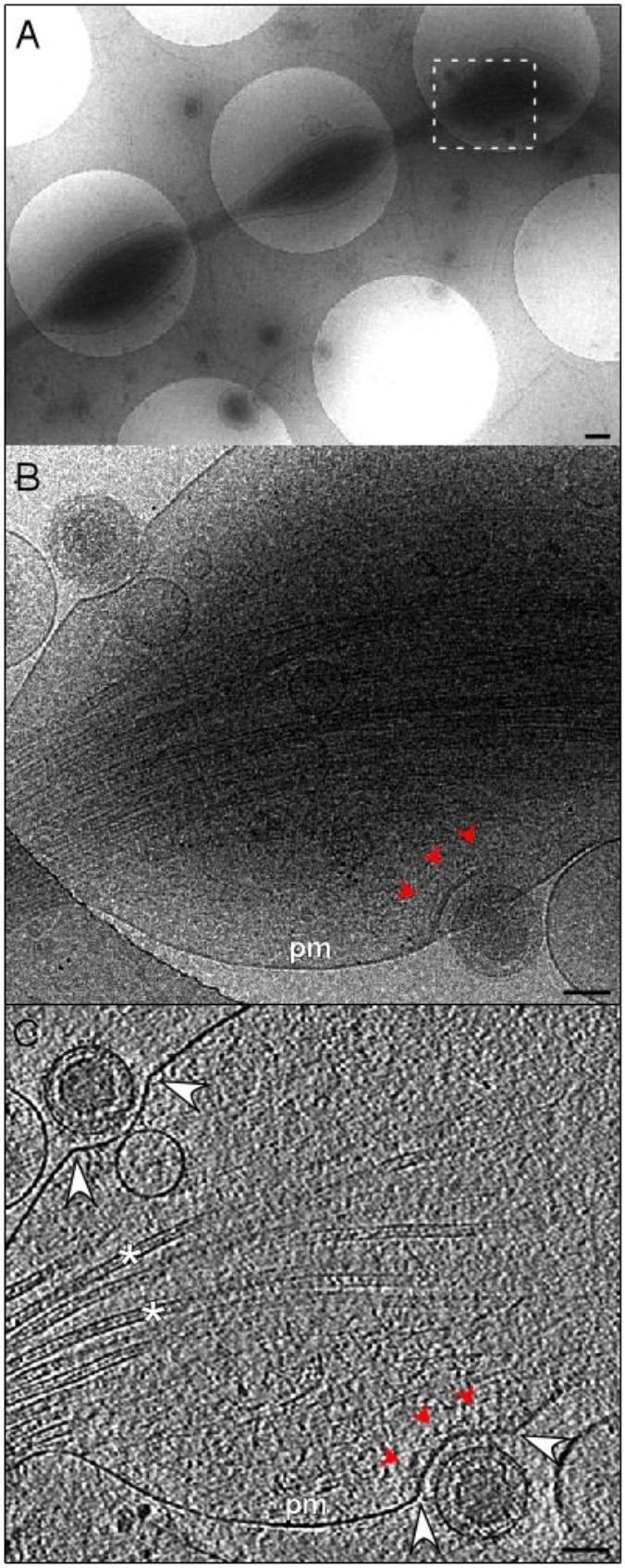

Figure 32. Exit of virions from varicosities. (A) Projection image of the axon of an infected vitrified neuron on a holey carbon film Au grid. The white dashed square marks a varicosity with two virions exiting the neuron. Bar = 400 nm. (B) Close-up of the area framed in (A). (C) Slice through a tomogram from the framed area. Microtubules (asterisks) are present along the whole axon and actin can be seen at both sides of the varicosity, close to the exit sites. The plasma membrane (pm) shows sharp kinks (white arrows) at the rim of the exit site, and sometimes there are coat-like densities recognizable on the cytoplasmic side (red arrow heads, see also **Figure 33**). Bar: 100 nm.

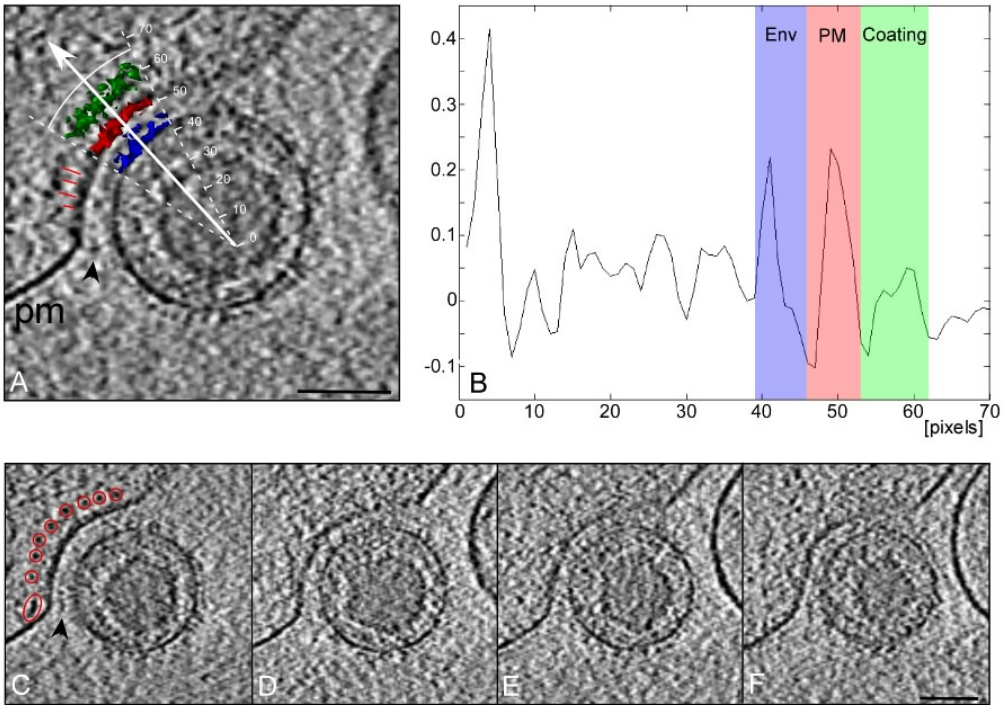

Figure 33. Plasma membrane coat at the exit sites. (A) Slice through a tomogram of a virus exiting a varicosity. The arrow shows the origin and the direction of the radial density plot (B). The origin was determined by fitting a spherical reference to the plasma membrane. The direction of the plot was chosen so it is pointing towards the centre of the exit site and was calculated within a cone with a 30° opening. (B) Radial density plot that shows the density peaks which correspond to the envelope and glycoproteins (Env, blue), plasma membrane (PM, red) and coating at the cytoplasmic side of the plasma membrane (Coating, green). These peaks were selected and segmented in the tomogram (rendering shown in A). Red lines in (A) mark the maximal distance of the coat from the plasma membrane, measured to be 25 to 32 nm. (C-F) Gallery of consecutive parallel slices through the tomogram. Coat densities are highlighted by red circles in (C). The black arrow points to extra density located in between the virion and the plasma membrane. pm: plasma membrane; bar: 100 nm.

4.7.3 Orientation of the virion towards the exit site

The orientation of viral particles towards the exit site was analyzed in terms of their polarity, i.e. location of the capsid proximal vs. capsid distant pole of the virus envelope membrane (Grünewald *et al.* 2003; Maurer *et al.* 2008). For all viral particles exiting varicosities (**Figure 34**), the capsid distant pole, where the majority of the tegument density is found, was located close to the exit site. To proof this preferred orientation of the viral particles, the relative distance of the capsid to the exit site within the virus was calculated (from 0 to 1). The relative distance was measured in 3D along the vector that

goes from the centre of the exit site at the plasma membrane to the centre of the virion. The mean relative distance of all measured cases was 0.54, i.e. a value >0.5. The angle of deviation of the capsid from the vector varied from 1.5 to 10.7 degrees.

Not only virions were observed exiting varicosities, but also an L-particle (**Figure 34 E, J**). This L-particle contained an inclusion vesicle (IV) instead of a capsid. As observed for the released and still attached virions, within the L-particle most of the tegument was found close to the exit site and the inclusion vesicle was closer to the opposite side.

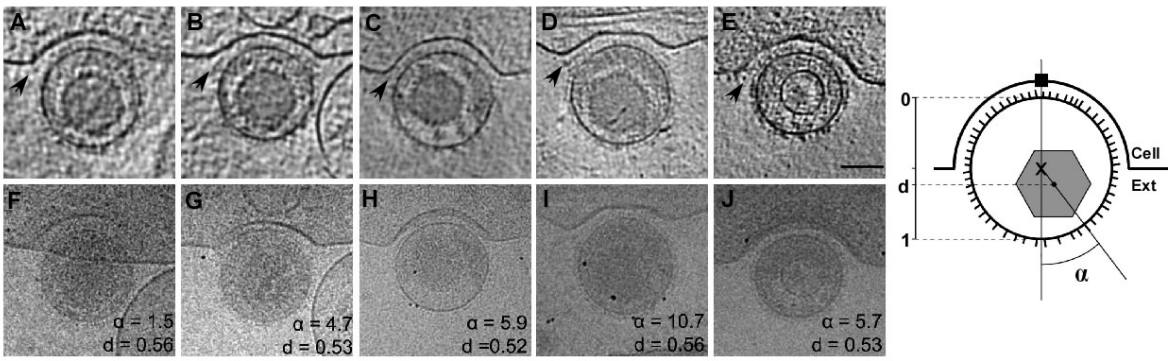

Figure 34. Orientation of the virion towards the exit site. (A-E) Slices from five different tomogram showing viral particles exiting varicosities. (F, J) Corresponding projection images. In (E, J) an L-particle exits a varicosity containing an IV instead of a capsid. The diagram at the right side of the figure explains how the relative distance (d) for each capsid was calculated in 3D, taking into account the vector that goes from the exit site centre at the plasma membrane (black square) through the virion centre (x). The angle of deviation (α) of the capsid was also measured. In all cases, most of the tegument was located close to the exit site at the capsid distal pole of the virion, and the capsid was located at the opposite side (see relative distances (d) >0.5). The black arrows point to the extra density located in between virus and plasma membrane. Bar: 100 nm.

5 Discussion

In this study, *in vivo* cryo-ET imaging of virus-host interactions was successfully established. In particular, these interactions were imaged in adherently grown epithelial cells and in neurons, the natural hosts of HSV-1. These native host-cell interaction models are also potentially suitable for the investigation of other processes, since neurons grown on holey carbon support gold grids present extended flat areas, particularly axons.

By using fluorescence microscopy (FM) in neurons infected with fluorescence labelled viruses, the different stages of infection were characterised. This allowed determining the time-points for vitrification. Correlation between FM and cryo electron microscopy (cryo-EM) at the individual virus level was not possible with the current available correlation microscopy techniques, since the virus-host interaction processes occur too fast, e.g. capsids are transported at a speed of 1-2 μm/sec. This means that the elapsed time between FM observations and vitrification was too long to trace individual viruses. Current developments (J. M. Plitzko, MPI Biochemistry; personal communication) in FM of vitrified specimens based on a previous tested prototype (Sartori *et al.* 2007) might offer the localization by FM of individual viruses on the grid in vitrified specimens and will such facilitate the latter identification of events by cryo-EM.

5.1 Interaction of viral structures with molecular motors and cytoskeletal elements of the host allowing for directional capsid transport

5.1.1 Capsid-tegument-motor interactions in neurons

Neurons vitrified 16 hours p.i. with HSV-1 showed often naked capsids inside axons. This clearly supports the envelopment-deenvelopment-reenvelopment theory of HSV-1 assembly (Skepper *et al.* 2001; Mettenleiter 2002; Mettenleiter *et al.* 2006) (assembly discussed in **5.3**). Most of the time, these capsids contained DNA (cytosolic C-capsids) but sometimes were empty or contained the scaffolding protein (‘defective’ capsids). Simian cytomegalovirus (another herpesvirus) capsids containing the scaffolding protein but not DNA were previously observed in the cytoplasm of cells associated with tegument (Trus *et*

al. 1999). The amount of elapsed time between infection and vitrification suggests that both cytosolic C-capsids and 'defective' capsids visualized inside axons were newly produced by the cell and were being transported towards the cell periphery for assembly and exit. Since the inner tegument proteins are essential for the transport of capsids (Spear *et al.* 1972; Luxton *et al.* 2005; Luxton *et al.* 2006), there is a strong interest in visualizing the tegument that is attached to the capsids during egress and this way, elucidate its structure and distribution.

5.1.1.1 Density differences between cytosolic C-capsids and 'defective' capsids

Surprisingly, big differences were found in the amount of tegument present at 'defective' capsids (cytosolic A- and B-capsids) and cytosolic C-capsids. The average of cytosolic C-capsids showed a significant amount of extra density on top of the pentons that connected to the right side of the adjacent hexons and to the triplexes. Recently, the protein UL25 has previously been detected in cryo-EM reconstructions of nuclear C-capsids forming a heterodimer with the protein UL17 and connecting to the two triplexes closest to the penton (triplexes Tc and Ta) and to the side of the neighbouring hexon (Trus *et al.* 2007). In this study, the heterodimer was not observed in nuclear A- and B-capsids. UL25 is assumed to be important for the stabilization of the DNA-filled capsid (Newcomb *et al.* 2006) and for the exit of capsids from the nucleus (Klupp *et al.* 2006; Trus *et al.* 2007). Since the amount of tegument associated to cytosolic C-capsids and 'defective' capsids in neurons was found here to be very different, it is possible that the heterodimer UL25-UL17 is as well involved in the recruitment of tegument in the cytoplasm. This way, cytosolic C-capsids would have more copies of the heterodimer and therefore would recruit more tegument than 'defective' capsids. Nevertheless, the 'defective' capsids found in the cytoplasm had enough UL25 to be able to leave the nucleus. This finding supports the view that the A- and B-capsids can egress the nucleus, potentially with lower efficiency than C-capsids. It also could be that the requirement of UL25 is cell dependent.

'Defective' capsids had ~50% of the vertices covered with tegument. These covered vertices correspond most probably to the vertices that had UL25 and UL17. It was

estimated that in nuclear A- and B-capsids there should be ~15-40 copies of these proteins (Trus *et al.* 2007). Assuming that there is one heterodimer attached to every triplex adjacent to a penton, our data suggests that there would be ~30 copies of the heterodimer per 'defective' capsid. Cytosolic C-capsids had 91% of the 'one fifth' subvolumes classified as 'with tegument', which would mean that there are at least 55 copies of UL25-UL17 per cytosolic C-capsid. The fact that almost all vertices are classified as 'with tegument' means that cytosolic C-capsids recruited tegument evenly and at the same time point of the infection. The 9% 'one fifths' classified as 'without tegument' were distributed throughout all vertices, meaning that there was no vertex in the capsid specifically free of tegument. This suggests that during anterograde transport the portal of the capsid is also covered by tegument.

It seems that close to 100% coverage of tegument is not required for transport, since 'defective' capsids were found in mid-axon regions. An apparent cooperativity was observed (**Figure 19**) in binding density around the pentons, e.g. pentons were either almost 'clean' or almost full of tegument. The vertices with inner tegument bound apparently have the proteins necessary for capsid transport. In these vertices the extra density was attached to the closest triplex Ta and to the right side of the hexons, where the VP5 protein is located (**Figure 18**). This capsid protein sits on top of the hexons. Thus, it was not in contact with the extra density found in 'defective' capsids. In agreement with previous studies (Antinone *et al.* 2006; Döhner *et al.* 2006), VP26 should therefore not be essential for the transport of capsids as it was previously proposed by Douglas *et al.* 2004. UL25-UL17 is probably part of the extra density found since it is located at the place where the heterodimer is supposed to be (Ta triplex and VP5 protein from hexon). In 'defective' capsids the channels of the pentons were open, as was previously detected for A- and B-capsids (Zhou *et al.* 1999). In cytosolic C-capsids the channel was closed. This is consistent with the idea that once the DNA is packed the closure of the channels would be necessary not to lose the DNA.

Cytosolic C-capsids had more extra density attached than 'defective' capsids (**Figure 18**). This density linked to the top of the penton, to the side of the neighbouring hexons and to the adjacent vertices Tc and Ta. This density could in part belong to molecular motors attached to the capsid. It is assumed that since the molecular motor complexes are

structures that change conformation continuously, that at least their flexible domains might be invisible in the average. It is also possible that only one vertex per capsid is binding with motors (8.3% occupancy) or even just one fifth of a penton could serve as the binding platform. Since the motor complex was not identified in the tomograms, the occupancy is likely too low to be visible in the average. According to studies with hepatitis B virus capsids binding to Fab fragments, an occupancy of ~20% is the minimum for a structure to be visible (Conway *et al.* 2003).

Fluorescence microscopy experiments showed that anterograde transport is bidirectional, which suggest that several molecular motors are attached to the capsid at the same time as reported previously (Gross 2003), or subsequent to each other and having fast on and off states (U.F. Greber, University Zurich; personal communication).

5.1.1.2 Tegument protein candidates involved in transport

In a mature virion there are at least 20 different tegument proteins. Some of them seem not to have any specific function while others are essential for virus replication and in particular for viral transport (Spear *et al.* 1972; Luxton *et al.* 2005; Luxton *et al.* 2006; Fields 2007).

Previous studies have shown that VP1-2 is most likely to be involved in transport (Luxton *et al.* 2005; Luxton *et al.* 2006). Chemically, it binds very tightly to the capsid (Spear *et al.* 1972; Batterson *et al.* 1983) and it seems to be essential for capsid egress since its absence results in the accumulation of capsids in the cytoplasm (Desai 2000). Zhou et al. suggested that the extra density attached to the pentons found in an average from virion capsids could be VP1-2. No biochemical evidence for this was presented and part of the observed density was later attributed to the UL25/UL17 heterodimer (Trus *et al.* 2007). There are 60 to 120 molecules of VP1-2 present per virion (Heine *et al.* 1974), meaning that every vertex could have 5 to 10 molecules attached. The size of one molecule is approximately 270 kDa (McNabb *et al.* 1992), which is larger than what is observed for ‘defective’ capsids. Here, the extra density is not connecting to the pentons but is rather associated to the area where theoretically the heterodimer UL25-UL17 is located. This finding suggests that UL25-UL17 mediates the attachment of tegument to capsids, which

agrees with the findings of an interaction between VP1-2 and UL25 in PrV (Coller *et al.* 2007). If that is the case, the presence of UL25-UL17 would be a prerequisite for the attachment of VP1-2.

Taken all this into account, the extra density that is observed in cytosolic C-capsids should correspond at least to the heterodimer UL25-UL17 and VP1-2, which would connect the penton to the heterodimer. Now the question arises, is VP1-2 not present in 'defective' capsids? This would imply that they are not able to be transported, but the observations made here confirm that they in fact do undergo transport, since viral particles without DNA or with scaffolding protein are found after secondary envelopment in axon terminals. The amount of extra density in 'defective' capsids does not belong only to UL25-UL17, since the difference of density was calculated against nuclear C-capsids, which are supposed to already have the heterodimer attached. VP1-2 could be present in 'defective' capsids but would bind only partially to the capsid by interacting with UL25-UL17. VP1-2 has been detected in L-particles so the capsid is not an essential prerequisite for its presence (Szilagyi *et al.* 1991; Roberts *et al.* 2008). The binding of VP1-2 to the pentons is likely mediated by some other tegument protein that attaches to the vertex of cytosolic C-capsids but not to 'defective' capsids. A candidate for the binding of VP1-2 to the penton would be UL37, which interacts with VP1-2 in PrV (Klupp *et al.* 2002). This way, the domain of VP1-2 that does not bind to the penton would be more flexible and could bend towards different positions and therefore, is not resolved in the average of 'defective' capsids.

5.1.2 Capsid-tegument-motor interactions *in vitro*

5.1.2.1 Capsid-tegument interactions in isolated detegumented capsids

To characterize the tegument attached to capsids during transport in more detail, subtomogram averaging and classification was applied in capsids extracted from virions that were treated with different salt concentrations (100 mM, 500 mM and 1000 mM KCl). The '500 mM' and '1000 mM' capsids showed previously motility in an *in vitro* system together with microtubules and molecular motors (Wolfstein *et al.* 2006). In the same study the authors characterized every group of capsids by their tegument protein

content: all treated capsids contained the tegument proteins VP1-2 and UL37, while VP13/14, VP22, vhs and US11 were extracted from the capsid treated with 1000 mM and 500 mM KCl but not with 100 mM KCl.

As expected, every group of salt-treated capsids showed differences in the amount of associated tegument. The averages of whole capsids (**Figure 20**) showed that in all groups the extra density was located at the vertices. These densities decreased with increasing salt concentrations applied. One would expect to find much more extra density than observed in the averages, since all treated capsids should at least contain the tegument proteins VP1-2 and UL37.

Classification using one fifth of a penton was performed to improve the results and show that salt treated capsids are heterogeneous and not all vertices have the same amount of tegument. From the asymmetric positioning of the capsid inside the virion and the varying thickness of the tegument, it was likely that once the viral membrane is disrupted, the inner tegument is more exposed to KCl buffer in certain areas and more easily removed than other areas of the capsid where the tegument layer is thicker. After classification it became obvious that KCl-treated capsids were detegumented in a heterogeneous way. Vertices were classified into 'with' or 'without tegument'. The class 'with tegument' showed much more extra density than when all capsids were averaged. The 1000 mM KCl treated capsids were expected to have more extra density also after classification (**Figure 21**). From this it is concluded that this group of capsids was not anymore fully associated to the inner tegument proteins VP1-2 and UL37. The observed differences probably originated from the partial occupancy of the triplexes with either the heterodimer UL25-UL17 or with a VP1-2 fraction. The presence of extra density at the pentons could be due to partial occupancy with UL37 or again a fraction of VP1-2. The performed classification could still be refined in the future by upcoming improved classification tools for tomographic subvolumes (Stölken *et al*., in preparation).

Capsids treated with 100 mM KCl needed to be masked before classification to get rid of the gold beads that were sticking to the capsid surface, since they were influencing the classification. This affected the average of the class 'with tegument' since the extra

density is cut on the top by the mask. It is expected that the tegument expands further out than the masked area.

In shape and extension, the density found in ‘500 mM’ capsids best resembles the extra density found in cytosolic C-capsids inside neurons. This is consistent with the observations from Kerstin Radtke (Hannover Medical School, personal communication). She observed that ‘500 mM’ capsids showed best binding to dynein. Therefore, the density observed in cytosolic C-capsids during egress inside neurons corresponds at least to VP1-2 and UL37, which have been detected by western blotting in ‘500 mM’ capsids (Wolfstein *et al.* 2006). A more direct assignment of the densities to specific proteins was unfortunately not possible in this study. This could be achieved best with an *in vitro* tegumentation assay based on baculovirus expressed proteins. Unfortunately, such an assay is currently not available.

5.1.2.2 *In vitro* binding of capsids to molecular motors and microtubules

In an attempt to visualize the interactions between capsid, tegument and molecular motors *in vitro*, 500 mM KCl treated capsids were incubated with microtubules and with *Xenopus laevis* cytosol of high protein concentration. As it was the case inside neurons, it was not possible to identify any larger densities that could be attributed to molecular motors attached to the capsids. However, the immunogold labelling experiments performed suggest that at least the intermediate chain of dynein was bound to capsids. To be able to average the interaction between motors and capsid it would be necessary to recognize them and this way, select only the capsid vertices that are interacting with motors. Otherwise, motors would become invisible in the average as it was the case *in vivo*. Since motors were not recognized in the tomograms, it was not possible to visualize the interactions between capsid and cellular components like motors and microtubules. Here again, the improved classification algorithms currently being developed might offer an approach to identify at least part of the motor complex densities in the future.

5.2 Capsid binding to nuclear pores

In situ investigation of this aspect of the viral life cycle is not possible. Therefore, various *in vitro* investigation systems were explored here. Mammalian nuclei isolated from cultured cells could not be separated from adhering vesicular and tubular structures that potentially represent parts of ER cisternae. Thus, this approach did not provide a suitable source of nuclei for the experiments. It can not be excluded that it would be possible to optimize the purification but this would require a long term dedicated commitment.

Instead, the possibility to use nuclei from *X. laevis* oocytes was explored as these had been used successfully in structural studies of the nuclear pore complexes (NPCs) (Jarnik *et al.* 1991; Stoffler *et al.* 2003). Salt treated capsids and isolated *X. laevis* nuclei were used to study the interaction between capsid and nuclear pore during attachment to the nucleus. Attachment conditions were tested by fluorescence. In cryo-ET the spread nuclear envelope was always found perpendicular to the field of view so the capsid-nuclear pore interaction was always located in the direction most affected by the missing wedge (Lucic *et al.* 2005). Therefore, the structures mediating the interaction between capsid and nuclear pore were not resolved.

Nevertheless, this system might hold potential to be used for such a study. A recent 3D tomographic averaging of the NPC showed an overall missing wedge of 30% (Frenkiel D. *et al*.; submitted), likely benefiting from an imperfect flatness of the support film. Furthermore, one could explore the possibility of using a wavy support film, and this way reducing the missing wedge effect in the averaged structure. Besides this system, one might also consider to use *in vitro* reconstituted nuclei. Preliminary experiments show that this system will also need dedicated optimization to be suitable for cryo-ET. The source and quality of the cytosol is also a crucial criterion and optimization could benefit the frequency of found capsid binding events.

5.3 Assembly of viral particles

In this study it was possible to visualize the egress pathway of HSV-1 in neurons in quite some detail. As already mentioned, this aspect is still under dispute and two main

theories exist: one is the envelopment-deenvelopment-reenvelopment pathway and the other is the single envelopment theory (**1.1.3.4**). In the first one the capsids travel naked without an envelope in the cytoplasm towards the site of secondary envelopment (Miranda-Saksena *et al.* 2000; Skepper *et al.* 2001; Mettenleiter 2002; Luxton *et al.* 2005; De Regge *et al.* 2006; Mettenleiter *et al.* 2006; Snyder *et al.* 2006; Diefenbach *et al.* 2008) while in the second theory the virions are assumed to be in the perinuclear space already assembled and are transported inside the ER to the Golgi and finally to the plasma membrane (Darlington *et al.* 1968; Lycke *et al.* 1988; Leuzinger *et al.* 2005).

Here, capsids were found most of the time naked in middle regions of neuronal axons. Envelopment sites were observed in axon terminals. Sometimes, virions were also seen inside a membranous compartment in middle regions of axons but not as frequently as naked capsids. These virions were found most of the time in areas resembling sites of envelopment due to the presence of vesicles associated with glycoprotein-like densities and tegument, implying that these particles were just enveloped in this area. In other cases, it was not possible to know whether the virions travelled already mature from the nucleus or were just formed, since they were beside microtubules in regions that did not seem to be envelopment sites. Transport of virions inside an enveloping compartment would not be surprising since the topology of these compartments is identical to that of the vesicles that are transported to the envelopment sites, associated with tegument and glycoproteins.

Taking all these observations into account, it can be suggested that the envelopment of capsids in hippocampal neurons occurs mainly close to the exit sites, where the naked capsids arrive transported by using microtubules and molecular motors. The single envelopment theory can not be totally excluded since by cryo-ET it is not possible to visualize the cell body of neurons. Therefore, it is not possible to observe in which way capsids leave the nucleus, but it is a fact that capsids were found naked more frequently than enveloped virions inside middle regions of axons. It is possible but probably not always necessary that once enveloped, virions are further transported inside the membranous compartment along microtubules. The presence in some cases of actin close to the exit sites suggests that the viral particles could also be transported along actin filaments during the last stage before exit.

The envelopment-deenvelopment-reenvelopment theory seems to be in any case the most logical and 'easy' option for the virus to be transported since the diameter of naked capsids is much smaller than the diameter of an enveloped virion and the cytoplasm is a very crowded environment packed with organelles, cytoskeleton and high amounts of proteins. In humans, viral particles are supposed to go from the dorsal root ganglia to the original site of infection once reactivation occurs. With such a long distance the transport of naked capsids and the formation of virions close to the exit sites are the most efficient strategy.

5.3.1 Sites of secondary envelopment

Secondary envelopment sites were characterized by the presence of many capsids and vesicles with both glycoprotein-like densities and associated tegument. These vesicles were not always large enough in 3D to be able to envelope a capsid but they still formed a curvature towards the capsid, such resembling an intermediate stage of envelopment. It seems possible that these vesicles would be able to fuse with each other to form a compartment big enough to envelope the capsid. This theory would support the concept of an easier transport through the cytoplasm if vesicles are smaller. It seems that most of the tegument accumulates between the capsid or inclusion vesicle (IV) and the enveloping compartment, forming the distal pole, which suggests that certain tegument proteins trigger secondary envelopment. Thereby, secondary envelopment would start at the distal pole of virions, as was proposed earlier (Grünewald *et al.* 2003).

5.3.2 Role of clathrin during particle assembly

Surprisingly, L-particles were found undergoing envelopment with the contribution of coated envelopment compartments. The coat resembled clathrin since it had a pentagonal-hexagonal arrangement of the typical dimensions (Cheng *et al.* 2007). Clathrin coated vesicles can be formed at the trans-Golgi network, endosomes and the plasma membrane. The coat is the result of the assembly of clathrin triskelions and in isolated vesicles it has the characteristic appearance of a pentagonal and hexagonal lattice

(Kirchhausen 2000; Fotin *et al.* 2006; Cheng *et al.* 2007; Spang 2008). Two hypotheses might explain why clathrin is present during particle formation:

1) Clathrin-coated vesicles are transported from the trans-Golgi network to the site of envelopment and fuse with the enveloping compartment. It is possible that these vesicles carry glycoproteins since in some cases the inner side of the membrane in contact with the coat showed an accumulation of material. Coated vesicles have been observed close to areas of secondary envelopment, which also supports this hypothesis.

2) Clathrin triskelions might attach to the enveloping compartment during secondary envelopment and influence the formation of curvature. As a result, the enveloped viral particle would be surrounded by a membranous compartment that is coated with clathrin on the outside. The whole structure would be transported to the cell membrane and the viral particle would exit the cell by fusion of the coated compartment with the plasma membrane. This hypothesis is supported by the observation of viral particles (both L-particles and virions) that were exiting the cell and left their coat at the exit site (see discussion in **5.4.2**).

However, it seems that clathrin is not necessarily essential during HSV-1 egress since it was not observed in all the envelopment and exit events. The exact role of clathrin in HSV-1 egress has to be determined in future studies using high speed life cell imaging with respective markers and knock-out mutants.

5.4 Exit of viral particles from host cells

5.4.1 Orientation of HSV-1 towards the exit site after fusion

The here obtained data support that HSV-1 has a preferred orientation during exit from neurons once the membranous compartment surrounding the virion fuses with the plasma membrane: the capsid proximal pole of the virion is situated at the opposite side from the exit site (**Figure 34**). As observed before, the glycoproteins seem to be associated in higher amounts to the distal pole of the virion than to the proximal pole (Grünewald *et al.* 2003; Maurer *et al.* 2008). Recently, it was observed that the virus has a preference of entering cells by its proximal pole (Maurer *et al.* 2008). Therefore, a

preferred orientation for exit with the proximal pole facing the extracellular space would facilitate the infection of the next cell.

The distance between virus and plasma membrane is ~30 nm, almost double the length of the largest glycoprotein present at the viral surface, gB, which has a length of ~16 nm (Stannard *et al.* 1987; Heldwein *et al.* 2006). The viral particle could remain temporally hooked to the plasma membrane using the glycoproteins, which are more concentrated at the distal pole. The distance between viral particle and cell suggests that the glycoproteins at the viral surface cannot be in direct contact with the plasma membrane, but rather by interacting with another protein sitting at the cell surface that makes the contact with the glycoproteins of the viral particle. These proteins are most probably also viral glycoproteins coming from the cytoplasmic membranous compartment that envelopes the virus during secondary envelopment. The presence of a dense area located at the middle distance from viral and plasma membrane could mean that certain glycoprotein domains are interacting with each other in this area. A model of interaction would be the intercalation of glycoproteins extruding from the virus and the plasma membrane.

There were structures connecting to the cell membrane at the cytoplasmic site in the areas where the sharp kinks present at both sides of the exit site are located. These could potentially be SNARE or exocyst proteins that have been involved in the previous fusion of the compartment surrounding the viral particle with the cell membrane (Sutton *et al.* 1998; Munson *et al.* 2006). The nature of these structures is unclear but it is possible that the sharp kinks are stabilized by some protein so the cell membrane does not recover its original shape, such helping the virus to stay in contact with the cell. The fact that in one instance two virions appeared to just have exited the same varicosity, this statistically supports the likeliness of a longer contact after exit. This type of event would be very unlikely if the particles would leave the exit sites quickly. The concave curvature at the exit site supporting the contact is likely also stabilized by the coat on the cytoplasmic face of the plasma membrane.

5.4.2 Coating of the cell membrane at the exit site after fusion

The occasional presence of coat-like densities at the cytoplasmic side of the cell membrane at the exit site were previously observed by conventional EM and described as a thickened crescent-shaped invagination of the plasma membrane (Saksena *et al.* 2006). In cryo-ET, the plasma membrane seems to have a protein layer of regular appearance at the cytoplasmic side. The coat had a thickness of 25 to 32 nm. The possibility of being formed by viral glycoproteins can be discarded since the longest HSV-1 glycoprotein has a length of ~16 nm. Such a coat was observed during exit of both, virions and L-particles. During envelopment of L-particles, a similar sized coat at the enveloping compartment was seen, which suggests that after envelopment some viral particles could be transported inside a coated membranous compartment to the site of exit (see discussion in **5.3.2**). This coat had a pentagonal-hexagonal arrangement that resembled clathrin (**Figure 27**, **Figure 28**). At the exit sites this typical lattice was less obvious. Nevertheless, the distances and appearance of the coat from the side suggested that clathrin was coating the exit site (**Figure 32C**).

5.4.3 Exit of L-particles

L-particles were found surrounded by a membranous compartment inside axon terminals similar to virions. There were also cases of L-particles that shared the same membranous compartment with virions before exiting the cell. During exit, L-particles seem to behave the same way as virions. In the observed case the cell membrane also seemed to be thickened and presented a coating at the cytoplasmic side (**Figure 34E, J**). Like virions, the L-particle had most of the tegument close to the exit site and the distance between both membranes was also ~30 nm. An extra density appeared at middle distance suggesting the same hypothesis of glycoprotein intercalation as for the virions. Therefore, the discussion for exit behaviour in virions would apply as well to L-particles.

Overall this study supports the view that L-particles and virions share most likely the same secondary envelopment sites and exit pathway, as was already suggested in previous studies (Aleman *et al.* 2003).

5.4.4 Polarity of HSV-1 egress in neurons

From the cryo-ET experiments here presented, it can be concluded that axons and varicosities are the sites of exit for HSV-1. This supports previous reports (Saksena *et al.* 2006). Due to the high concentration of extracellular virions and the massive amount of viral particles present at 16h p.i., axons terminals seem to be the main sites of exit for HSV-1 in neurons. Varicosities do not present such high amounts of both intra- and extracellular virions and seem to be used as exit sites more occasionally. The biological significance of the exit in varicosities is unclear but it seems to occur also *in vivo* since these middle regions of axons served as exit sites for PrV after infecting the retina of rats (Tomishima *et al.* 2002).

Before exiting the axon terminal, viral particles were seen inside cytoplasmic membranous compartments likely originated from trans-Golgi derived vesicles. In most of the cases, only one particle was present inside the same compartment. Groups of several particles sharing a compartment were rarely found, which supports the view that capsid budding into multivesicular bodies does not occur.

The appearance of 'defective' viral particles containing A-capsids and B-capsids suggests that these capsids are also produced by the cell and were able to follow the whole replicative cycle, recruiting tegument, envelope and glycoproteins. The presence of these particles in axon terminals inside a compartment suggests that they would also exit the cell (in fact they are found in viral preparations partially to a substantial amount), and most likely also enter other cells.

5.5 Structure and formation of L-particles: similarities to virions

Cryo-ET allowed to distinguish the tegument accumulation between the enveloping membranous compartment and the inclusion vesicle (IV) or capsid at the site of envelopment. Glycoprotein spikes were clearly present in these compartments. Interestingly, enveloping vesicles were also coated in some cases. The appearance of many vesicles in the secondary envelopment sites associated to glycoproteins which were not big enough to envelope a capsid indicates that they might fuse with each other to

form a compartment big enough for envelopment. A- and B-capsids probably follow the same secondary envelopment pathway as L-particles and virions since they were found in the same secondary envelopment sites.

Although capsid preparations were isolated carefully, there was a bigger amount of diversity in sizes and shapes for L-particles than inside neurons. This clearly indicates that the L-particles inside cells give more precise information about their morphology than viral preparations, since L-particles might break or deform during the purification procedure. In neurons, most of the L-particles contained one IV which was usually eccentrically located inside the particle, leaving space for most of the tegument in one side, as was previously described for virions (Grünewald *et al.* 2003; Maurer *et al.* 2008). For both L-particles and virions, the area with most tegument seemed to be associated with more glycoproteins than the opposite side. This was also the case during envelopment of L-particles, where the area of membrane that was in contact with most of the tegument and that surrounded the IV in the first place was associated to more glycoproteins than the rest of the membrane.

The frequent appearance of at least one IV per L-particle suggests that they trigger L-particle formation and envelopment, but obviously L-particles can also be formed without an IV. In viral preparations and inside cells (data not shown), IVs were also observed inside virions although most of them lack an IV, so it seems that IVs are not specific only for L-particles as was suggested before (Szilagyi *et al.* 1994), but they are much more present here than in virions. IVs contained certain electron-dense material of different appearance than the tegument, which corroborates previous studies that suggest that IVs might have a different chemical composition than the rest of the L-particle. Most probably some of their components are polypeptides that are unique to L-particles (Szilagyi *et al.* 1991; Szilagyi *et al.* 1994).

6 Conclusions

1. The main egress pathway of HSV-1 in hippocampal neurons follows the envelopment-deenvelopment-reenvelopment hypothesis since most of the time capsids are transported naked during egress along axons.

2. The inner tegument attached to capsids during anterograde transport in neurons is located at the vertices. In cytosolic C-capsids it is situated on top of the pentons and connects with the right side of the neighbouring hexons and adjacent triplexes. The localized tegument most likely corresponds at least to the tegument protein VP1-2 and the minor capsid proteins UL25-UL17.

3. 'Defective' capsids present less amount of tegument than cytosolic C-capsids but they are still able to be transported during egress along axons. The tegument is not located at the pentons but only at the neighbouring hexons and adjacent triplexes. The amount of tegument is smaller than in cytosolic C-capsids, probably because 'defective' capsids have less amounts of UL25-UL17. Therefore, the heterodimer UL25-UL17 is most likely responsible for the recruitment of inner tegument in the cytoplasm.

4. Clathrin is at least in some cases involved in secondary envelopment and exit of viral particles from neurons.

5. HSV-1 virions show a preferred orientation during exit from neurons once the membranous compartment surrounding the virion fuses with the plasma membrane: the capsid proximal pole of the virus is situated opposite from the exit site. The virions seem to remain temporarily attached to the cell surface after exit by interaction of viral glycoproteins on the outer side of the cell membrane and glycoproteins from the viral envelope.

6. L-particles share the same envelopment and exit pathway as virions.

7 Appendix: Introducción y conclusiones en castellano

7.1 Introducción

7.1.1 HSV-1: clasificación, propiedades y aspectos clínicos

Los Herpesviruses están muy extendidos en la naturaleza e infectan a muchos organismos diferentes como mamíferos, aves y reptiles (*Herpesviridiae*), peces y anfibios (*Alloherpesviridiae*) y ostras (*Malacoherpesviridiae*) (McGeoch *et al.* 2006). Los *Herpesviridiae* son una familia muy numerosa de virus de ADN bicatenario que causan diversas enfermedades en humanos, como por ejemplo lesiones mucocutaneas, queratitis, encefalitis, meningitis, varicela, roséola y sarcoma de Karposi (Sedy *et al.* 2008). Los miembros de esta familia comparten cuatro propiedades biológicas significativas (Fields 2007):

- Especifican muchas encimas relacionadas con el metabolismo de ácidos nucleicos, síntesis de ADN y procesamiento de proteínas.
- La síntesis de ADN viral y el ensamblaje de la cápsida tiene lugar en el núcleo de la célula hospedadora. El ensamblaje final del virus maduro infeccioso (virión) tiene lugar en el citoplasma.
- La producción de virus infecciosos provoca en última instancia la destrucción de la célula infectada.
- Tienen la capacidad de permanecer latentes en sus huéspedes naturales, y más tarde pueden producir infecciones recurrentes.

Esta familia está dividida en tres subfamilias: *Alphaherpesvirinae*, *Betaherpesvirinae* y *Gammaherpesvirinae* (**Tabla I**). Herpes Simplex Virus 1 (HSV-1) es el prototipo de la subfamilia *Alphaherpesvirinae.* Esta subfamilia está caracterizada por su ciclo reproductor relativamente corto y por su capacidad de invadir y vivir en el tejido neuronal, donde permanece latente y puede ser posteriormente reactivado. La investigación de HSV-1 es muy elevada debido a estas propiedades biológicas, las cuales proveen un modelo y herramienta para el estudio de translocación de proteínas, conexiones sinápticas del

sistema nervioso, estructura de membranas, regulación genética, terapia genética, terapia contra el cáncer y otros problemas biológicos y médicos (Fields 2007).

En humanos, HSV-1 infecta inicialmente la piel de la cavidad oral o peri-oral y posteriormente se adentra en las terminaciones nerviosas que están en contacto con las células epidérmicas infectadas. Desde aquí, es transportado a lo largo de axones hasta que alcanza el núcleo de la neurona (transporte anterógrado) en el ganglio de la raíz dorsal, donde permanece latente. Se puede producir una reactivación debida a diferentes causas como exposición solar, estrés o fiebre. Es entonces cuando el virus es transportado a el área inicialmente infectada o a sus proximidades (**Figura 1**). Estas infecciones recurrentes causan normalmente lesiones cerca de la cavidad bucal, pero también pueden dar lugar a úlceras oculares e incluso en raros casos a encefalitis, la cual puede llegar a tener resultados catastróficos, incluso muerte (Fields 2007).

7.1.2 Estructura

7.1.2.1 Viriones

Las partículas infecciosas de HSV-1 (viriones) tienen un tamaño considerable (180-220 nm) y poseen una gran complejidad (**Figura 2**). Contienen un ADN bicatenario de 152 kpb elevadamente condensado, el cual está rodeado por una cápsida icosahédrica de unos 125 nm de diámetro. La cápsida ha sido estudiada en detalle en crio microscopía electrónica (crio-ME) (Schrag *et al.* 1989; Zhou *et al.* 1994; Zhou *et al.* 2000; Bowman *et al.* 2003). Está compuesta mayoritariamente por cinco proteínas diferentes: VP5 (149 kD), VP26 (12 kD), VP23 (34 kD), VP19C (50 kD) y UL6 (700 kD). La estructura cristalina de la proteína mayor VP5 ha sido resuelta (Bowman *et al.* 2003). Las unidades morfológicas mayores dentro de la cápsida son los capsómeros: 12 son pentagonales (pentámeros, situados en los vértices) y 150 son hexagonales (hexámeros). Están formados por cinco y seis copias de VP5 respectivamente. Los hexámeros contienen también seis copias de la proteína VP26 que forman un anillo sobre las subunidades VP5. Los tripletes forman conexiones entre los capsómeros y están compuestos por una molécula de VP19C y dos de VP23 (Newcomb *et al.* 1993). Uno de los vértices de la cápsida tiene una conformación ligeramente diferente. Está formado por un anillo dodecamérico formado por 12 copias

de la proteína UL6, en vez de las cinco unidades de VP5 presentes en el resto de los vértices. Este vértice único recibe el nombre de portal, ya que sirve de conducto de entrada y posiblemente también de salida del ADN (Newcomb *et al.* 2001; Trus *et al.* 2004; Cardone *et al.* 2007; Chang *et al.* 2007). Se ha sugerido que la proteína UL25 retiene el ADN dentro de la cápsida y puede que también provea de una señal para la salida del núcleo (Ogasawara *et al.* 2001; Rode 2007).

La cápsida se encuentra rodeada por una envoltura lipídica que contiene más de once glicoproteínas integradas en su superficie (**Tabla III**). Algunas de estas glicoproteínas son esenciales durante la entrada a la célula (Spear 2004) (**7.1.3.1**). Otras están probablemente relacionadas con el ensamblaje del virión (Mettenleiter 2006).

Una capa amorfa de al menos 20 proteínas diferentes está situada entre la envoltura y la cápsida. Es el llamado tegumento, de estructura irregular (Grünewald *et al.* 2003), aunque parece estar organizado más regularmente alrededor de los vértices de la cápsida (Zhou *et al.* 1999; Zhou *et al.* 2000). Algunas de las proteínas que forman el tegumento son de especial interés debido a su supuesta importancia durante el transporte de la cápsida hacia el núcleo y periferia celular (**Tabla IV, 7.1.3.2, 7.1.3.4**). La cápsida está asimétricamente localizada dentro del virión (Grünewald *et al.* 2003). El polo donde la cápsida se encuentra más cerca de la envoltura casi no contiene tegumento (polo proximal) mientras que el polo opuesto del virión contiene la mayoría del tegumento (polo distal) (Grünewald *et al.* 2003) (**Figura 2**).

7.1.2.2 Partículas ligeras

A principios de los años 90 se observó que la infección de diferentes líneas celulares con HSV-1 no solo producía viriones sino también partículas ligeras no infecciosas (partículas-L), caracterizadas por la ausencia de cápsida y ADN (Szilagyi *et al.* 1991). La morfología de estas partículas no infecciosas ha sido analizada en preparaciones virales y parece ser bastante heterogénea. Cubren un amplio rango de tamaños y a veces contienen vesículas de inclusión (VIs) que varían en tamaño y número. Estas VIs podrían estar asociadas con determinadas fosfoproteínas (Szilagyi *et al.* 1994). Algunos de los polipéptidos detectados en partículas-L (175K, 132K, 92K, 60K, 55K) no se observan en viriones (Szilagyi *et al.*

1991). Uno de ellos (175K) ha sido identificado como el polipéptido trans-activador IE (McLauchlan *et al.* 1992). Las partículas-L no sólo están presentes en HSV-1 sino en todos los alphaherpesvirus testados hasta ahora (McLauchlan *et al.* 1992; Dargan *et al.* 1997). Estas partículas desempeñan una función durante la infección, ya que son capaces de fusionarse con la célula y de este modo diseminan proteínas tegumentales adicionales necesarias durante la replicación de HSV-1 (McLauchlan *et al.* 1992; Dargan *et al.* 1997).

Por medio de la infección con el mutante sensitivo a la temperatura ts1203, el cual es incapaz de formar cápsidas a temperaturas no permisivas, se ha demostrado que la formación de partículas-L es independiente de la producción de viriones. A temperaturas no permisivas había producción de partículas-L pero no se daba el ensamblaje de viriones (Rixon *et al.* 1992). Estudios previos con microscopía electrónica clásica (ME) han mostrado que las partículas-L se forman con la inclusión de tegumento condensado en vesículas del Golgi. Han sido observadas formándose en una misma vesícula junto con cápsidas, lo cual sugiere que viriones y partículas-L comparten las mismas áreas de envoltura secundaria (Aleman *et al.* 2003).

7.1.3 Ciclo replicativo

7.1.3.1 Entrada a la célula

El acoplamiento a la célula de HSV-1 está mediado por la interacción entre determinadas glicoproteínas de la envoltura viral y de sus receptores en la membrana celular. Existen por lo menos 11 glicoproteínas diferentes en la envoltura (**Tabla IV**) pero sólo cinco juegan un papel importante durante la entrada a la célula: gB, gC, gD, gH y gL (Spear 2004).

El virión se acopla a la membrana celular por medio de la interacción de las glicoproteínas gC y gB con cadenas de sulfato de heparano presentes en la superficie de la célula (Campadelli-Fiume *et al.* 2000; Carfi *et al.* 2001) (**Figura 3A**). Tras el acoplamiento, la entrada de HSV-1 puede llevarse a cabo de dos maneras diferentes según el tipo celular (Milne *et al.* 2005):

1) Ruta primaria: entrada por fusión de la envoltura viral con la membrana celular (Pelkmans *et al.* 2003). La glicoproteína gD provoca cambios de conformación en la membrana tras su interacción con receptores celulares *herpesvirus-entry-mediator* (HVEM), nectina-1 o con áreas específicas del sulfato de heparano (Shukla *et al.* 1999). La unión de gD con cualquiera de estos receptores induce la fusión. Una vez se da la unión, determinados dominios de los receptores quedan expuestos e interactúan con las glicoproteínas gB, gH y gL, dando como resultado la fusión de las membranas (Spear 2004). Recientemente se ha descubierto que la interacción entre gB y el receptor celular PILRα es esencial para la infección en determinados tipos celulares (Satoh *et al.* 2008). Tras la fusión de la envuelta viral con la membrana plasmática, la cápsida queda liberada en el citoplasma celular dejando tras de sí la mayor parte del tegumento (Maurer *et al.* 2008), pero conservando el llamado tegumento interno asociado con determinadas áreas de la cápsida. Esta vía de entrada se da en células HFF, Ptk2 y Vero, además de en neuronas, las hospedadoras naturales de HSV-1.

2) Ruta secundaria: entrada viral por medio de endocitosis (Smith *et al.* 2004). Es seguida por la fusión de la envoltura viral con la membrana del endosoma. Esta fusión es probablemente también mediada por la interacción de glicoproteínas virales con receptores de la membrana del endosoma. En la mayoría de los casos, la fusión tiene lugar sólo después de una acidificación del medio. Esta vía de entrada se ha observado en células CHO y HeLa (Nicola *et al.* 2003; Milne *et al.* 2005). La liberación de la cápsida en el citoplasma está también caracterizada por la pérdida de la mayoría del tegumento y la conservación del tegumento interno asociado a la cápsida. Este tegumento interno parece tener un papel crucial durante el transporte de la cápsida hacia el núcleo celular (Bearer *et al.* 2000; Antinone *et al.* 2006; Luxton *et al.* 2006). Algunas de las proteínas tegumentales, como vhs, se separan de la cápsida después de la fusión y actúan en el citoplasma. Otras, como en el caso de VP16, son transportadas independientemente al núcleo.

7.1.3.2 Transporte hacia el núcleo

Una vez la cápsida se encuentra en el citoplasma, se aprovecha de la maquinaria celular para ser transportada hacia el núcleo de la célula (**Figura 3C;** para más detalle ver **7.1.4**). El motor molecular usado por la cápsida para ser transportada a lo largo de microtúbulos desde la periferia celular hasta el núcleo (transporte retrógrado) es la dineína y su cofactor dinactina (Sodeik *et al.* 1997; Döhner *et al.* 2002; Greber *et al.* 2006; Radtke *et al.* 2006). Se ha observado cómo las cápsidas se acumulan en el centro organizador de microtúbulos (COMT) y desde aquí se distribuyen sobre la membrana nuclear (Sodeik *et al.* 1997; Döhner *et al.* 2002; Mabit *et al.* 2002). Se desconoce cómo las cápsidas consiguen llegar a la membrana nuclear desde el COMT. Es probable que se de transporte activo a lo largo de microtúbulos por medio de la utilización de motores dirigidos al extremo (+) como la kinesina-1 (Janus 2008).

7.1.3.3 Acoplamiento al núcleo, liberación del ADN y replicación

Cuando la cápsida llega al núcleo se adhiere a los poros nucleares de la membrana nuclear y libera el ADN en su interior (**Figura 3D**). Parece ser que importin-ß favorece el acoplamiento de las cápsidas a los poros nucleares (Ojala *et al.* 2000). Los poros nucleares son enormes complejos supramoleculares que atraviesan las membranas nucleares interna y externa y que sirven como mediadores del transporte bidireccional de muchas macromoléculas. Se componen de un cuerpo central con forma de donut y de fibras que se extienden desde el cuerpo central hacia el citoplasma y el núcleo. Las fibras nucleares forman una estructura en forma de canasta por debajo del cuerpo central (Stewart 2007). La estructura de los poros nucleares ha sido estudiada en crio tomografía electrónica (crio-TE) (Beck *et al.* 2004; Beck *et al.* 2007).

La orientación de la cápsida hacia el poro nuclear y los mecanismos que inducen la liberación del ADN se desconocen. Algunos estudios sugieren que uno de los vértices, se encuentra dirigido hacia la apertura del poro durante el acoplamiento (Sodeik *et al.* 1997; Ojala *et al.* 2000), probablemente el portal ya que es el medio de entrada del ADN en la cápsida (Newcomb *et al.* 2001). Por tanto, puede que la liberación de ADN en el núcleo tenga lugar en uno de los vértices de la cápsida. Parece ser que la liberación es

dependiente de ATP y puede que otros factores sean también requeridos (Ojala *et al.* 2000; Whittaker 2003). La liberación de ADN en cápsidas aisladas ha sido estudiada en un sistema *in vitro* donde las cápsidas eran capaces de liberar el ADN en núcleos aislados de células mamíferas. Cuando estas cápsidas eran tratadas con tripsina, perdían las proteínas VP1-2, VP13/14, VP16 y VP22, y la liberación de ADN se veía muy afectada. Esto indica que por lo menos algunas de estas proteínas están involucradas en el proceso (Ojala *et al.* 2000). VP1-2 está probablemente involucrada ya que HSV-1 tsB7, mutante con una expresión de VP1-2 defectuosa, puede acoplarse a los poros nucleares pero no puede liberar el ADN a temperaturas no permisivas (Batterson *et al.* 1983).

Tras la liberación del ADN, la cápsida vacía queda acoplada a una distancia de 50 nm del centro del poro hasta que es eventualmente liberada al citoplasma y es degradada (Sodeik *et al.* 1997).

Una vez el ADN se encuentra en el núcleo empieza la replicación (**Figura 3E**). La nuevas cápsidas se ensamblan gracias a una proteína andamio que ayuda a formar como primer resultado las procápsidas, de forma esférica y frágil consistencia. Esta procápsida irá madurando para dar lugar a las características cápsidas icosahédricas (Heymann *et al.* 2003). Tras la maduración de la cápsida, el ADN bicatenario entra en la cápsida a través del vértice portal y se da el empaquetamiento. En núcleos infectados se pueden encontrar tres tipos de cápsidas (cápsidas-A, -B y -C). Las cápsidas-C contienen ADN y pueden madurar hasta convertirse en viriones infecciosos. Las cápsidas-A y -B no tienen ADN, pero las cápsidas-B todavía retienen parcialmente la proteína andamio. Se cree que las cápsidas-A son el producto de un empaquetamiento de ADN fallido (Newcomb *et al.* 1991). Estudios recientes han demostrado que las cápsidas-C tienen mayor cantidad de las proteínas UL25 y UL17 que las cápsidas-A y -B. Estas proteínas menores forman un heterodímero en los vértices de la cápsida (Trus *et al.* 2007) y están relacionadas con el empaquetamiento de ADN y con la maduración de la cápsida (Salmon *et al.* 1998). Todas las cápsidas nucleares están libres de tegumento y el reclutamiento empieza durante la adquisición de la envoltura primaria y continúa mayoritariamente en el citoplasma (Miranda-Saksena *et al.* 2002; Naldinho-Souto *et al.* 2006), aunque estudios recientes sugieren que las cápsidas nucleares podrían estar ya asociadas con las proteínas tegumentales VP1-2 y UL37 (Bucks *et al.* 2007).

7.1.3.4 Transporte hacia la periferia, ensamblaje y salida

Después de la replicación y ensamblaje y una vez que el ADN está empaquetado, la cápsida madura sale del núcleo. La ruta de salida ha creado mucha controversia. Existen tres hipótesis de salida diferentes:

1) Modelo de envoltura-desenvoltura-reenvoltura (**Figura 3F**): la cápsida adquiere una envoltura primaria en la membrana nuclear interna al adentrarse en el espacio perinuclear (Epstein 1962). Las proteínas pUL31 y pUL34 interactúan en la membrana nuclear interna y forman un complejo que es requerido para la formación de la envoltura primaria. La quinasa US3 es esencial para la distribución de pUL31 y pUL34 en la membrana nuclear (Reynolds *et al.* 2002; Klupp *et al.* 2007). De esta manera el virus con envoltura primaria contendría por lo menos las proteínas tegumentales pUL31, pUL34 y US3. La proteína tegumental VP16 ha sido también detectada en partículas virales primarias (Naldinho-Souto *et al.* 2006). Estas partículas salen del espacio perinuclear por medio de la fusión de la envoltura primaria con la membrana nuclear externa (Skepper *et al.* 2001; Mettenleiter 2002; Mettenleiter 2006). Una vez liberada al citoplasma, la cápsida pierde el tegumento primario y es transportada a la periferia celular (transporte anterógrado) probablemente mediante el motor molecular kinesina-1 (para más detalle ver **7.1.4**). El proceso de tegumentación que las cápsidas sufren en el citoplasma no está muy bien definido. Se sabe que ciertas proteínas tegumentales son esenciales para el transporte de cápsidas (ver **7.1.4.3**). En la zona de ensamblaje final del virión, las cápsidas interaccionan con vesículas asociadas con algunas de las proteínas tegumentales y con glicoproteínas virales. Estas vesículas son originadas en la región trans-Golgi y probablemente usan también un tipo de kinesina para el transporte anterógrado (Loomis *et al.* 2001; Turcotte *et al.* 2005; Mettenleiter *et al.* 2006). Los complejos multiproteínicos ESCRT (*Endosomal Sorting Complexes Required for Transport*) podrían estar también relacionados con la adquisición de envoltura secundaria en HSV-1 (Crump *et al.* 2007). El resultado de la envoltura secundaria es un virión incluido en una vesícula derivada de la región trans-Golgi. El virión viaja dentro de esta vesícula hasta la membrana plasmática y sale de la célula por la fusión, equivalente a el proceso de exocitosis, de la vesícula que rodea al virión con la membrana plasmática (Mettenleiter 2002).

El área donde se da la envoltura secundaria es también un tema de mucha controversia. En neuronas se ha sugerido por un lado que ocurre principalmente en la periferia celular, en concreto en las terminales axonales y esporádicamente también en varicosidades. En este caso, el transporte anterógrado se daría en cápsidas desnudas (sin envuelta) (Miranda-Saksena *et al.* 2000; Luxton *et al.* 2005; De Regge *et al.* 2006; Snyder *et al.* 2006; Diefenbach *et al.* 2008). Las varicosidades son dilataciones del axón que representan conos de crecimiento residuales que han quedado atrás durante el crecimiento del la terminal del axón. Presentan microtúbulos y vesículas en su interior (Lucic *et al.* 2007; Diefenbach *et al.* 2008). Por otro lado, estudios realizados en Pseudorrabies virus (PrV), otro miembro de la familia *Alphaherpesviriniae*, sugieren que la cápsida adquiere la envoltura secundaria cerca del cuerpo celular y que el transporte anterógrado ocurre una vez la cápsida se ve rodeada de la envoltura (Antinone *et al.* 2006; Lyman *et al.* 2007; Lyman *et al.* 2008).

HSV-1 abandona la neurona desde varicosidades y desde la terminal del axón (Miranda-Saksena *et al.* 2000; Smith *et al.* 2001; Smith *et al.* 2004; Luxton *et al.* 2005; Saksena *et al.* 2006; Snyder *et al.* 2006).

2) Modelo de envoltura única: una vez en el espacio perinuclear, la cápsida con envoltura es transportada hasta las cisternas de Golgi a través de las cisternas del retículo endoplasmático que están en conexión directa con el espacio perinuclear. De este modo, utiliza la ruta secretora del Golgi para su transporte por medio de vacuolas que pueden contener uno o más viriones (Darlington *et al.* 1968; Lycke *et al.* 1988; Leuzinger *et al.* 2005). Estas vacuolas son transportadas hacia la periferia celular a lo largo de microtúbulos, probablemente mediante el motor kinesina-1. Una vez que la vacuola llega a la membrana celular, ambas membranas se funden y los viriones son liberados al espacio extracelular. En este modelo, los virus abandonan el espacio perinuclear conteniendo ya todo el tegumento y las glicoproteínas características de los viriones, y son transportados en el citoplasma utilizando microtúbulos en su forma ya madura e infectiva. Debido a que prácticamente todas las proteínas tegumentales son exclusivamente citoplasmáticas, este modelo es poco probable.

3) Modelo de expansión de los poros nucleares: es el modelo más controvertido. Se llegó a proponer que los poros nucleares pueden expandirse de tal manera que la cápsida es capaz de abandonar el núcleo atravesándolos (Leuzinger *et al.* 2005). Una vez libre en el citoplasma, adquiriría el tegumento y se adentraría en las cisternas del Golgi para adquirir la envoltura y formar un virión maduro. De aquí pasaría a utilizar la ruta secretora del Golgi al igual que en el primer y segundo modelo para salir de la célula. Este modelo es también poco probable ya que los poros nucleares expandidos de tal manera ya no serían funcionales y la célula moriría rápidamente. En cambio, la microscopía de luz *in vivo* demuestra que las células infectadas siguen vivas durante bastantes horas durante la producción de virus.

7.1.4 Tráfico intracelular de partículas virales

El transporte intracelular está mediado por los motores moleculares de la célula. Estos son complejos proteínicos capaces de moverse a lo largo de microtúbulos y son usados por la célula para el transporte de diferentes tipos de carga, como por ejemplo vesículas y orgánulos. El mecanismo de obtención de energía para el movimiento es la hidrólisis de ATP. Esta reacción causa un pequeño cambio conformacional en uno de los dominios globulares del motor, el cual es amplificado y convertido en movimiento (Schliwa *et al.* 2003). Los motores moleculares son esenciales para el transporte de HSV-1 ya que el citoplasma contiene una elevada concentración de diferentes orgánulos, citoesqueleto y proteínas, los cuales restringen la difusión libre de partículas mayores que 500kDa (Dauty *et al.* 2005).

7.1.4.1 Microtúbulos

Los microtúbulos forman parte del citoesqueleto de las células eucariotas y se forman mediante la polimerización de dímeros de tubulina α y ß. Son cilindros de 25 nm de diámetro y longitud variable (Nogales 2000). Originariamente fueron descritos como cilindros huecos pero recientemente se ha observado que en neuronas de mamífero el lumen de los microtúbulos puede contener partículas globulares (Garvalov *et al.* 2006). El extremo (-) de un microtúbulo está localizado en el MTOC y el extremo (+) está orientado

hacia la periferia celular. Este extremo está en continua polimerización y depolimerización. Los microtúbulos tienen diferentes funciones dentro de la célula. Son parte del citoesqueleto y ayudan a mantener la estructura de la célula, además actúan como 'autopistas' para el transporte de diversos orgánulos y vesículas y forman el huso mitótico, el cual segrega las cromátidas durante la división celular.

7.1.4.2 Motores moleculares

El transporte dirigido hacia el extremo (-) de los microtúbulos se realiza mediante el motor dineína, la cual tiene un peso molecular de 1.4 MDa. Contiene dos cadenas pesadas (DHC, 520 kDa) que se acoplan al microtúbulo e hidrolizan ATP para producir movimiento (**Figura 4**). También tiene seis cadenas ligeras que pertenecen a tres familias de proteínas (LC8/PIN, tctex and LC7/roadblock), dos cadenas intermedias ligeras (LIC, 53-57 kDa) y dos cadenas intermedias (IC, 74 kDa) (Vale 2003). LCs, LICs y ICs están involucrados en el acoplamiento de la partícula viral al motor (Vallee *et al.* 2003; Greber *et al.* 2006; Radtke *et al.* 2006). Se ha demostrado que el motor dineína da pasos de 8-32 nm de longitud dependiendo de la carga (Mallik *et al.* 2004; Reck-Peterson *et al.* 2006). Para ser capaz de realizar el movimiento, dineína requiere del complejo proteínico dinactina (**Figura 5**) (Sodeik *et al.* 1997; Döhner *et al.* 2002; Culver-Hanlon *et al.* 2006).

El transporte dirigido hacia el extremo (+) se realiza probablemente mediante el motor kinesina-1 (**Figura 4**). Este motor se compone de dos cadenas pesadas (KHC, 120 kDa) y dos cadenas ligeras (KLC, 64 kDa). Cada cadena pesada tiene una cabeza motora que se acopla al microtúbulo, un cuello conector y una cola globular. Las cadenas ligeras se acoplan a la partícula viral. La kinesina-1 es responsable del transporte de orgánulos celulares desde el núcleo a la periferia celular. Parece ser que kinesina-1 interactúa con dineína por medio de las KLC y DIC (Ligon *et al.* 2004). Se mueve a lo largo de microtúbulos moviendo las dos cabezas motoras dando pasos de 8 nm de longitud (Yildiz *et al.* 2005).

El tráfico intracelular de partículas no es siempre continuo, sino que puede variar de sentido y ser bidireccional (Gross 2003). Esto indica que no solo un motor está presente en la cápsida, sino que el motor responsable del movimiento en la dirección opuesta

también se encuentra asociado al mismo tiempo (**Figura 6**). En peroxisomas *in vivo* se ha observado que hasta 11 kinesinas o dineínas pueden trabajar juntas para transportar la misma carga a mayor velocidad (Kural *et al.* 2005). Por ello debe de existir algún tipo de regulación de la actividad motora para que los motores dineína y kinesina no se obstaculicen al moverse en direcciones opuestas. Esta coordinación del movimiento es probablemente llevada a cabo por dinactina, la cual tiene una zona de acoplamiento llamada p150/Glued que se acopla con los dominios DIC en la dineína y con el dominio XCAP en la kinesina-1 induciendo su activación (Schroer 2004). Se cree que sólo uno de los motores puede acoplarse a dinactina al mismo tiempo. Por ello, cuando uno de los motores se acopla a la dinactina se activa y permanece en contacto con el microtúbulo, mientras que el otro motor permanece desactivado y alejado del microtúbulo pero todavía en conexión con la carga (Gross 2003).

7.1.4.3 Interacciones cápsida – tegumento - motor

Dónde está la zona de la cápsida en la que se da el acoplamiento con los motores moleculares y cuáles son las proteínas virales relacionadas con dicho acoplamiento son cuestiones sólo parcialmente resueltas hasta el momento. Algunas de las proteínas tegumentales son esenciales durante el transporte intracelular de partículas virales y son probablemente mediadoras del acoplamiento de los motores a la cápsida. Estudios con PrV indican que las proteínas tegumentales VP1-2 y UL37 son requeridas para el transporte intracelular de cápsidas (Luxton *et al.* 2005; Luxton *et al.* 2006). La eliminación del gen UL36 (su producto es VP1-2) resulta en la acumulación de cápsidas de HSV-1 en el citoplasma que no son capaces de liberar su ADN en el núcleo (Desai 2000). El hecho de que VP1-2 parece estar fuertemente asociada con la cápsida en comparación con otras proteínas tegumentales corrobora la hipótesis de que VP1-2 juega un papel importante durante el transporte intracelular (Spear *et al.* 1972). Estudios previos realizados en viriones aislados muestran que una pequeña porción de tegumento está conectada con los vértices de la cápsida, en particular con la proteína VP5 (Zhou *et al.* 1999). Basándose en el tamaño de la densidad, el autor sugiere a VP1-2 como posible candidata. Más aun, hay estudios con microscopía electrónica tradicional que muestran cápsidas en células

con densidades suplementarias localizadas en los vértices (Sodeik *et al.* 1997). Esto sugiere que los motores moleculares podrían acoplarse a los vértices de la cápsida, probablemente mediante la interacción de algunas proteínas tegumentales como VP1-2 y UL37. Existen otras proteínas tegumentales como VP16, VP13-14 y VP22 que pudieran estar implicadas en el transporte de las nuevas cápsidas hacia la periferia celular, ya que han sido localizadas junto con cápsidas durante el transporte hacia la periferia celular (Luxton *et al.* 2005).

7.1.4.4 Interacciones proteína de membrana-motor

Asumiendo que el transporte anterógrado de HSV-1 tiene lugar cuando el virión está ya completamente ensamblado y dentro de una vesícula (ver **7.1.3.4**), deben de existir zonas de acoplamiento en la vesícula para los motores moleculares. Una candidata es la proteína UL34, la cual parece interactuar con la subunidad DIC de la dineína (Ye *et al.* 2000). UL34 está localizada en la membrana nuclear interna y tras la envoltura primaria se localizaría en la envoltura del virión. Otra candidata podría ser la proteína de membrana UL56, la cual interactúa en HSV-2 con KIF1A, un miembro de la familia de las kinesinas-3 (Koshizuka *et al.* 2005).

7.1.5 Fundamentos metodológicos

7.1.5.1 Microscopía electrónica de transmisión

El microscopio electrónico fue inventado por Ernst Ruska y Max Knoll a principios de los años treinta, desbancando al microscopio de luz como técnica de visualización de mayor resolución hasta el momento. A partir de ahí fue evolucionando hasta llegar a alcanzar mucha mayor resolución. Hoy en día, los microscopios electrónicos de transmisión (METs) pueden alcanzar una resolución de 3-4 nanómetros para especímenes biológicos, aunque los conceptos básicos siguen siendo los mismos (**Figura 7**). Los electrones emitidos desde un cañón de electrones sol acelerados por medio de un alto voltaje (normalmente 100-300 KeV para especímenes biológicos) para formar el haz de electrones. Este haz es enfocado por medio de lentes electroestáticas y electromagnéticas sobre una muestra

colocada en la columna del microscopio Esta columna se mantiene con alto vacío para prevenir la desviación de los electrones por la interacción con moléculas del aire (Yonekura *et al.* 2002).

El haz es enfocado por medio de las lentes condensadores hacia la muestra. Parte de los electrones la atraviesan sin interferir con ella, mientras que otros son retenidos o dispersados por los átomos de la muestra. Hay dos tipos distintos de dispersión: elástica e inelástica. En la dispersión elástica no hay pérdida de energía cinética. Es esencial para el aumento de contraste en la imagen final (ver **7.1.5.2**). En la dispersión inelástica se produce una excitación de la muestra y pérdida de energía (Reimer 1997). Además, los electrones dispersados inelásticamente producen ruido que degrada la calidad de la imagen final. La proporción de electrones dispersados es directamente proporcional al grosor de la muestra y a su densidad.

De este modo, se crea una imagen con los electrones que atraviesan la muestra. La lente objetivo y las lentes proyectoras magnifican la imagen, la cual se ve reflejada en una pantalla fluorescente situada al final de la columna. Alternativamente, la imagen final puede ser también captada por una cámara de televisión, por películas fotográficas o por un detector CCD (*charge-coupled device*). Este último es capaz de formar imágenes digitales directamente, convirtiendo primero la imagen de electrones en una imagen de luz y transfiriéndola después al sensor CCD.

Algunos microscopios electrónicos están dotados de un filtro de energía, lo cual les permite deshacerse de electrones que han sido inelásticamente dispersados. De este modo, la imagen resultante aparece con menos ruido y mayor contraste. Hay dos tipos diferentes de filtro de energía: *in-column* (ej. diseño Omega; creado por Zeiss y JEOL) y *post-column* (ej. *Gatan Imaging Filter*; GIF).

7.1.5.2 Formación de imagen

Una micrografía electrónica es una proyección bidimensional (2D) del objeto a observar en MET. La resolución de la imagen viene limitada esencialmente por el contraste, que se define como la diferencia relativa de intensidad entre un punto en la imagen y lo que le

rodea, y que es necesario para diferenciar los elementos de la imagen con respecto del fondo.

En preparaciones con tinción de metales pesados el contraste es aumentado gracias a la elevada densidad de la muestra. Es el contraste de amplitud, también llamado contraste de dispersión, causado por los electrones que son dispersados en la columna con grandes ángulos de desviación cuando interactúan con áreas de elevada densidad en la muestra, no contribuyendo por tanto a la formación de imagen. En muestras biológicas vitrificadas es más importante el contraste de fase, también llamado contraste de interferencia. Es el resultado de la interferencia entre los electrones dispersados elásticamente y los electrones no dispersados (Erickson 1971). Sin tinción, los átomos de la muestra tienen una densidad muy parecida a la de la capa de hielo que la rodea (ver **7.1.5.4**) y producen muy poca dispersión. Por ello, en este caso el contraste de fase adquiere más importancia. El contraste de fase se ve incrementado por la combinación del desenfoque y una aberración en las lentes. Aplicando desenfoque las longitudes de onda de los electrones dispersados varía más que las de los no dispersados, por lo que se incrementa el contraste de fase. Sin embargo, un desenfoque excesivo limitaría la resolución y daría lugar a la aparición de detalles en la imagen que no son reales. Para las muestras biológicas, el desenfoque óptimo que hace balance entre contraste y resolución se sitúa ligeramente por debajo del enfoque perfecto (defoco).

La función de transferencia de contraste (FTC) especifica el contraste relativo de detalles en la imagen como una función de frecuencia espacial y depende de la aberración esférica del desenfoque de la lente-objetivo y de la energía de los electrones. La FTC se describe dentro del espacio de Fourier, donde las imágenes están representadas por las frecuencias espaciales que contienen. El principio de Fourier dice que cualquier función periódica puede ser dividida en una suma infinita de senos y cosenos, y de esta manera tiene una representación única en el espacio de Fourier. Por ello, la transformación al espacio de Fourier es muy útil a la hora de procesar imágenes.

7.1.5.3 Preparación de muestras biológicas para microscopía electrónica

Las muestras biológicas contienen normalmente elevadas cantidades de agua (hasta un 90%). Debido al alto vacío existente en la columna del microscopio y a la exposición de las muestras al haz de electrones, una muestra biológica sería completamente destruida si no se le somete a un tratamiento anterior que elimine o inmovilice su contenido en agua. Por ello, las muestras destinadas a la observación en MET son fijadas previamente.

El método tradicional de preparación consiste en una fijación química seguida por una tinción con metales pesados, deshidratación con disolventes orgánicos y la inclusión en plástico o resina. Tras ello la muestra se secciona en láminas que se someten de nuevo a tinción para aumentar más su contraste. Estos tratamientos son muy duros para la muestra y pueden causar daños en las distintas estructuras.

La crio-fijación apareció a finales de los años ochenta como la solución a este problema, y desde entonces ha revolucionado el mundo de la microscopía electrónica de muestras biológicas (Adrian *et al.* 1984; Dubochet *et al.* 1988). Con este método la muestra es vitrificada y se conserva hidratada. Por ello, las estructuras se mantienen en un estado cercano al nativo y no sufren ningún tratamiento químico. Para lograr la vitrificación de la muestra, esta es congelada rápidamente en etano líquido a una temperatura de unos -180 °C. La congelación rápida previene la formación de cristales de hielo (se expandirían y destruirían la muestra), así como la formación de hielo hexagonal (provocaría la difracción de electrones no deseada). Por el contrario, con la vitrificación el agua líquida pasa a ser hielo de consistencia amorfa, similar a la de un líquido pero con una elevada viscosidad (**Figura 8**). Además, las bajas temperaturas tienen un efecto crio-protector que reduce el daño causado por el haz de electrones durante la exposición con MET. Por otro lado, una muestra con un grosor mayor que 10 µm no puede ser vitrificada correctamente con el método descrito previamente. Existen métodos alternativos elaborados recientemente para muestras más gruesas, como son la congelación por alta presión con la posterior sección de la muestra congelada a una temperatura de -140 a -160°C (CEMOVIS; (Al-Amoudi *et al.* 2004).

7.1.5.4 Crio microscopía electrónica

Una vez vitrificadas, las muestras son almacenadas en nitrógeno líquido (-196 °C). Las muestras son insertadas en la columna del microscopio dentro de un brazo de soporte crio. Este tipo de soporte puede ser enfriado con nitrógeno líquido y es capaz de mantener la muestra a una temperatura de unos -180°C. Una vez es introducida, es importante exponer la muestra a una dosis de electrones baja que la dañe lo menos posible. Debido a que no hay tinción con metales pesados, el contraste que se adquiere en la imagen viene sólo del material de la muestra. Las muestras biológicas se componen principalmente de hidrógeno, carbono, oxígeno, fósforo, nitrógeno y sulfuro. Estos son materiales blandos que producen bajo contraste comparado con los metales pesados (ej. oro).

7.1.5.5 Crio tomografía electrónica

La tomografía es una técnica que permite producir volúmenes tridimensionales (3D) de objetos, los llamados tomogramas. Cuando se combina con crio ME, se le denomina crio tomografía electrónica (crio-TE). La TE se basa en un principio descubierto por Radón en 1917, el cual describe cómo que un tomograma puede ser formado a partir de la suma de las diferentes proyecciones de un objeto. Este principio fue elaborándose más adelante y se puso finalmente en práctica en 1968 (De Rosier 1968). mediante el uso de la crio-TE se pueden conseguir tomogramas de un amplio rango de materiales biológicos, desde células hasta moléculas, permitiendo el estudio de la relación estructura–función en dichos materiales (Lucic *et al.* 2005). En concreto, la crio-TE permite observar detalles del objeto que no pueden ser detectados en las proyecciones aisladas aplicando la misma dosis total de electrones (**Figura 9**). Los detalles son captados mejor en tomografía mientras que en 2D, las estructuras pueden superponerse entre sí y pueden ser obstruidas por otro objeto. La resolución de un tomograma en crio-TE se sitúa en el rango de los 5 nm.

7.1.5.6 Adquisición de una serie de proyecciones

El procedimiento consiste en la obtención de una serie de micrografías electrónicas de un espécimen a diferentes ángulos (**Figura 10, izda.**). Hay dos requerimientos fundamentales

que deben darse: el objeto de interés debe permanecer en el campo de visión durante la adquisición de imágenes y todas las proyecciones deben ser tomadas con la misma magnificación y bajo similares niveles de defoco y dosis de electrones. Para conseguir las proyecciones de la muestra a diferentes ángulos, el brazo de soporte de la muestra es girado en torno a su eje perpendicular al haz de electrones. Este brazo y el goniómetro que realiza la rotación no son mecánicamente perfectos y tras la rotación se dan normalmente desplazamientos del espécimen de interés en el campo de visión. Por ello es necesario reajustar estos desplazamientos y centrar el espécimen de nuevo en el campo de visión.

Los ajustes manuales requieren una gran cantidad de tiempo, por lo cual se han desarrollado procedimientos automáticos de adquisición de datos (Koster *et al.* 1992; Dierksen 1993). La adquisición automática requiere de tres pasos diferentes: enfoque, *tracking* y *exposure*. Con el enfoque se compensa el cambio de defoco que se produce a rotar el espécimen (Koster 1989). El defoco es determinado mediante la comparación de dos imágenes adquiridas a diferentes ángulos. Con el *tracking* se corrige el desplazamiento de la imagen con respecto a la imagen anterior. Para ello se adquiere una micrografía con una dosis de electrones muy baja y es comparada con una imagen de la misma área tomada en un ángulo de rotación previo. *Exposure* es la adquisición de la imagen final. Normalmente, las áreas de enfoque y *tracking* se encuentran situadas algo alejadas del área de *exposure*, para minimizar los daños por radiación.

7.1.5.7 Reconstrucción tridimensional

Para reconstruir el volumen en 3D del conjunto de proyecciones de un objeto se necesita primero alinear las diferentes micrografías entre si y después juntarlas creando el volumen (**Figura 10**). La alineación de las proyecciones entre sí compensa los pequeños movimientos del espécimen dentro del campo de visión. Puede llevarse a cabo por medio de marcadores o por correlación entre imágenes (*cross-correlation*). Los marcadores son partículas pequeñas y electron-densas que se añaden homogéneamente a la muestra. Normalmente, se usan partículas de oro coloidal, aunque recientemente se han empezado a utilizar *quantum dots* como marcadores para secciones vitrificadas (Masich

et al. 2006; Gruska *et al.* 2008). Las coordenadas de cada marcador son localizadas en cada una de las imágenes de forma manual o automática. La reconstrucción del tomograma es llevada a cabo una vez la alineación está definida. La manera en la que se consiguen recuperar los datos en 3D a partir de imágenes en 2D puede ser explicada en el espacio de Fourier: la transformada de Fourier de una proyección corresponde a un corte central similar a una rodaja en el espacio tridimensional de Fourier del objeto visualizado. Por ello, desde distintas direcciones las proyecciones muestrearán diferentes áreas de la representación Fourier del objeto. El modo de reconstrucción más común en TE es el de *weighted back-projection*. En este método las proyecciones son proyectadas 'hacia atrás' para conseguir el volumen en 3D. Las frecuencias más bajas se ven aumentadas artificialmente por lo que es necesario realizar el denominado *weighting*, que elimina este efecto en el Espacio de Fourier (Harauz G. 1986).

7.1.5.8 Limitaciones por la exposición a los electrones

La mayor limitación en crio-TE está en el daño que se produce en la muestra cuando se ve expuesta al haz de electrones. En muestras fijadas químicamente y teñidas con metales pesados, la dosis que se puede utilizar es mucho mayor que cuando se trabaja con muestras crio. Cuando se expone la muestra crio esta se ve alterada produciéndose ionización y formación de radicales libres. Aunque estos procesos no dependen de la temperatura, el daño resultante, pérdida de masa y la difusión de radicales libres sí dependen de ella (Lucic *et al.* 2005). Por esta razón, la dosis total de electrones debe mantenerse bajo el límite crítico donde se empieza a quemar la muestra. Como consecuencia el contraste es menor que en muestras fijadas químicamente, en las que se puede aplicar mayor dosis. En general, la dosis total tolerada por una muestra biológica en crio es de 60-80 $e^-/Å^2$, pero depende de la muestra y debe ser determinada experimentalmente.

Las muestras más gruesas (ej. células) dispersarán y absorberán más electrones. Para estos especímenes, es necesario un voltaje de aceleración lo suficientemente elevado (300 KeV) con mayor penetración.

7.1.5.9 Limitaciones por el *missing wedge*

Existe una limitación en TE debido al diseño del brazo de soporte de la muestra: no es capaz de girar sobre su eje más allá del rango ± 70 grados. Esto obstruye la visualización de ciertas áreas en la muestra. La información de las áreas no muestreadas se pierde y se forma el llamado *missing wedge*. Por ello, la reconstrucción del objeto no puede completarse (para una reconstrucción completa, sería necesaria una rotación de ±90 grados del objeto) (**Figura 11**). Como consecuencia de esta carencia, la resolución del tomograma es dependiente de la dirección en la que se obtiene (anisotrópica). Los objetos reconstruidos pueden mostrarse elongados en la dirección del haz de electrones y algunos elementos estructurales quedan sin resolver (**Figura 11**). La adquisición de tomogramas por el método de doble rotación puede minimizar este efecto. En este caso se adquieren dos series tomográficas del mismo objeto rotando la muestra 90 grados en el plano horizontal tras adquirir la primera serie. Esto debe hacerse con la misma dosis total aplicada en una sola serie, es decir, o bien los incrementos de rotación se amplían en ambas series o la dosis de electrones aplicada en cada imagen es reducida.

7.2 Conclusiones

1. La principal ruta de salida de HSV-1 en neuronas del hipocampo sigue el modelo de envoltura-desenvoltura-reenvoltura, ya que la mayoría de las cápsidas son transportadas desnudas a lo largo de axones hacia la periferia celular.

2. El tegumento asociado con las cápsidas durante el transporte anterógrado en neuronas se encuentra en los vértices. En las C-cápsidas citosólicas se sitúa encima de los pentones y conecta con la cara derecha de los hexones y triplexes adyacentes. Este tegumento se corresponde probablemente con la proteína tegumental VP1-2 y el heterodímero UL25-UL17.

3. Las cápsidas 'defectuosas' presentan menos cantidad de tegumento que las C-cápsidas citosólicas, pero son de cualquier manera transportadas a lo largo de axones hacia la periferia celular. El tegumento no está situado sobre los pentones sino sobre los triplexes y hexones adyacentes. La cantidad de tegumento es más pequeña que en las C-cápsidas citosólicas, probablemente porque las cápsidas 'defectuosas' tienen menor cantidad de heterodímeros UL25-UL17. Es por esto que UL25-UL17 es probablemente responsable de la adquisición de tegumento interno en el citoplasma.

4. La clatrina está involucrada al menos en algunos casos en la envoltura secundaria y en la salida de partículas virales en neuronas.

5. Los viriones de HSV-1 presentan una orientación preferente durante la salida de neuronas una vez que el compartimento membranoso que rodea al virión se funde con la membrana plasmática: el polo proximal de la cápsida se sitúa en el lado opuesto al área de salida. Parece ser que los viriones quedan amarrados temporalmente a la superficie de la célula tras la salida, por medio de la interacción de glicoproteínas virales en la cara exterior de la membrana celular y glicoproteínas de la envoltura viral.

6. Las partículas ligeras comparten una misma ruta de envoltura y salida con los viriones.

Acknowledgements

At this point I would like to thank everyone that contributed in many different ways to this work and therefore made it possible:

Wolfgang Baumeister and Jose Lopez Carrascosa for giving me the opportunity to elaborate and present my work.

Kay Grünewald for the continuous supervision of my work, for his always positive attitude and for his great support.

Everyone else in the 'virus' group: Juha, Lars, Ulrike, Niina, Christoph, Patrick and Stefan (the adopted member). Thank you all for your help inside the lab and for all the fun we had outside. I will never forget the great atmosphere we had in this group.

Beate Sodeik, Kerstin Radtke, André Wolfstein and Katinka Döhner for all the supplied material and productive discussions.

Frank Bradke, Boyan Garvalov and Liane Meyn for the neuron preparations, Valentin Stein and Nancy Meyer for providing *Xenopus Laevis* oocytes and Prashant Desai for providing VP26-GFP-HSV-1.

Ulrike Maurer, Stefan Bohn, Lars Anders Carlson, Juha Huiskonen and Ruben Fernandez for proofreading the manuscript.

My colleagues at the Baumeister department for help with the microscopes and others, as well as for the good atmosphere.

Maria Victoria San Martin and Paula Serrano for being my 'spanish connections' and helping me with all the organization and paper work.

Especialmente agradezco a mis padres su cariño y apoyo incondicional durante todos mis estudios y durante mi estancia en Alemania. A ellos les debo esta tesis.

Muchas gracias a todos!

References

Adrian, M., J. Dubochet, J. Lepault and A. W. McDowall (1984). "Cryo-electron microscopy of viruses." Nature 308(5954): 32-6.

Al-Amoudi, A., J. J. Chang, A. Leforestier, A. McDowall, L. M. Salamin, L. P. Norlen, K. Richter, N. S. Blanc, D. Studer and J. Dubochet (2004). "Cryo-electron microscopy of vitreous sections." EMBO J 23(18): 3583-8.

Aleman, N., M. I. Quiroga, M. Lopez-Pena, S. Vazquez, F. H. Guerrero and J. M. Nieto (2003). "L-particle production during primary replication of pseudorabies virus in the nasal mucosa of swine." J Virol 77(10): 5657-67.

Antinone, S. E., G. T. Shubeita, K. E. Coller, J. I. Lee, S. Haverlock-Moyns, S. P. Gross and G. A. Smith (2006). "The Herpesvirus capsid surface protein, VP26, and the majority of the tegument proteins are dispensable for capsid transport toward the nucleus." J Virol 80(11): 5494-8.

Antinone, S. E. and G. A. Smith (2006). "Two modes of herpesvirus trafficking in neurons: membrane acquisition directs motion." J Virol 80(22): 11235-40.

Batterson, W., D. Furlong and B. Roizman (1983). "Molecular genetics of herpes simplex virus. VIII. further characterization of a temperature-sensitive mutant defective in release of viral DNA and in other stages of the viral reproductive cycle." J Virol 45(1): 397-407.

Bearer, E. L., X. O. Breakefield, D. Schuback, T. S. Reese and J. H. LaVail (2000). "Retrograde axonal transport of herpes simplex virus: evidence for a single mechanism and a role for tegument." Proc Natl Acad Sci U S A 97(14): 8146-50.

Beck, M., F. Forster, M. Ecke, J. M. Plitzko, F. Melchior, G. Gerisch, W. Baumeister and O. Medalia (2004). "Nuclear pore complex structure and dynamics revealed by cryoelectron tomography." Science 306(5700): 1387-90.

Beck, M., V. Lucic, F. Forster, W. Baumeister and O. Medalia (2007). "Snapshots of nuclear pore complexes in action captured by cryo-electron tomography." Nature 449(7162): 611-5.

Bowman, B. R., M. L. Baker, F. J. Rixon, W. Chiu and F. A. Quiocho (2003). "Structure of the herpesvirus major capsid protein." EMBO J 22(4): 757-65.

Bucks, M. A., K. J. O'Regan, M. A. Murphy, J. W. Wills and R. J. Courtney (2007). "Herpes simplex virus type 1 tegument proteins VP1/2 and UL37 are associated with intranuclear capsids." Virology 361(2): 316-24.

Campadelli-Fiume, G., F. Cocchi, L. Menotti and M. Lopez (2000). "The novel receptors that mediate the entry of herpes simplex viruses and animal alphaherpesviruses into cells." Rev Med Virol 10(5): 305-19.

Cardone, G., D. C. Winkler, B. L. Trus, N. Cheng, J. E. Heuser, W. W. Newcomb, J. C. Brown and A. C. Steven (2007). "Visualization of the herpes simplex virus portal in situ by cryo-electron tomography." Virology 361(2): 426-34.

Carfi, A., S. H. Willis, J. C. Whitbeck, C. Krummenacher, G. H. Cohen, R. J. Eisenberg and D. C. Wiley (2001). "Herpes simplex virus glycoprotein D bound to the human receptor HveA." Mol Cell 8(1): 169-79.

Chang, J. T., M. F. Schmid, F. J. Rixon and W. Chiu (2007). "Electron cryotomography reveals the portal in the herpesvirus capsid." J Virol 81(4): 2065-8.

Cheng, Y., W. Boll, T. Kirchhausen, S. C. Harrison and T. Walz (2007). "Cryo-electron tomography of clathrin-coated vesicles: structural implications for coat assembly." J Mol Biol 365(3): 892-9.

Coller, K. E., J. I. Lee, A. Ueda and G. A. Smith (2007). "The capsid and tegument of the alphaherpesviruses are linked by an interaction between the UL25 and VP1/2 proteins." J Virol 81(21): 11790-7.

Conway, J. F., N. R. Watts, D. M. Belnap, N. Cheng, S. J. Stahl, P. T. Wingfield and A. C. Steven (2003). "Characterization of a conformational epitope on hepatitis B virus core antigen and quasiequivalent variations in antibody binding." J Virol 77(11): 6466-73.

Crump, C. M., C. Yates and T. Minson (2007). "Herpes simplex virus type 1 cytoplasmic envelopment requires functional Vps4." J Virol 81(14): 7380-7.

Culver-Hanlon, T. L., S. A. Lex, A. D. Stephens, N. J. Quintyne and S. J. King (2006). "A microtubule-binding domain in dynactin increases dynein processivity by skating along microtubules." Nat Cell Biol 8(3): 264-70.

Dargan, D. J. and J. H. Subak-Sharpe (1997). "The effect of herpes simplex virus type 1 L-particles on virus entry, replication, and the infectivity of naked herpesvirus DNA." Virology 239(2): 378-88.

Darlington, R. W. and L. H. Moss, 3rd (1968). "Herpesvirus envelopment." J Virol 2(1): 48-55.

Dauty, E. and A. S. Verkman (2005). "Actin cytoskeleton as the principal determinant of size-dependent DNA mobility in cytoplasm: a new barrier for non-viral gene delivery." J Biol Chem 280(9): 7823-8.

De Regge, N., H. J. Nauwynck, K. Geenen, C. Krummenacher, G. H. Cohen, R. J. Eisenberg, T. C. Mettenleiter and H. W. Favoreel (2006). "Alpha-herpesvirus glycoprotein D interaction with sensory neurons triggers formation of varicosities that serve as virus exit sites." J Cell Biol 174(2): 267-75.

De Rosier, D. J., Klug A. (1968). "Reconstruction of three dimensional structures from electron micrographs." Nature 217: 130-134.

Desai, P. and S. Person (1998). "Incorporation of the green fluorescent protein into the herpes simplex virus type 1 capsid." J Virol 72(9): 7563-8.

Desai, P. J. (2000). "A null mutation in the UL36 gene of herpes simplex virus type 1 results in accumulation of unenveloped DNA-filled capsids in the cytoplasm of infected cells." J Virol 74(24): 11608-18.

Diefenbach, R. J., M. Miranda-Saksena, M. W. Douglas and A. L. Cunningham (2008). "Transport and egress of herpes simplex virus in neurons." Rev Med Virol 18(1): 35-51.

Dierksen, K., D. Typke, R. Hegerl, W. Baumeister (1993). "Towards automatic electron tomography .2. Implementation of autofocus and low-dose procedures." ultramicroscopy 49: 109-120.

Döhner, K. (2006). Herpes simplex virus type 1 nuclear targeting is mediated by dynein and dynactin, but does not require the small capsid protein VP26, Hannover University.

Döhner, K., K. Radtke, S. Schmidt and B. Sodeik (2006). "Eclipse phase of herpes simplex virus type 1 infection: Efficient dynein-mediated capsid transport without the small capsid protein VP26." J Virol 80(16): 8211-24.

Döhner, K., A. Wolfstein, U. Prank, C. Echeverri, D. Dujardin, R. Vallee and B. Sodeik (2002). "Function of dynein and dynactin in herpes simplex virus capsid transport." Mol Biol Cell 13(8): 2795-809.

Douglas, M. W., R. J. Diefenbach, F. L. Homa, M. Miranda-Saksena, F. J. Rixon, V. Vittone, K. Byth and A. L. Cunningham (2004). "Herpes simplex virus type 1 capsid protein VP26 interacts with dynein light chains RP3 and Tctex1 and plays a role in retrograde cellular transport." J Biol Chem 279(27): 28522-30.

Dubochet, J., M. Adrian, J. J. Chang, J. C. Homo, J. Lepault, A. W. McDowall and P. Schultz (1988). "Cryo-electron microscopy of vitrified specimens." Q Rev Biophys 21(2): 129-228.

Epstein, M. D. (1962). "Observations of the mode of release of Herpes Virus from infected Hela cells." J. Cell biol 12: 589-597.

Erickson, H. P., Klug. A. (1971). "Measurements and compensation of defocusing and aberrations by Fourier processing of electron micrographs." Phil. Trans. Roy. Soc. Lond. 261: 105-118.

Fields, B. N. (2007). Fields Virology, Lippincott Williams & Wilkins.

Fotin, A., T. Kirchhausen, N. Grigorieff, S. C. Harrison, T. Walz and Y. Cheng (2006). "Structure determination of clathrin coats to subnanometer resolution by single particle cryo-electron microscopy." J Struct Biol 156(3): 453-60.

Frangakis, A. S. and R. Hegerl (2001). "Noise reduction in electron tomographic reconstructions using nonlinear anisotropic diffusion." J Struct Biol 135(3): 239-50.

Garvalov, B. K., B. Zuber, C. Bouchet-Marquis, M. Kudryashev, M. Gruska, M. Beck, A. Leis, F. Frischknecht, F. Bradke, W. Baumeister, J. Dubochet and M. Cyrklaff (2006). "Luminal particles within cellular microtubules." J Cell Biol 174(6): 759-65.

Greber, U. F. and M. Way (2006). "A superhighway to virus infection." Cell 124(4): 741-54.

Gross, S. P. (2003). "Dynactin: coordinating motors with opposite inclinations." Curr Biol 13(8): R320-2.

Grünewald, K., P. Desai, D. C. Winkler, J. B. Heymann, D. M. Belnap, W. Baumeister and A. C. Steven (2003). "Three-dimensional structure of herpes simplex virus from cryo-electron tomography." Science 302(5649): 1396-8.

Gruska, M., O. Medalia, W. Baumeister and A. Leis (2008). "Electron tomography of vitreous sections from cultured mammalian cells." J Struct Biol 161(3): 384-92.

Harauz G., M. v. H. (1986). "Exact filter for general geometry three-dimensional reconstruction." Optik 73: 146-156.

Hegerl, R. (1996). "The EM Program Package: A Platform for Image Processing in Biological Electron Microscopy." J Struct Biol 116(1): 30-4.

Heine, J. W., R. W. Honess, E. Cassai and B. Roizman (1974). "Proteins specified by herpes simplex virus. XII. The virion polypeptides of type 1 strains." J Virol 14(3): 640-51.

Heldwein, E. E., H. Lou, F. C. Bender, G. H. Cohen, R. J. Eisenberg and S. C. Harrison (2006). "Crystal structure of glycoprotein B from herpes simplex virus 1." Science 313(5784): 217-20.

Heymann, J. B. and D. M. Belnap (2007). "Bsoft: image processing and molecular modeling for electron microscopy." J Struct Biol 157(1): 3-18.

Heymann, J. B., N. Cheng, W. W. Newcomb, B. L. Trus, J. C. Brown and A. C. Steven (2003). "Dynamics of herpes simplex virus capsid maturation visualized by time-lapse cryo-electron microscopy." Nat Struct Biol 10(5): 334-41.

Janus, J. (2008). Kinesin-1 mediates Herpes simplex virus capsid transport from the MTOC to the nucleus, Abstract book from the 33rd International Herpesvirus Workshop.

Jarnik, M. and U. Aebi (1991). "Toward a more complete 3-D structure of the nuclear pore complex." J Struct Biol 107(3): 291-308.

Kirchhausen, T. (2000). "Clathrin." Annu Rev Biochem 69: 699-727.

Klupp, B. G., W. Fuchs, H. Granzow, R. Nixdorf and T. C. Mettenleiter (2002). "Pseudorabies virus UL36 tegument protein physically interacts with the UL37 protein." J Virol 76(6): 3065-71.

Klupp, B. G., H. Granzow, W. Fuchs, G. M. Keil, S. Finke and T. C. Mettenleiter (2007). "Vesicle formation from the nuclear membrane is induced by coexpression of two conserved herpesvirus proteins." Proc Natl Acad Sci U S A 104(17): 7241-6.

Klupp, B. G., H. Granzow, G. M. Keil and T. C. Mettenleiter (2006). "The capsid-associated UL25 protein of the alphaherpesvirus pseudorabies virus is nonessential for cleavage and encapsidation of genomic DNA but is required for nuclear egress of capsids." J Virol 80(13): 6235-46.

Koshizuka, T., Y. Kawaguchi and Y. Nishiyama (2005). "Herpes simplex virus type 2 membrane protein UL56 associates with the kinesin motor protein KIF1A." J Gen Virol 86(Pt 3): 527-33.

Koster, A., W. d. Ruijter, A. v. d. Bos, K. D. v. d. Mast (1989). "Autotuning of a TEM using minimum electron dose." Ultramicroscopy 27: 251-272.

Koster, A. J., H. Chen, J. W. Sedat and D. A. Agard (1992). "Automated microscopy for electron tomography." Ultramicroscopy 46(1-4): 207-27.

Kremer, J. R., D. N. Mastronarde and J. R. McIntosh (1996). "Computer visualization of three-dimensional image data using IMOD." J Struct Biol 116(1): 71-6.

Kural, C., H. Kim, S. Syed, G. Goshima, V. I. Gelfand and P. R. Selvin (2005). "Kinesin and dynein move a peroxisome in vivo: a tug-of-war or coordinated movement?" Science 308(5727): 1469-72.

Leuzinger, H., U. Ziegler, E. M. Schraner, C. Fraefel, D. L. Glauser, I. Heid, M. Ackermann, M. Mueller and P. Wild (2005). "Herpes simplex virus 1 envelopment follows two diverse pathways." J Virol 79(20): 13047-59.

Ligon, L. A., M. Tokito, J. M. Finklestein, F. E. Grossman and E. L. Holzbaur (2004). "A direct interaction between cytoplasmic dynein and kinesin I may coordinate motor activity." J Biol Chem 279(18): 19201-8.

Loomis, J. S., J. B. Bowzard, R. J. Courtney and J. W. Wills (2001). "Intracellular trafficking of the UL11 tegument protein of herpes simplex virus type 1." J Virol 75(24): 12209-19.

Loret, S., G. Guay and R. Lippe (2008). "Comprehensive characterization of extracellular herpes simplex virus type 1 virions." J Virol 82(17): 8605-18.

Lucic, V., F. Forster and W. Baumeister (2005). "Structural studies by electron tomography: from cells to molecules." Annu Rev Biochem 74: 833-65.

Lucic, V., A. H. Kossel, T. Yang, T. Bonhoeffer, W. Baumeister and A. Sartori (2007). "Multiscale imaging of neurons grown in culture: from light microscopy to cryo-electron tomography." J Struct Biol 160(2): 146-56.

Luxton, G. W., S. Haverlock, K. E. Coller, S. E. Antinone, A. Pincetic and G. A. Smith (2005). "Targeting of herpesvirus capsid transport in axons is coupled to association with specific sets of tegument proteins." Proc Natl Acad Sci U S A 102(16): 5832-7.

Luxton, G. W., J. I. Lee, S. Haverlock-Moyns, J. M. Schober and G. A. Smith (2006). "The pseudorabies virus VP1/2 tegument protein is required for intracellular capsid transport." J Virol 80(1): 201-9.

Lycke, E., B. Hamark, M. Johansson, A. Krotochwil, J. Lycke and B. Svennerholm (1988). "Herpes simplex virus infection of the human sensory neuron. An electron microscopy study." Arch Virol 101(1-2): 87-104.

Lyman, M. G., D. Curanovic and L. W. Enquist (2008). "Targeting of pseudorabies virus structural proteins to axons requires association of the viral Us9 protein with lipid rafts." PLoS Pathog 4(5): e1000065.

Lyman, M. G., B. Feierbach, D. Curanovic, M. Bisher and L. W. Enquist (2007). "Pseudorabies virus Us9 directs axonal sorting of viral capsids." J Virol 81(20): 11363-71.

Mabit, H., M. Y. Nakano, U. Prank, B. Saam, K. Döhner, B. Sodeik and U. F. Greber (2002). "Intact microtubules support adenovirus and herpes simplex virus infections." J Virol 76(19): 9962-71.

Mallik, R., B. C. Carter, S. A. Lex, S. J. King and S. P. Gross (2004). "Cytoplasmic dynein functions as a gear in response to load." Nature 427(6975): 649-52.

Masich, S., T. Ostberg, L. Norlen, O. Shupliakov and B. Daneholt (2006). "A procedure to deposit fiducial markers on vitreous cryo-sections for cellular tomography." J Struct Biol 156(3): 461-8.

Maurer, U. E., B. Sodeik and K. Grünewald (2008). "Native 3D intermediates of membrane fusion in herpes simplex virus 1 entry." Proc Natl Acad Sci U S A 105(30): 10559-64.

McGeoch, D. J., F. J. Rixon and A. J. Davison (2006). "Topics in herpesvirus genomics and evolution." Virus Res 117(1): 90-104.

McLauchlan, J., C. Addison, M. C. Craigie and F. J. Rixon (1992). "Noninfectious L-particles supply functions which can facilitate infection by HSV-1." Virology 190(2): 682-8.

McLauchlan, J. and F. J. Rixon (1992). "Characterization of enveloped tegument structures (L particles) produced by alphaherpesviruses: integrity of the tegument does not depend on the presence of capsid or envelope." J Gen Virol 73 (Pt 2): 269-76.

McNabb, D. S. and R. J. Courtney (1992). "Characterization of the large tegument protein (ICP1/2) of herpes simplex virus type 1." Virology 190(1): 221-32.

Medalia, O., I. Weber, A. S. Frangakis, D. Nicastro, G. Gerisch and W. Baumeister (2002). "Macromolecular architecture in eukaryotic cells visualized by cryoelectron tomography." Science 298(5596): 1209-13.

Mettenleiter, T. C. (2002). "Herpesvirus assembly and egress." J Virol 76(4): 1537-47.

Mettenleiter, T. C. (2006). "Intriguing interplay between viral proteins during herpesvirus assembly or: the herpesvirus assembly puzzle." Vet Microbiol 113(3-4): 163-9.

Mettenleiter, T. C., B. G. Klupp and H. Granzow (2006). "Herpesvirus assembly: a tale of two membranes." Curr Opin Microbiol 9(4): 423-9.

Milne, R. S., A. V. Nicola, J. C. Whitbeck, R. J. Eisenberg and G. H. Cohen (2005). "Glycoprotein D receptor-dependent, low-pH-independent endocytic entry of herpes simplex virus type 1." J Virol 79(11): 6655-63.

Miranda-Saksena, M., P. Armati, R. A. Boadle, D. J. Holland and A. L. Cunningham (2000). "Anterograde transport of herpes simplex virus type 1 in cultured, dissociated human and rat dorsal root ganglion neurons." J Virol 74(4): 1827-39.

Miranda-Saksena, M., R. A. Boadle, P. Armati and A. L. Cunningham (2002). "In rat dorsal root ganglion neurons, herpes simplex virus type 1 tegument forms in the cytoplasm of the cell body." J Virol 76(19): 9934-51.

Munson, M. and P. Novick (2006). "The exocyst defrocked, a framework of rods revealed." Nat Struct Mol Biol 13(7): 577-81.

Naldinho-Souto, R., H. Browne and T. Minson (2006). "Herpes simplex virus tegument protein VP16 is a component of primary enveloped virions." J Virol 80(5): 2582-4.

Newcomb, W. W. and J. C. Brown (1990). "Structure of the Herpes Simplex Virus capsid: Effects of extraction with Guanidine Hydrochloride and partial reconstitution of extracted capsids." J Virol 65(2): 613-620.

Newcomb, W. W. and J. C. Brown (1991). "Structure of the herpes simplex virus capsid: effects of extraction with guanidine hydrochloride and partial reconstitution of extracted capsids." J Virol 65(2): 613-20.

Newcomb, W. W., F. L. Homa and J. C. Brown (2006). "Herpes simplex virus capsid structure: DNA packaging protein UL25 is located on the external surface of the capsid near the vertices." J Virol 80(13): 6286-94.

Newcomb, W. W., R. M. Juhas, D. R. Thomsen, F. L. Homa, A. D. Burch, S. K. Weller and J. C. Brown (2001). "The UL6 gene product forms the portal for entry of DNA into the herpes simplex virus capsid." J Virol 75(22): 10923-32.

Newcomb, W. W., B. L. Trus, F. P. Booy, A. C. Steven, J. S. Wall and J. C. Brown (1993). "Structure of the herpes simplex virus capsid. Molecular composition of the pentons and the triplexes." J Mol Biol 232(2): 499-511.

Nickell, S., F. Forster, A. Linaroudis, W. D. Net, F. Beck, R. Hegerl, W. Baumeister and J. M. Plitzko (2005). "TOM software toolbox: acquisition and analysis for electron tomography." J Struct Biol 149(3): 227-34.

Nicola, A. V., A. M. McEvoy and S. E. Straus (2003). "Roles for endocytosis and low pH in herpes simplex virus entry into HeLa and Chinese hamster ovary cells." J Virol 77(9): 5324-32.

Nogales, E. (2000). "Structural insights into microtubule function." Annu Rev Biochem 69: 277-302.

Ogasawara, M., T. Suzutani, I. Yoshida and M. Azuma (2001). "Role of the UL25 gene product in packaging DNA into the herpes simplex virus capsid: location of UL25 product in the capsid and demonstration that it binds DNA." J Virol 75(3): 1427-36.

Ojala, P. M., B. Sodeik, M. W. Ebersold, U. Kutay and A. Helenius (2000). "Herpes simplex virus type 1 entry into host cells: reconstitution of capsid binding and uncoating at the nuclear pore complex in vitro." Mol Cell Biol 20(13): 4922-31.

Pelkmans, L. and A. Helenius (2003). "Insider information: what viruses tell us about endocytosis." Curr Opin Cell Biol 15(4): 414-22.

Radtke, K., K. Döhner and B. Sodeik (2006). "Viral interactions with the cytoskeleton: a hitchhiker's guide to the cell." Cell Microbiol 8(3): 387-400.

Reck-Peterson, S. L., A. Yildiz, A. P. Carter, A. Gennerich, N. Zhang and R. D. Vale (2006). "Single-molecule analysis of dynein processivity and stepping behavior." Cell 126(2): 335-48.

Reimer, L. (1997). Transmission electron microscopy, Physics of image formation and microanalysis, Springer.

Reynolds, A. E., E. G. Wills, R. J. Roller, B. J. Ryckman and J. D. Baines (2002). "Ultrastructural localization of the herpes simplex virus type 1 UL31, UL34, and US3 proteins suggests specific roles in primary envelopment and egress of nucleocapsids." J Virol 76(17): 8939-52.

Rixon, F. J., C. Addison and J. McLauchlan (1992). "Assembly of enveloped tegument structures (L particles) can occur independently of virion maturation in herpes simplex virus type 1-infected cells." J Gen Virol 73 (Pt 2): 277-84.

Roberts, A. P., F. Abaitua, P. O'Hare, D. McNab, F. J. Rixon and D. Pasdeloup (2008). "Differing Roles of Inner Tegument Proteins pUL36 and pUL37 During Entry of Herpes Simplex Virus Type 1 (HSV-1)." J Virol.

Rode, K. (2007). The role of the UL25 Protein of Herpes simplex virus 1 during assembly, cell entry and nuclear import of the viral genome, Hannover University.

Saksena, M. M., H. Wakisaka, B. Tijono, R. A. Boadle, F. Rixon, H. Takahashi and A. L. Cunningham (2006). "Herpes simplex virus type 1 accumulation, envelopment, and exit in growth cones and varicosities in mid-distal regions of axons." J Virol 80(7): 3592-606.

Salmon, B. and J. D. Baines (1998). "Herpes simplex virus DNA cleavage and packaging: association of multiple forms of U(L)15-encoded proteins with B capsids requires at least the U(L)6, U(L)17, and U(L)28 genes." J Virol 72(4): 3045-50.

Sartori, A., R. Gatz, F. Beck, A. Rigort, W. Baumeister and J. M. Plitzko (2007). "Correlative microscopy: bridging the gap between fluorescence light microscopy and cryo-electron tomography." J Struct Biol 160(2): 135-45.

Satoh, T., J. Arii, T. Suenaga, J. Wang, A. Kogure, J. Uehori, N. Arase, I. Shiratori, S. Tanaka, Y. Kawaguchi, P. G. Spear, L. L. Lanier and H. Arase (2008). "PILRalpha is a herpes simplex virus-1 entry coreceptor that associates with glycoprotein B." Cell 132(6): 935-44.

Schliwa, M. and G. Woehlke (2003). "Molecular motors." Nature 422(6933): 759-65.

Schrag, J. D., B. V. Prasad, F. J. Rixon and W. Chiu (1989). "Three-dimensional structure of the HSV1 nucleocapsid." Cell 56(4): 651-60.

Schroer, T. A. (2004). "Dynactin." Annu Rev Cell Dev Biol 20: 759-79.

Schweikert, G. (2004). Quantitativer Vergleich der Strahlschädigung biologischer Proben in TEM bei Stickstoff und Helium Temperatur., Technical University Munich.

Sedy, J. R., P. G. Spear and C. F. Ware (2008). "Cross-regulation between herpesviruses and the TNF superfamily members." Nat Rev Immunol 8(11): 861-73.

Shukla, D., J. Liu, P. Blaiklock, N. W. Shworak, X. Bai, J. D. Esko, G. H. Cohen, R. J. Eisenberg, R. D. Rosenberg and P. G. Spear (1999). "A novel role for 3-O-sulfated heparan sulfate in herpes simplex virus 1 entry." Cell 99(1): 13-22.

Skepper, J. N., A. Whiteley, H. Browne and A. Minson (2001). "Herpes simplex virus nucleocapsids mature to progeny virions by an envelopment --> deenvelopment --> reenvelopment pathway." J Virol 75(12): 5697-702.

Smith, A. E. and A. Helenius (2004). "How viruses enter animal cells." Science 304(5668): 237-42.

Smith, G. A., S. P. Gross and L. W. Enquist (2001). "Herpesviruses use bidirectional fast-axonal transport to spread in sensory neurons." Proc Natl Acad Sci U S A 98(6): 3466-70.

Smith, G. A., L. Pomeranz, S. P. Gross and L. W. Enquist (2004). "Local modulation of plus-end transport targets herpesvirus entry and egress in sensory axons." Proc Natl Acad Sci U S A 101(45): 16034-9.

Snyder, A., T. W. Wisner and D. C. Johnson (2006). "Herpes simplex virus capsids are transported in neuronal axons without an envelope containing the viral glycoproteins." J Virol 80(22): 11165-77.

Sodeik, B., M. W. Ebersold and A. Helenius (1997). "Microtubule-mediated transport of incoming herpes simplex virus 1 capsids to the nucleus." J Cell Biol 136(5): 1007-21.

Spang, A. (2008). "The life cycle of a transport vesicle." Cell Mol Life Sci 65(18): 2781-9.

Spear, P. G. (2004). "Herpes simplex virus: receptors and ligands for cell entry." Cell Microbiol 6(5): 401-10.

Spear, P. G. and B. Roizman (1972). "Proteins specified by herpes simplex virus. V. Purification and structural proteins of the herpesvirion." J Virol 9(1): 143-59.

Stannard, L. M., A. O. Fuller and P. G. Spear (1987). "Herpes simplex virus glycoproteins associated with different morphological entities projecting from the virion envelope." J Gen Virol 68 (Pt 3): 715-25.

Stewart, M. (2007). "Molecular mechanism of the nuclear protein import cycle." Nat Rev Mol Cell Biol 8(3): 195-208.

Stewart, P. L., C. Y. Chiu, D. A. Haley, L. B. Kong and J. L. Schlessman (1999). "Review: resolution issues in single-particle reconstruction." J Struct Biol 128(1): 58-64.

Stoffler, D., B. Feja, B. Fahrenkrog, J. Walz, D. Typke and U. Aebi (2003). "Cryo-electron tomography provides novel insights into nuclear pore architecture: implications for nucleocytoplasmic transport." J Mol Biol 328(1): 119-30.

Stoffler, D., K. N. Goldie, B. Feja and U. Aebi (1999). "Calcium-mediated structural changes of native nuclear pore complexes monitored by time-lapse atomic force microscopy." J Mol Biol 287(4): 741-52.

Sutton, R. B., D. Fasshauer, R. Jahn and A. T. Brunger (1998). "Crystal structure of a SNARE complex involved in synaptic exocytosis at 2.4 A resolution." Nature 395(6700): 347-53.

Szilagyi, J. F. and J. Berriman (1994). "Herpes simplex virus L particles contain spherical membrane-enclosed inclusion vesicles." J Gen Virol 75 (Pt 7): 1749-53.

Szilagyi, J. F. and C. Cunningham (1991). "Identification and characterization of a novel non-infectious herpes simplex virus-related particle." J Gen Virol 72 (Pt 3): 661-8.

Tomishima, M. J. and L. W. Enquist (2002). "In vivo egress of an alphaherpesvirus from axons." J Virol 76(16): 8310-7.

Trus, B. L., N. Cheng, W. W. Newcomb, F. L. Homa, J. C. Brown and A. C. Steven (2004). "Structure and polymorphism of the UL6 portal protein of herpes simplex virus type 1." J Virol 78(22): 12668-71.

Trus, B. L., W. Gibson, N. Cheng and A. C. Steven (1999). "Capsid structure of simian cytomegalovirus from cryoelectron microscopy: evidence for tegument attachment sites." J Virol 73(3): 2181-92.

Trus, B. L., W. W. Newcomb, N. Cheng, G. Cardone, L. Marekov, F. L. Homa, J. C. Brown and A. C. Steven (2007). "Allosteric signaling and a nuclear exit strategy: binding of UL25/UL17 heterodimers to DNA-Filled HSV-1 capsids." Mol Cell 26(4): 479-89.

Turcotte, S., J. Letellier and R. Lippe (2005). "Herpes simplex virus type 1 capsids transit by the trans-Golgi network, where viral glycoproteins accumulate independently of capsid egress." J Virol 79(14): 8847-60.

Vale, R. D. (2003). "The molecular motor toolbox for intracellular transport." Cell 112(4): 467-80.

Vallee, R. B. and P. Hook (2003). "Molecular motors: A magnificent machine." Nature 421(6924): 701-2.

Whittaker, G. R. (2003). "Virus nuclear import." Adv Drug Deliv Rev 55(6): 733-47.

Wolfstein, A., C. H. Nagel, K. Radtke, K. Döhner, V. J. Allan and B. Sodeik (2006). "The inner tegument promotes herpes simplex virus capsid motility along microtubules in vitro." Traffic 7(2): 227-37.

Ye, G. J., K. T. Vaughan, R. B. Vallee and B. Roizman (2000). "The herpes simplex virus 1 U(L)34 protein interacts with a cytoplasmic dynein intermediate chain and targets nuclear membrane." J Virol 74(3): 1355-63.

Yildiz, A. and P. R. Selvin (2005). "Kinesin: walking, crawling or sliding along?" Trends Cell Biol 15(2): 112-20.

Yonekura, K., S. Maki-Yonekura and K. Namba (2002). "Quantitative comparison of zero-loss and conventional electron diffraction from two-dimensional and thin three-dimensional protein crystals." Biophys J 82(5): 2784-97.

Zhou, Z. H., D. H. Chen, J. Jakana, F. J. Rixon and W. Chiu (1999). "Visualization of tegument-capsid interactions and DNA in intact herpes simplex virus type 1 virions." J Virol 73(4): 3210-8.

Zhou, Z. H., M. Dougherty, J. Jakana, J. He, F. J. Rixon and W. Chiu (2000). "Seeing the herpesvirus capsid at 8.5 A." Science 288(5467): 877-80.

Zhou, Z. H., B. V. Prasad, J. Jakana, F. J. Rixon and W. Chiu (1994). "Protein subunit structures in the herpes simplex virus A-capsid determined from 400 kV spot-scan electron cryomicroscopy." J Mol Biol 242(4): 456-69.